Stimulus-Dependent Regulation of 2-Arachidonoyl Glycerol Signaling and the Mechanism of its Hydrolysis by ABHD6

Simar R. Singh

A dissertation

submitted in partial fulfillment of the

requirements for the degree of

Doctor of Philosophy

University of Washington

2023

Reading Committee:

Nephi Stella, Chair

Ning Zheng

Smita Yadav

Program Authorized to Offer Degree:

Pharmacology

University of Washington

Abstract

Stimulus-Dependent Regulation of 2-Arachidonoyl Glycerol Signaling and the Mechanism of its Hydrolysis by ABHD6

Simar R. Singh

Chair of the Supervisory Committee:
Nephi Stella
Department of Pharmacology

Cannabis has been used for thousands of years for recreational and therapeutic effects. The efficacy of medicinal cannabis for conditions such as epilepsy and pain has resulted in the discovery of the molecular targets of the bioactive compounds, or phyto-cannabinoids, found in cannabis. These targets are part of a signaling system called the endocannabinoid (eCB) system, which is a neuromodulatory system consisting of the receptors targeted by phyto-cannabinoids, the endogenously produced lipid neuromodulators, or eCBs, that act at these targets, and the machinery that regulates eCB levels, including biosynthetic and degradative enzymes. Enhancing eCB signaling in the brain can provide therapeutic benefit for neurological diseases like epilepsy and chronic pain.

A strategy for enhancing eCB signaling is by inhibiting its enzymatic hydrolysis. One of the eCB hydrolyzing enzymes expressed in the brain is α/β hydrolase domain containing 6 (ABHD6). ABHD6 hydrolyzes the eCB 2-arachidonoyl glycerol (2-AG), which is the most abundant eCB in the central nervous system. Production of neuronal 2-AG is activity-dependent, resulting in localized and tightly regulated signaling at targets such as the cannabinoid receptors (CBRs). Therefore, inhibiting ABHD6 can increase intrinsic 2-AG levels and resulting CBR activation. Thus, inhibition will have an effect only when and where activated cells produce 2-AG. Recent studies have demonstrated efficacy of ABHD6 inhibition in preclinical models of epilepsy and neuropathic pain, which are pathological conditions that share key elements: hyperexcitability of neurons and neuroinflammation. While 2-AG's role in reducing neuronal activity has been well-described, the mechanism of neuronal 2-AG production following inflammation and the effect of ABHD6 inhibition on enhancing these 2-AG levels remains unclear.

Here, we characterize a genetically encoded sensor, the $GRAB_{eCB2.0}$, and then use the sensor to show that two inflammatory mediators, ATP and bradykinin (BK), can stimulate 2-AG production in neuro2a mouse neuroblastoma cells through separate receptor-dependent mechanisms. I discovered that, in a co-culture model system, ATP and BK-stimulated 2-AG can participate in paracrine activation of $GRAB_{eCB2.0}$. These findings describe a potential molecular mechanism by which inflammatory mediators may act directly on sensory CB_1R-expressing neurons and engage the eCB system, which can function in a negative feedback loop to decrease hyperactivity of peripheral nociceptors that underlies hyperalgesia. Since ABHD6 inhibition has the potential to enhance 2-AG signaling and produces analgesia in neuropathic pain models, we further

described the mechanism of ABHD6 hydrolysis activity and discovered that an undescribed membrane factor increases in vitro ABHD6 activity and are now testing a first-in-class ABHD6 inhibitor. This work expands our understanding of the pathophysiological role of 2-AG and describes the function of ABHD6, a potential therapeutic target which can allow for the development selective inhibitors with a clinical benefit.

TABLE OF CONTENTS

LIST OF FIGURES

LIST OF TABLES

ACKNOWLEDGEMENTS

I want to start by thanking Nephi Stella for being an excellent mentor. Starting from the time he interviewed me as a prospective graduate student, I greatly appreciated and admired Nephi's excitement about research. His trust in my abilities and confidence that the winding path we were one would lead us to an interesting finding gave me confidence as I explored new ideas and techniques. Nephi has patiently guided me through the long process of attaining this degree and I feel lucky to have had him has a mentor.

I also want to acknowledge rest of the Stella Lab, both past and present members, for their support and friendship throughout this process. In particular, I want to thank Katie Viray, Cong Xu, Anthony English, Dennis Sarroza, Kainat Khan, and Jackson Yu. Stella Lab collaborators and friends at the University of Washington that I also want to thank include Ruth Westenbroek, Domnita Rusnac, Xiao-Bo Tang, and the entirety of the Wordeman Lab (Linda, Mike, and Juan Jesus Vicente). I also want to thank members of the UW Cannabinoid Network (Michael Bruchas, Ben Land, David Marcus, and Kaylin Ellioff), my cohort (namely Kimya Nourbakhsh, Nicole Marsh, Ashley Tsue), my committee and the Department of Pharmacology and University of Washington at large. I have thoroughly enjoyed working with all of you and this experience would not have been as fulfilling or fun without the experiences, both scientific and otherwise, that I've shared with all of you.

Next, I want to thank all my friends who supported me in the days when the idea of graduate school was still a dream. I want to specifically thank Raj Kadiyala for his contribution to this thesis, since no one asked more about how close I was to finishing the thesis than he did. I also want to thank everyone else for refraining from this habit. I have known some of you for over a decade during a formative period in my life, and I wouldn't be the person I am today without this friendship. I am proud to call you my friends and I hope we can spend many more decades together!

Finally, I want to thank my entire family for their unwavering support. To my grandparents and extended family: your words of encouragement have carried a lot of weight for me. To my parents: thank you for your sacrifices that have allowed me to follow any path I wanted to and for modeling the importance of primarily being a kind and loving person over all else. To my sister: thank you for being an amazing sibling and one of my closest friends who probably knows me better than I know myself. I am looking forward to spending more time with all of you in the future!

To sum up my experience, both scientific and personal, I want to end with this quote: "…straight linearity, which we have come to take for granted in everything from physics to fiction, simply does not exist. Linearity is an artificial way of viewing the world. Real life isn't a series of interconnected events occurring one after another like beads strung on a necklace. Life is actually a series of encounters in which one event may change those that follow in a wholly unpredictable, even devastating way."

Michael Crighton

Chapter 1.

Introduction

The therapeutic effects of cannabinoids

Cannabis is a genus of plant that originated in central Asia that has a wide range of effects in humans, with reports of its therapeutic use dating back to 2737 BC in China[1]. The biological effects of cannabis use include 1] recreational effects: hallucinations, altered perceptions of time, euphoria, dissociation, and are associated with feeling high; 2] medicinal effects: analgesic, antiemetic, anticonvulsant, and sedative effects; 3] and adverse effects: paranoia, anxiety, memory impairment, and other symptoms of intoxication[2-4]. This diversity in effects resulting from cannabis use is attributed to the more than 100 phyto-cannabinoids found in the plant. Phyto-cannabinoids are a class of lipophilic, 21-carbon polyketides[5]. The most abundant on average is Δ^9-tetrahydrocannabinol (THC), although the amount of THC relative to the other cannabinoids varies based on strain[6,7]. Other cannabinoids found in the plant that have a lower abundance than THC but contribute to the biological effects of cannabis include cannabidiol (CBD), cannabinol, and Δ^8-THC, among others[3]. To date, THC and CBD are also the most studied in terms of their mechanism of action and therapeutic potential.

Due to their therapeutic benefits, cannabinoids have been approved by the FDA for multiple therapeutic uses. Dronabinol, a synthetic form of THC, and nabilone (a synthetic THC analog) are approved for chemotherapy-induced nausea and vomiting[8,9]. CBD was approved in 2018 by the FDA to combat the pharmacoresistant epilepsies Dravet syndrome and Lennox-Gestaut syndrome[10]. Furthermore, following decades of federal

prohibition in the United States, cannabis is slowly being decriminalized and cannabis use is increasing. As of today, legal access to recreational cannabis can be found in 23 states and the District of Columba, while another 15 states have legalized cannabis for medical purposes[11].

THC and CBD, exert their effects on the body by acting at a number of receptors in the body. The first targets to be identified were the CB_1 and CB_2 cannabinoid receptors (CB_1R and CB_2R, respectively), although the number of targets has expanded in recent years. The discovery of the CB_1R and CB_2R was the first step in characterizing a novel signaling system in the body: the endocannabinoid signaling system.

2-arachidonoyl glycerol signaling

The eCB system is a signaling system involved in multiple physiological processes, including neurotransmission, inflammation, and metabolism, all of which are mediated by a class of lipid signaling molecules known as endocannabinoids (eCBs). The best characterized eCBs are N-arachidonoylethanolamine (AEA) and 2-arachidonoyl glycerol (2-AG), which differ from one another in several key characteristics, including their: 1] relative abundance in the brain; 2] biosynthetic mechanisms; 3] properties at target proteins; 4] and how they are degraded[12]. For instance, 2-AG acts as a low affinity full agonist at both the CB_1R and CB_2R while AEA is as a high-affinity partial agonist at CB_1R with low activity at the CB_2R. Furthermore, the levels of 2-AG in the brain are approximately 100-1000-fold greater than AEA levels in select brain areas (as determined by mass spectrometry in bulk brain tissue)[13,14]. Due to 2-AG's abundance and activity at the CB_1R and CB_2R's, it can be considered the predominant eCB in the brain.

2-AG is a monoacylglycerol derivative of the ω-6 polyunsaturated fatty acid, arachidonic acid. 2-AG synthesis in neurons is activity-dependent, which refers to its on-demand production stimulated by an increase in intracellular calcium[15,16]. The role of calcium in 2-AG production is demonstrated with receptor-independent 2-AG synthesis. Increasing intracellular calcium using the calcium ionophore, ionomycin, which bypasses receptor activation, is sufficient for increasing 2-AG levels in neurons[17,18]. This increase in calcium is not only sufficient for 2-AG synthesis but is also necessary, which can be highlighted using a more physiologically relevant model of 2-AG biosynthesis: receptor-dependent 2-AG production. For example, activation of the group 1 metabotropic glutamate receptors (mGLUR1/5) results in an increase in activity of calcium-sensitive phospholipase C-β (PLCβ), which hydrolyzes the membrane phosphoinositide PIP_2 to form IP_3, a second messenger that mobilizes endoplasmic reticulum calcium stores, and diacylglycerol (DAG)[19,20]. DAG serves as a precursor for 2-AG synthesis, which occurs through the hydrolysis of DAG at the sn-1 position by the enzyme diacylglycerol lipase (DAGL)[16,19]. Decreasing intracellular calcium either with the chelators EGTA and BAPTA-AM, or by depletion of intracellular calcium stores using thapsigargin, results in decreased receptor-dependent 2-AG synthesis[17,21,22]. Thus, the regulation of 2-AG biosynthesis by intracellular calcium levels suggests that 2-AG production is activity-dependent and tightly coupled to neuronal activity.

Molecular Targets of 2-arachidonoyl glycerol

Following its synthesis, 2-AG can act at several target proteins. 2-AG's actions have been best characterized as a full agonist at the CB_1R and CB_2R, which are G-protein coupled receptors (GPCRs). The CB_1R is widely expressed in the brain and estimated to

be one of the most abundant GPCRs expressed in the brain[23]. Specifically, CB_1R is expressed by GABAergic and glutamatergic neurons in various brain regions including the cortex and the hippocampus[24,25] as well as at lower levels in astrocytes[26] and in microglia, although microglial CB_1R expression can increase when the cells in an activated state[27]. CB_1R is also expressed in neurons outside of the brain, such as by the trigeminal ganglia and dorsal root ganglia, as well as peripheral tissues (GI tract, including both enteric neurons and enteroendocrine cells, liver and reproductive tissues)[14].

CB_2R expression has traditionally been thought to be contained to microglia, the resident immune cells in the brain that sense damage and respond to the insult, and in peripheral myeloid cells, including macrophages, monocytes, and natural killer cells[28]. CB_2R expression is correlated with the activation state of these cells. A healthy brain expresses low levels of CB_2R while neuroinflammation and neurodegeneration is correlated with increase CB_2R expression[28]. CB_2R expression in neurons is controversial due to a lack of validated antibodies; however, there is some evidence of neuronal CB_2R mRNA expression in several brain regions, including the hippocampus, cortex, and brainstem[29,30]. Due to the conflicting results regarding CB_2R expression in neurons, studies regarding 2-AG's action as a neuromodulator generally focus on the CB_1R.

Since CB_1R is widely expressed in multiple cell and tissue types, the signaling of these receptors upon activation by 2-AG is cell-type specific. For instance, expression of the CB_1R does not always correlate with its G-protein activity. This was demonstrated by cell-specific CB_1R knock-out studies in the hippocampus showing that glutamatergic neurons account for about 20% of the CB_1R protein expression but accounts for about 50% of the G-protein activation induced by a CB_1R agonist as measured by GTPγS

binding, while GABAergic-CB_1R expression contributes to about 80% of the total CB_1R expression and only 20% of the CB_1R-dependent G-protein activation[25]. This cell-specific activity has several potential mechanisms, including differences in expression of CB_1R-interacting proteins, such as CRIP1α and other GPCRs that the CB_1R is known to dimerize with like D2 dopamine receptor, as well as the potential for CB_1R to couple to different G_α-proteins, including $G_{i/o}$, G_s, and $G_{q/11}$[31]. To date, the best characterized CB_1R signaling is mediated by the receptors coupling to the pertussis-toxin sensitive $G_{i/o}$ proteins. In this context, CB_1R activation results several downstream effects: 1] $G_{i/o}$-mediated inhibition of adenylyl cyclase and subsequent decrease in cAMP levels; 2] $G_{\beta y}$-mediated inhibition of several voltage-gated calcium channels (N-, P/Q-, and R-type channels specifically) and activation of G-protein inward rectifying potassium channels; 3] increased MAPK and PI3K/Akt signaling[14]. Some of these downstream signaling pathways, namely phosphorylation of MAPK proteins, can also be mediated by β-arrestin1[32]. Although the cumulative effects of this downstream signaling is dependent on cell type, in general, 2-AG activation of neuronal CB_1R is associated with a decrease in neuronal excitability.

2-AG's action at the CB_1R can regulate neuronal activity through several mechanisms. One of the first mechanisms to be characterized was CB_1R-dependent retrograde signaling which modulates synaptic function. This signaling involves post-synaptic, activity-dependent synthesis of 2-AG, which travels to the pre-synaptic nerve terminal (hence the name retrograde) where it activates CB_1R and inhibits pre-synaptic neurotransmitter release[33]. Retrograde eCB signaling was first demonstrated at inhibitory GABAergic synapses in hippocampal neurons and slices, where depolarization (in the

form of a high frequency train of action potentials) of post-synaptic neurons and resulting increase in intracellular calcium decreased inhibitory post-synaptic currents (IPSC), indicating a reduction in pre-synaptic GABA release, and was blocked by a CB_1R antagonist[34-36]. Similarly, retrograde eCB signaling can also occur at excitatory synapses where it can decrease pre-synaptic glutamate release. This form of short-term synaptic plasticity, which only lasts for tens of seconds, at inhibitory and excitatory synapses has been named Depolarization induced Suppression of Inhibition (DSI) or Depolarization-induced Suppression of Excitation (DSE), respectively[12]. Short-term synaptic depression mediated by retrograde eCB signaling can also be triggered by neurotransmitters acting at metabotropic GPCRs: activation of post-synaptic group I mGluR or M1/M3 muscarinic receptors decreases excitatory post-synaptic currents (EPSCs), indicating a reduction in pre-synaptic glutamate release, and can be blocked by CB_1R antagonist and DAGL inhibitors, helping identify 2-AG as the eCB mediating this retrograde signaling[34]. Since the description of retrograde 2-AG signaling and its role in CB_1R-dependent short-term synaptic depression, 2-AG's role as a neuromodulator has expanded to include more forms of signaling involving different cell types and molecular targets, including: 1] long-term depression (LTD) in at excitatory and inhibitory synapses, which also depend on 2-AG retrograde signaling; 2] 2-AG autocrine signaling, including acting at post-synaptic $GABA_A$ receptors[37]; 3] activation of astrocytic CB_1R which indirectly modulate synaptic function; 4] and tonic 2-AG signaling[38,39]. Although the mechanisms and physiological roles of 2-AG's signaling modalities continues to be investigated, it is clear that 2-AG can regulate neuronal activity throughout the brain. With the potential therapeutic benefits of targeting the CB_1R, as demonstrated using cannabis, enhancing the activity-dependent

signaling of the endogenous CB_1R agonist 2-AG could be a promising therapeutic approach to increase CB_1R activation in a targeted and localized manner, which may help avoid the widespread activation and resulting adverse effects associated with the exogenous phyto-cannabinoids. A potential strategy for increasing 2-AG signaling is to inhibit 2-AG degradation.

2-AG's degradation by enzymatic hydrolysis is the primary mechanism by which 2-AG signaling is terminated. The major enzymes involved in 2-AG hydrolysis in the brain are monoacylglycerol lipase (MAGL), α/β-hydrolase domain containing 12 (ABHD12), and α/β-hydrolase domain containing 6 (ABHD6), all of which degrade 2-AG to produce arachidonic acid and glycerol[40]. Despite the shared mechanism of 2-AG hydrolysis, MAGL, ABHD12, and ABHD6 differ in several key aspects, namely their relative contribution to brain 2-AG hydrolysis, their subcellular localization, which determines what pool of 2-AG they regulate, and the physiological effects of their respective inhibition. In neurons, MAGL has presynaptic localization, which means it is co-expressed in the same cellular compartment as the pre-synaptic CB_1Rs that are involved in DSI/DSE[41]. MAGL also accounts for an estimated 85% of 2-AG hydrolysis in the brain[42,43]. Due to its large contribution to 2-AG hydrolysis, genetic deletion or chronic inhibition of MAGL increases 2-AG levels in the brain, producing therapeutic effects, such as analgesia, as well as other CB_1R -mediated physiological effects such as hypothermia and hypolocomotion, indicating widespread CB_1R activation throughout the brain and the potential for off-target effects if inhibitors are used clinically[44]. Furthermore, the sustained increase in 2-AG results in CB_1R desensitization in mice, which points toward a risk of developing tolerance to inhibitors of MAGL if needed for a chronic/long term conditions such as neuropathic

pain or epilepsy[44]. ABHD12 accounts for approximately 10% of 2-AG hydrolysis in the brain[40]. Unlike MAGL and ABHD6, which are cytosolic or cytosolic-facing enzymes respectively, ABHD12 is membrane-protein that faces the extracellular space[40]. While ABHD12 can hydrolyze 2-AG, global knock-out models of ABHD12 show that it is also a regulator of lysophosphatidylserine, and mice lacking ABHD12 exhibit symptoms associated with the neurodegenerative disorder PHARC (polyneuropathy, hearing-loss, ataxia, retinosis pigmentosa, and cataract)[45]. The last major 2-AG hydrolyzing enzyme is ABHD6, which accounts for an estimated 5% of 2-AG hydrolysis in the brain[40]. It has a post-synaptic localization, which is also the major site of 2-AG synthesis as it co-localizes with DAGL[41,46]. ABHD6 knock-out and inhibition do not result in CB_1R mediated off-target effects (tetrad effects) and CB_1R desensitization, while still having a potential therapeutic benefit when used in preclinical models of epilepsy and pain[47-49]. Therefore, ABHD6 inhibition can allow for a localized increases in 2-AG levels, allowing for a therapeutic benefit while potentially minimizing the risk of adverse effects and CB_1R desensitization.

ABHD6: A Therapeutic Target to Increase 2-AG Signaling

ABHD6 was first identified as a 2-AG hydrolyzing enzyme in mouse brain membrane fraction[40]. This was confirmed in the BV-2 microglial cell line and in mouse neurons in primary culture, where ABHD6 was found to hydrolyze 2-AG in intact cells[46,50]. ABHD6's role in regulating 2-AG dependent neurotransmission was also discovered in neuron in primary culture, where ABHD6 inhibition enhanced CB_1R-dependent long-term depression in mouse cortical slices[46]. At the synapse, ABHD6 was found to localize to the post-synaptic neuron, which is where the 2-AG involved in retrograde signaling is

produced[41,46]. Thus, ABHD6 is a post-synaptic enzyme that regulates activity-dependent 2-AG levels at the site of 2-AG synthesis and 2-AG's activity at the CB_1R.

Following the identification of ABHD6's role as a regulator of 2-AG neuronal signaling, more recent biochemical and pharmacological studies have further characterized the molecular mechanism underlying ABHD6 activity. ABHD6 is an enzyme in the serine hydrolase superfamily, which encompasses hundreds of enzymes characterized by a conserved catalytic mechanism that relies on three amino acid residues in the active site called the catalytic triad[42]. In the case of ABHD6, these residues are Ser148, Asp278, and His306, and mutating any of these residues abolishes hydrolysis activity of the enzyme[51]. Aside from the catalytic triad, ABHD6 consists of a short amino terminal sequence followed by a single transmembrane domain within the first 30 amino acids, and lastly an intracellular catalytic domain[40,52]. While the function of the amino terminal and transmembrane domain remains elusive, the catalytic domain has been more extensively characterized. The catalytic domain is made up of the α/β hydrolase domain, which consists of a central core made up of eight β-sheets surrounded by six alpha helices (two on one side and four on the other), and a lid domain made up of four α-helices[53]. Between these two domains is the active site of the enzyme, which is predicted to transverse through the entirely of the enzyme, and which also contains the residues of the catalytic triad on the loops connecting the α-helices to the β-sheets in the α/β hydrolase fold. The active site can accommodate the binding and hydrolysis of other substrates aside from 2-AG with disparate chemical structures.

ABHD6 substrate specificity has been studied using a combination of in vitro enzymatic assays and lipidomic analysis of ABHD6 knock-out mice. ABHD6 can

hydrolyze monoacylglycerols with varying acyl chain lengths and levels of saturation, ranging from 8:0 to 20:4[51]. The in vitro studies also indicate that ABHD6 can hydrolyze the 18:1, 18:2, and 20:4 monoacylglycerols in either the 1,3 or 2 configurations, but with a preference for the 1,3-position, and has a significantly lower preference for diacyl- and triacylglycerols[51]. ABHD6's substrate selectivity extends beyond the monoacylglycerols, as it also degrades lysophospholipids and glycerophospholipids in the liver, including lysophosphotidylglcyerol and bis(monoaclyglycero)phosphate[54,55]. In part due to this broad substrate specificity, ABHD6 has been shown to be involved in multiple pathophysiological processes. However, ABHD6's role is likely tissue specific as it is expressed throughout the body in multiple cell types, including the brain (where it was first discovered), testis, liver, and adipose tissue.

In the brain, the highest ABHD6 mRNA expression and activity is found in the hippocampus, cortex, striatum, and cerebellum[56]. In terms of cell specific expression in the brain, ABHD6 protein can be detected in principle glutamatergic cells, GABAergic interneurons, and astrocytes, with low expression in microglia in a healthy state[46]. ABHD6 CNS expression, along with its role in regulating CB_1R dependent synaptic plasticity indicate that ABHD6 regulates 2-AG neuromodulation, making it a potential target for enhancing 2-AG signaling. The use of ABHD6 inhibitors in rodent models is evidence of this therapeutic strategy.

ABHD6 inhibitors have demonstrated efficacy in various preclinical disease models and indicate that ABHD6 is involved in multiple pathophysiological processes. ABHD6's role in regulating neuronal activity is apparent in models of epilepsy, a condition characterized by aberrant neuronal firing in the brain[57]. ABHD6 inhibition decreases

seizure incidence and severity in multiple mouse models, including in pentylenetetrazole induced seizures and in the R6/2 mouse model of juvenile Huntington's which have spontaneous seizures[48]. ABHD6 inhibition and its heterozygous expression also decreased seizure incidence and duration of thermally induced seizures in $Scn1a^{+/-}$ mice, which are a model of Dravet syndrome[49]. Different ABHD6 inhibitors have also been efficacious in mouse models of diseases associated with neuro-inflammation, including traumatic brain injury, multiple sclerosis, and inflammatory pain[53,58]. In all preclinical studies published thus far, a couple common issues are present: 1] many of these results are reliant on ABHD6 inhibitors which can have limited selectivity; 2] the mechanism of action of ABHD6 inhibition is not yet clear since there is little evidence that ABHD6 inhibition in these disease models affects 2-AG levels. Addressing these questions requires a combination of novel classes of ABHD6 inhibitors with improved selectivity and new tools that allow for the measurement of 2-AG levels in intact cells and tissues at a cellular level.

Mass Spectrometry-based methods of measuring eCBs

Analyzing tissue eCB levels is not a trivial task since they are lipids, which are a diverse group of hydrophobic macromolecules with a wide range of functions in the cell, ranging from maintaining membrane integrity to intracellular signaling[59]. This means that eCBs and other ABHD6 substrates are a minority of all the lipids present in our tissues. To account for this complex lipid environment and relative low abundance of the eCBs, the most common technique for quantifying the eCBs entail several key steps: 1] lipid extraction along with optional enrichment/purification, 2] chromatographic separation, and 3] a detection method such as mass spectrometry[13]. This multi-step process allows for

specific and sensitive detection of many lipids, but each step has its drawbacks that can limit the efficiency and accuracy of the technique. Fully capturing both the advantages and disadvantages of mass spectrometry-based methods requires dissecting the rationale and general methodology for each of these steps.

The first step is lipid extraction and involves isolating the lipids from complex biological matrices, such as cells or tissues. Lipid extraction removes cellular components such as proteins, carbohydrates, and other metabolites that might interfere with detection in later steps[60]. Well-described methods of lipid extraction include the Folch extraction or the Bligh and Dyer extraction, both of which use a mixture of a polar and water immiscible non-polar solvent, such as methanol and chloroform, respectively, to separate the aqueous and hydrophobic components of the cell[13]. Other extraction methods, such as a single solvent protein precipitation by acetonitrile, can also be effective[61]. Once the lipids are extracted, further optional purification and enrichment steps can be taken to enrich the eCB content since the eCBs are a small proportion of the total lipid content. The two most common methods of eCB enrichment are thin layer chromatography (TLC) and solid phase extraction. TLC consists of spotting the extracted lipids onto a silica plate, which is then developed using a combination of organic solvents to separate the lipids[62]. The lipids of interest can then be scraped off and re-extracted with an organic solvent before proceeded to detection. Similar to TLC, solid phase extraction can also be used to purify and enrich the sample by separating the eCBs from contaminants, and can be performed in normal phase (using a polar silica stationary phase) or reverse phase (with a non-polar C8 or C18 stationary phase)[63]. The sample is loaded onto the stationary phase, and

different combinations of solvents of varying polarity can be used to purify the eCBs[64]. Solid phase extraction and TLC can also be used in tandem.

Following extraction and optional enrichment, the samples can undergo chromatographic separation followed by detection using mass spectrometry. eCBs were identified using gas chromatography-mass spectrometry (GC-MS), although liquid chromatography-mass spectrometry (LC-MS) has become more common in recent years. GC can only separate volatile compounds, and while native AEA and 2-AG have been detected using GC-MS, a derivatization step can enhance the stability and volatility of the analytes, increasing the sensitivity of the method[63-65]. LC, which is most commonly done with a reverse phase C18 column, does not require analytes to be volatile and can separate native lipids without derivatization, making it increasingly popular for detecting eCBs[65]. Despite this difference, both GC and LC allow for the separation of structurally similar lipids. For instance, 2-AG and its isomer 1-AG have identical molecular weights, and therefore same mass-to-charge ratio when detected by mass spectrometry, but they have different retention times during the chromatography step, allowing for the differentiation of both lipid species from a single sample[18,66].

Chromatographic separation is then coupled to mass spectrometry to measure eCBs. Mass spectrometry is a highly sensitive detection method that quantifies eCBs using their mass-to-charge ratio (m/z). There are multiple mass spectrometry-based methods for quantifying eCBs, with a popular method for detecting 2-AG utilizing electrospray ionization in positive or negative mode, depending on the lipid, coupled to a quadrupole mass analyzer in single or selective reaction monitoring modes.

The two major advantages of using mass spectrometry to quantify eCBs is that it is sensitive and it can identify specific lipids simultaneously using their m/z and retention times. However, several limitations can affect the accuracy, interpretation, and utility of mass spectrometry. A major disadvantage is the low spatial resolution of mass-spectrometry-based analysis. Mass spectrometry is often preceded by lipid extraction, which requires homogenization of bulk tissue or cells. This processing step disrupts the spatial organization of the tissue at a subcellular level and making it difficult to determine which cells or cell compartments contribute to the eCB levels. Spatial resolution can be increased with techniques like MALDI-IM-MS and MALDI-MIS, which can detect changes in specific brain regions that would be difficult to isolate through dissection[67-69]. However, these techniques are often employed in samples that require tissue processing, such as brain slices. MALDI-based techniques, and mass spectrometry-based analysis in general, is also not suitable for detecting fast or transient changes. This can be somewhat overcome with microdialysis, which combines the spatial specificity of MALDI-MSI by sampling the interstitial fluid from a discrete brain region in an awake, freely behaving animal, with the sensitivity of LC-MS/MS[13]. This method does not rely on processing of bulk tissue; however, it only detects eCBs that are released into the extracellular space, which does not account for intracellular or plasma membrane associated eCBs.

Another limitation is linked to quantifying eCBs in the brain following decapitation since the ischemic conditions can increase the levels of AEA and 2-AG, although there are conflicting results as to how quickly this increase occurs[13]. There is also a potential of sample loss. This sample loss can take many forms, including lipids sticking to plastic, undergoing non-enzymatic acyl migration or peroxidation, and enzymatic degradation

during processing, all of which are also sensitive to the specific extraction method and may account for issues with reproducibility[65].

Thus, mass-spectrometry-based analytical methods for quantifying eCBs in complex biological matrices has traditionally involves multiple processing steps to achieve a highly sensitive method able to detect multiple lipids from single sample. However, these methods often cannot capture time-resolved/localized changes in eCBs.

Methods for Measuring ABHD6 Activity

Mass spectrometry-based methods are useful in studying multiple aspects of 2-AG signaling ranging from the mechanism of synthesis and degradation to the changes in 2-AG levels that occur in diseases states. However, ABHD6 is estimated to account for about 5% of brain 2-AG hydrolysis, and mass spectrometry might not capture the effects of ABHD6 inhibition. Therefore, several methods have been developed specifically to interrogate the function of 2-AG hydrolyzing enzymes like ABHD6. These techniques can be separated into two groups: 1] activity-based protein profiling, and 2] in vitro fluorescent assays.

Activity-based protein profiling (ABPP) is a way to measure enzyme active that relies on a small-molecule probe consisting of: 1] a warhead, which is the reactive group that covalently modifies the active site of the enzyme; 2] a reporter, such as a fluorophore or biotin, which allows for detection or further biochemical processing; and 3] a linker to join the reactive group and reporter together[70]. Depending on the reporter, various read-outs can be employed to quantify enzyme activity. A fluorescent reporter can be used with gel-electrophoresis and in-gel fluorescence detection as well as in microscopy, while

biotin-labeled enzymes can undergo streptavidin enrichment and be detected using mass spectrometry[71].

ABPP probes are essentially irreversible inhibitors and covalently modify the Ser148 in the active site of ABHD6 only when this active site is accessible, thereby measuring the functional state of the enzyme[71]. Aside from ABHD6, ABPP probes can also target multiple enzymes of a similar class, with the selectivity varying from probe to probe[72]. The labeled enzymes can then be resolved using gel-electrophoresis or mass spectrometry. Therefore, in a complex model system, such as brain tissue, ABPP probes can detect the activity of multiple serine hydrolases simultaneously[73]. ABPP has allowed for: 1] identification of new drug targets due to broad-spectrum probe activity; 2] discovery of drugs that inhibit enzyme activity, since inhibition decreases probe engagement with the enzyme; and 3] determining drug selectivity since multiple off-target enzyme activities can be detected in the same experiment.

ABHD6 activity can also be measured in vitro using substrate-based fluorescent assays. Since ABHD6 hydrolysis of 2-AG produces glycerol and arachidonic acid, an enzyme-linked reaction that couples glycerol levels to production of the fluorescent product resorufin can be used to measure ABHD6 activity[51]. Other methods use synthetic substrates such as 4-methylumbelliferyl-heptanoate (4-MUH)[74] and arachidonoyl, 7-hydroxy-6-methoxy-4-methylcoumarin ester (AHMMCE)[75], both of which are fluorogenic substrates. These methods have the advantage of being a high-throughput and time-resolved way to directly measure hydrolysis activity. However, a disadvantage is that these assays are often done in cell or tissue lysate, which prevents the measurement of localized, subcellular changes in ABHD6 activity.

Interrogation of 2-AG Signaling with a genetically encoded fluorescent eCB sensor

Due to its on-demand synthesis and multiple hydrolysis enzymes expressed in neurons, 2-AG signaling is fast and transient. For instance, 2-AG dependent short-term plasticity like DSI/DSE can be detected within seconds after depolarization but recovers in under two minutes. In fact, much of our understanding about cell-specific, time-resolved effects of 2-AG signaling on neuronal activity have come from electrophysiology; however, when it comes to measuring 2-AG, this is an indirect method and relies in pharmacological and genetic tools to identify the mechanism that regulate this signaling. Therefore, overcoming the lack of spatial and temporal resolution inherent in more direct methods of measuring 2-AG and ABHD6 activity, like mass spectrometry, is essential to study the mechanisms underlying regulation of 2-AG and the effects of targeting hydrolyzing enzymes such as ABHD6. The development of a novel, genetically encoded fluorescent sensor, $GRAB_{eCB2.0}$, promises to solve many of these problems since it allows for the measurement of changes in eCBs levels with subcellular and sub-second resolution in multiple model systems.

The $GRAB_{eCB2.0}$ was developed by first incorporating a circularly permutated-green fluorescent protein (cpGFP) into the third intracellular loop of the human CB_1R, then doing a randomized single-mutation screen to optimize the fluorescent-signal change induced by 2-AG[76]. Similar to other genetically encoded sensors, $GRAB_{eCB2.0}$ couples the conformational change of the CB_1R following the binding of a ligand to the conformation-dependent cpGFP. In other words, in the absence of a CB_1R agonist, the sensor has a conformation that elicits a low level of fluorescent signal. Upon binding to a CB_1R agonist, $GRAB_{eCB2.0}$ adopts a confirmation that stabilizes a cpEGFP conformation that elicits an

increased fluorescent signal. This increase in fluorescent signal can be elicited by multiple CB_1R agonists, including 2-AG, AEA, THC, and the synthetic cannabinoids CP55940 and WIN55212-2. Importantly, $GRAB_{eCB2.0}$ does not couple to intracellular signaling pathways, including G-proteins and β-arrestin, and does not appear to affect the coupling of the native CB_1R when expressed in the same cell. The $GRAB_{eCB2.0}$, has been tested in cells in culture, brain slices, and freely behaving animals and can detect exogenous application of cannabinoids and endogenous eCB production[77-79]. However, the in vivo application and interpretation of this sensor requires a more extensive characterization of $GRAB_{eCB2.0}$'s selectivity since it can be activated by multiple ligands. Furthermore, $GRAB_{eCB2.0}$ has not yet been used to study the molecular mechanisms regulating 2-AG signaling, such as the intracellular signal transduction pathways that are involved in 2-AG biosynthesis.

For my thesis work, I have characterized the pharmacological properties of the $GRAB_{eCB2.0}$ in HEK293 by testing the direct activation of the sensor by different classes of CB_1R targeting ligands, including eCBs, eCB analogs, phyto-cannabinoids, synthetic cannabinoids, and antagonists to determine selectivity of the sensor. I determined that the selectivity of the $GRAB_{eCB2.0}$ for detecting endogenous ligands extends beyond eCBs since it can be activated by other lipids found in the brain, including 2-OG and 2-LG, which indicates the need for pharmacological and genetic controls when using the $GRAB_{eCB2.0}$ in vivo. Next, I demonstrated that the $GRAB_{eCB2.0}$ can be used to interrogate mechanisms of 2-AG biosynthesis by elucidating the mechanism of 2-AG production in a neuronal model when stimulated with inflammatory mediators ATP and bradykinin. These inflammatory mediators are associated with hyperalgesia and neuropathic pain by acting

as peripheral sensitizers of sensory neurons, and they are known to stimulate 2-AG levels in neurons in culture. However, until now the mechanism of this neuronal 2-AG production, and thus the role 2-AG plays, has remained unclear. Here we show that ATP and bradykinin stimulate 2-AG production through ionotropic and metabotropic receptor-dependent mechanisms, respectively, and this 2-AG can act in an autocrine fashion, and can be released, allowing for paracrine activation at target proteins. Comparing the effects of ATP and bradykinin on 2-AG levels using LC-MS/MS and $GRAB_{eCB2.0}$ revealed that the two methods likely detect different pools of 2-AG and confirmed that the sensor has an increased spatiotemporal resolution, allowing it to detect changes in 2-AG levels not evident with mass spectrometry. Finally, testing the $GRAB_{eCB2.0}$ in two distinct mammalian cell models has also revealed cell-specific difference in $GRAB_{eCB2.0}$ function, specifically the potency and efficacy of direct-sensor activation by exogenous cannabinoids, indicating the need for validation of the $GRAB_{eCB2.0}$ prior to use in new cellular model systems. Having used the $GRAB_{eCB2.0}$ sensor to describe the mechanism of ATP- and bradykinin-stimulated 2-AG production, we tested whether $GRAB_{eCB2.0}$ could be used to study the mechanism underlying 2-AG hydrolysis. Thus, we measured changes in stimulated-2-AG levels in neuro2a cells following inhibition of ABHD6, which is endogenously expressed in neuro2a cells. Despite evidence that $GRAB_{eCB2.0}$ can detect changes in eCB hydrolysis of exogenous and endogenous eCBs, ABHD6 inhibition did not enhance stimulated 2-AG production. Therefore, we hypothesized that ABHD6 activity may be differentially regulated in a cell- or stimuli-specific manner. Thus, we revealed a novel regulatory mechanism by which ABHD6 activity is positively regulated by a membrane -enhancing factor. Furthermore, we show the initial target validation of a first-

in-class ABHD6 inhibitor that is designed to reversibly induce targeted proteasomal degradation of ABHD6, thereby reducing its hydrolysis-dependent and -independent activity.

Summary

I developed and validated a method for studying eCB signaling and identified the molecular mechanism of neuronal 2-AG production by two different inflammatory mediators: ATP and bradykinin. I also identified a novel mechanism regulating the activity of the 2-AG hydrolyzing enzyme ABHD6. This mechanism, which consists of a membrane-associated enhancing factor that is yet to be identified, brings us one step closer to elucidating how ABHD6 works so we can better understand its role in the body during both healthy and pathological states. ABHD6 is a potential therapeutic target to enhance 2-AG signaling for the treatment neurological disorders such as epilepsy and neuropathic pain. This work expands our understanding of how 2-AG signaling is regulated and the function of ABHD6, which can help us develop safe and selective inhibitors with clinical efficacy.

Chapter 2.

Pharmacological characterization of the endocannabinoid sensor GRAB$_{eCB2.0}$

2.1 INTRODUCTION

Many physiological functions and behaviors are differentially controlled by endogenously produced AEA and 2-AG that activate CB_1R.[14] Specifically, AEA or 2-AG production by select cells will partially or fully activate CB_1Rs ($EC_{50}s$: ≈10-100 nM and 30-300 nM, respectively) in an autocrine and paracrine fashion.[12] The effects of CB_1R activation are dependent on both cell type and coupling to intracellular signaling systems: CB_1R are expressed at remarkably different levels by distinct excitatory and inhibitory neurons and by glial cells where they couple to specific signaling pathways. Thus, cell-specific, differential activation of CB_1Rs by AEA and 2-AG in the brain fine-tunes excitatory and inhibitory neurotransmission and neuromodulation, and regulates neuronal metabolism and phenotype.[80,81] This fundamental signaling mechanism is modulated by Δ^9-THC via its binding to the orthosteric binding site of CB_1R where it acts as a partial agonist. For example, free CB_1Rs expressed throughout the brain are partially activated by THC, whereas CB_1R signaling stimulated by localized activity-dependent increases in 2-AG may be inhibited by THC.[82-85] CB_1R signaling is also modulated by cannabidiol (**CBD**) that interacts with a putative allosteric binding site on CB_1R.[86] Multiple lines of evidence suggest that CBD acts as a NAM of CB_1R, although its direct binding to CB_1R has still not been demonstrated.[87,88] Thus, CBD reduces 2-AG-stimulated CB_1R activity without influencing basal/tonic CB_1R signaling. This premise emphasizes a need to better

understand the role of endogenously produced AEA and 2-AG, their dynamics, and how the presence of THC and CBD affects their activation of the CB_1R.

Mass spectrometry has demonstrated that 2-AG is 10-1000 times more abundant than AEA in select cell types and tissues; however, little is known about the activity-dependent and spatio-temporal changes of 2-AG and AEA that occur within seconds.[14,65] Importantly, increased cellular activity not only enhances the production of AEA and 2-AG but also enhances the production of lipid analogues synthesized by the same enzymatic pathways. For example, 2-LG and 2-OG activate CB_1R yet with lower potency and efficacy than 2-AG.[89-91] Thus, localized activity-dependent increases in eCBs and their analogues will differentially activate CB_1R within seconds. The recent development of genetically encoded fluorescent sensors has enabled the real-time detection of changes in the levels of neurotransmitters and neuromodulators in live tissues.[92] This technology leverages the selective binding of endogenous agonists to specific receptors that stabilize their conformation. For example, the $GRAB_{eCB2.0}$ sensor was recently engineered starting from hCB_1R by introducing a circularly permutated-green fluorescent protein (**cpGFP**) in its third intracellular loop.[93,94] Thus, $GRAB_{eCB2.0}$ was developed by screening for constructs with functional insertion sites of cpGFP, followed by individual randomized mutations of amino acids that increased the fluorescent signal in response to 2-AG specifically.[95] Several laboratories reported that $GRAB_{eCB2.0}$ signal increases within seconds when exogenously applying 2-AG or AEA to cells in culture, as well as when endogenously stimulating eCB production in cells in culture, mouse brain slices, and behaving animals.[79,93,96,97]

In the current study, we measured $GRAB_{eCB2.0}$ signal in HEK293 cells in culture using live cell fluorescence microscopy and a high-throughput fluorescence plate reader assay. We found that 2-AG and SR1 formulated in buffer containing bovine serum albumin (**BSA**), a lipid binding protein known to assist eCB's activation of CB_1R, modulate $GRAB_{eCB2.0}$ fluorescent signal in HEK293 cells with potencies that closely mirror their reported activities at CB_1R.[93,98] Thus, we leveraged this experimental approach to characterize the pharmacological profile of eCB analogues and phyto-CBs at $GRAB_{eCB2.0}$.

2.2 RESULTS

Real-time activation and antagonism of $GRAB_{eCB2.0}$ fluorescent signals in HEK293 cells in culture: Live cell microscopy.

HEK293 cells in culture were transfected with *eCB2.0* DNA plasmid constructs containing the chimeric cytomegalovirus-chicken β-actin promoter to drive expression.[99-103] $GRAB_{eCB2.0}$ expression was confirmed by western blot using a goat polyclonal antibody developed against C-terminal amino acids of CB_1R that remained unchanged in $GRAB_{eCB2.0}$ (**Figure 1A** and Supplementary Figure S2.1 for amino acid sequence alignment).[93] Fluorescence confocal microscopy analysis of $GRAB_{eCB2.0}$ expression in fixed HEK293 cells using the CB_1R antibody showed abundant expression in many cells, consistent with transient transfection approaches (**Figure 1B**).

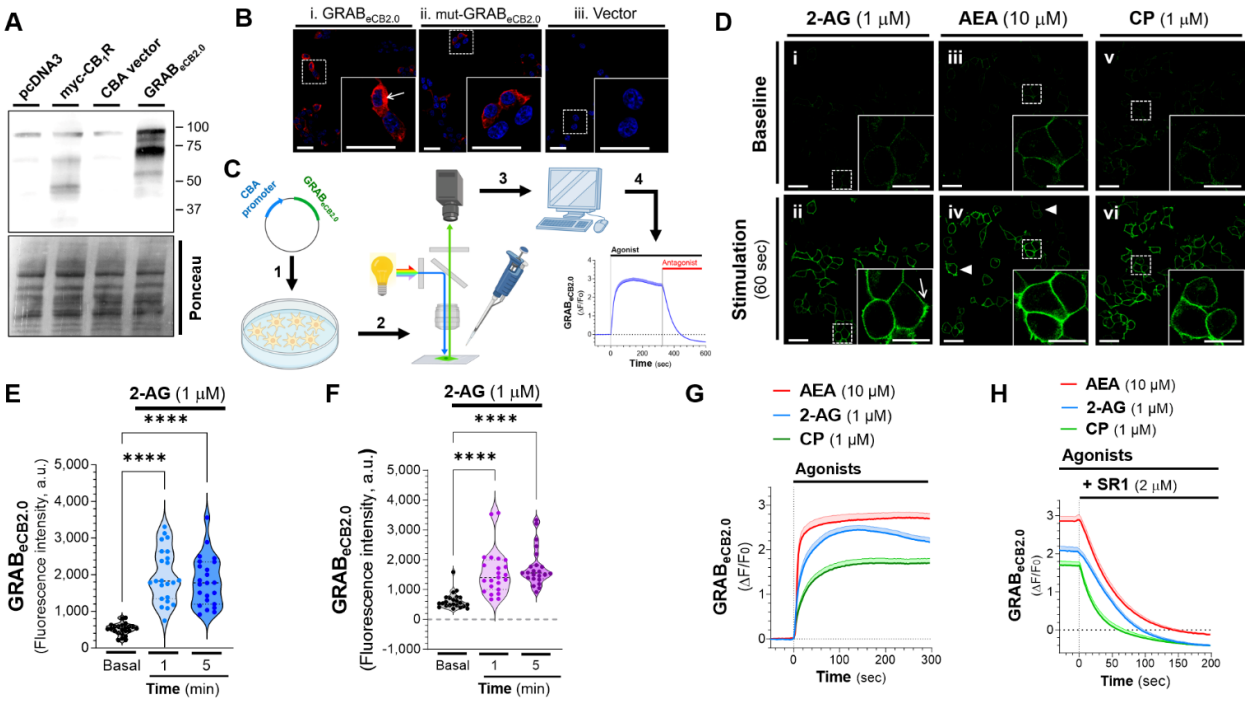

Figure 2.1: Agonist triggered changes in $GRAB_{eCB2.0}$ fluorescent signal in HEK293 cells detected by live-cell confocal microscopy. HEK293 cells were transfected with *eCB2.0* DNA plasmid and $GRAB_{eCB2.0}$ expression was measured by western blot and ICC, and changes in fluorescent signal measured by live-cell confocal microscopy when treated with the CB_1R agonists 2-arachidonoyl glycerol (**2-AG**), arachidonoyl ethanolamine (**AEA**), or CP55940 (**CP**). **A]** Detection of $GRAB_{eCB2.0}$ expression by western blot using lysates from HEK293 cells transfected with pcDNA3, myc-CB_1R (positive control), CBA plasmid, or $GRAB_{eCB2.0}$. Both CB_1R and $GRAB_{eCB2.0}$ were detected using an antibody against the CB_1R. Loading control: Ponceau stain. **B]** Detection of $GRAB_{eCB2.0}$ (i) or mut-GRABeCB2.0 (ii) expression by ICC of fixed and permeabilized HEK293 cells transfected with *eCB2.0* DNA plasmid (i), mut-*eCB2.0* DNA plasmid (ii), or CBA plasmid (iii). Scale bar = 20 μm (inset scale bar = 20 μm). **C]** Schematic of live cell confocal imaging of HEK293 cells: cells were transfected with *eCB2.0* DNA plasmid (1); 24 h later, cell growth media was exchanged for imaging PBS buffer and cells were placed on a confocal microscope (2); changes in $GRAB_{eCB2.0}$ fluorescent signal was determined by measuring fluorescent signal during baseline, spiking in treatments formulated with BSA (0.1%, 10X), and lastly spiking in SR141716 (**SR1**; 3 and 4). **D]** Live cell images of $GRAB_{eCB2.0}$-expressing HEK293 cells during baseline recording (i, iii, and v) and after 60 sec of treatment with 2-AG (1 μM, ii), AEA (10 μM, iv), or CP (1 μM, vi). Arrows indicate cells with different levels of fluorescent signal to show heterogeneous expression of $GRAB_{eCB2.0}$. Scale bars = 20 μm. **E]** Time courses of $GRAB_{eCB2.0}$ activation ($\Delta F/F_0$) following treatment with 2-AG (1 μM), AEA (10 μM), and CP (1 μM) as measured by live-cell confocal microscopy. **F]** Effect of SR1 (2 μM) on agonist-stimulated increase in $GRAB_{eCB2.0}$ fluorescent signal. Shaded area represents s.e.m. n= 42-66 cells from 3-5 independent experiments.

We used live-cell confocal microscopy (line scanning frequency: 200 Hz) to establish the time-course of changes in the dynamics of $GRAB_{eCB2.0}$ signal in response to 2-AG (the ligand used to develop this sensor) by adding a 10X concentration formulated in BSA directly into PBS buffer inside the imaging chamber (**Figure 1C**). **Figure 1D$_{i-ii}$** show that HEK293 cells exhibited low, yet clearly detectable basal fluorescent signal at the plasma membrane (treated with vehicle control, DMSO 0.1%); and that 2-AG (1 μM, 60 sec) increased this signal. Similarly, AEA (10 μM, 60 sec) and the potent, artificial CB_1R agonist CP (1 μM, 60 sec) increased $GRAB_{eCB2.0}$ signal at the plasma membrane (**Figure 1D$_{iii-iv}$**). Of note, both basal fluorescent signal and all agonist-triggered increases in $GRAB_{eCB2.0}$ signal reached different levels in HEK293 cells as expected by heterologous expression (for example, see **Figure 1D$_{iv}$** arrowheads).

It is important to note that significant levels of the $GRAB_{eCB2.0}$ protein were also present in the intracellular compartment of ≈70% of the HEK293 cells (see arrow in **Figure 1B,** insert and Supplementary Figure S2.2A-B). In these cells, 2-AG (1 μM) significantly increased the intracellular fluorescent signal; however, unlike the increase in the plasma membrane fluorescent signal, the intracellular signal was increased to a lesser extent (e.g., ≈124% increase in peak fluorescent signal after 5 min of treatment compared to 255% increase of the peak signal at the plasma membrane in the same cells; see arrow in **Figure 1E-F** and Supplementary Figure S2.2E). Furthermore, maximal increases in intracellular fluorescent signal occurred after ≈5 min of treatment, compared to the plasma membrane signal which peaked within 1-2 min (see arrow in **Figure 1E-F**). This delay may be a result of the time it takes 2-AG to travel to these intracellular compartments. Similarly, CP induced increases in both the plasma membrane and intracellular

fluorescent signal (≈180% and 110% increase in peak fluorescent signal, respectively, after 5 min treatment) (Supplementary Figure S2.2C, D, and F), indicating that activation of intracellular $GRAB_{eCB2.0}$ signal is likely not ligand selective. This indicates that activation of intracellular $GRAB_{eCB2.0}$ signal is likely not ligand selective specific and despite having a smaller activation and differing kinetics than the plasma membrane signal, it is detectable and has the potential be relevant for studying intracellular eCB signaling.[104]

Analysis of the time course of the increase in $GRAB_{eCB2.0}$ signal ($\Delta F/F_0$) at the plasma membrane triggered by these agonists indicated that each agonist increased $GRAB_{eCB2.0}$ signal within seconds and that these responses plateaued after approximately 60 sec (**Figure 1G**). **Figure 1H** shows that the CB_1R antagonist, SR1 (2 μM), reduced these responses within 100 sec, and this reduction reached levels below basal. Calculation of the onset of activation (i.e., slope of the fluorescent signal increase within the first 20 sec after start of treatment), the magnitude of the response (i.e., peak fluorescent signal and area under the curve), and the decay following SR1 treatment (i.e., τ value following start of SR1 treatment) showed that each agonist had significantly different pharmacological profiles at $GRAB_{eCB2.0}$ (**Table 1**). Specifically, 1] AEA triggered a 1.7- and 2.2-fold faster initial response compared to 2-AG and CP respectively, 2] 2-AG and AEA reached similar peak responses, and these were 47-58% greater than the CP maximal response, 3] 2-AG and AEA triggered a 1.4-1.6-fold overall greater response (area under the curve) compared to CP and 4] SR1 antagonized the CP and AEA responses with faster decay than the 2-AG response (24 sec < 37 sec < 43 sec, respectively). Together, these results

indicate that $GRAB_{eCB2.0}$ expressed by HEK293 cells are activated by the CB_1R agonists 2-AG ≈ AEA > CP, and these responses are differentially antagonized by SR1.

		CB_1R agonists		
PD parameter	**Units**	**2-AG**	**CP**	**AEA**
Initial response: slope	(x 10^{-2} $\Delta F/F_0$/sec)	6.6	4.5	10.9
Maximal response: peak	($\Delta F/F_0$)	2.5	1.7	2.7
Overall response	(area under the curve)	649	453	760
Antagonism response: τ	(sec)	42.7	24.3	36.8

Table 1: Parameters of $GRAB_{eCB2.0}$ activation and antagonism. Live cell images of $GRAB_{eCB2.0}$-expressing HEK293 cells treated with 2-AG (1 µM), AEA (10 µM), or CP (1 µM), followed by SR1 (2 µM) on agonist-stimulated increase in $GRAB_{eCB2.0}$ fluorescent signal. Calculation of the activation onset (i.e., the slope of the fluorescent signal increase within the first 20 sec after start of agonist treatment), the magnitude of the response (i.e., peak response and area under the curve), and the decay following SR1 treatment (i.e., τ value following treatment). Analysis of data presented in Figure 1, n= 42-66 cells from 3-5 independent experiments.

High-throughput measures of $GRAB_{eCB2.0}$ fluorescent signal in HEK293 cells in culture.

To further define the pharmacological profile and dynamics of $GRAB_{eCB2.0}$ signal, we developed and validated a fluorescent plate reader assay (96 wells, 3 Hz scanning frequency) (**Figure 2A**). **Figures 2B-C** show that 2-AG and AEA induced concentration-dependent increases in $GRAB_{eCB2.0}$ signals that were detected at the 0 sec timepoint (i.e., when the first Stimulation fluorescent signal was measured). For example, both the 10 nM and 100 nM 2-AG responses at 0 sec reached a $GRAB_{eCB2.0}$ signals value of 0.19 and 0.96 $\Delta F/F_0$ over basal, respectively; and both these responses reached an initial inflection point at 0.66 and 0.33 min, respectively (**Figures 2B**, see color coded arrows). Of note, 2-AG at 3 µM induced the strongest response that reached an inflection point at ≈0.66

min, whereas 2-AG at 10 μM induced a response had already reached a maximum plateau response at the 0 min timepoint (**Figures 2B**). Thus, 2-AG rapidly activated $GRAB_{eCB2.0}$ in a concentration dependent manner as calculated by its initial response (i.e., slope: $\Delta\Delta F/F_0$ between 0 min and the initial inflection time point) (**Figures 2D**). To calculate EC_{50} values, we averaged the $GRAB_{eCB2.0}$ signals between 4-5 min, and found 85 nM for 2-AG, a value that is consistent with its reported potency at CB_1R (e.g., EC_{50} = 12-100 nM for inhibiting cAMP production) (**Figures 2E**).[105,106] AEA also induced a concentration-dependent and rapid increase in $GRAB_{eCB2.0}$ signal that was detected at the 0 sec timepoint, but only reached a significant initial response starting at 30 nM, and a maximum plateau response at 10 μM (**Figures 2C-D**). Thus, AEA induced a concentration-dependent increase in $GRAB_{eCB2.0}$ with an EC_{50} = 815 nM, an activity that is approximately 10-fold less potent than AEA's potency at CB_1R (e.g., EC_{50} = 69 nM for inhibiting cAMP production) (**Figures 2E**).[106-108]

To further characterize these high-throughput measures, we tested the effect of CP and SR1 on $GRAB_{eCB2.0}$ signal. **Figures 2F** shows that CP induced a concentration-dependent increase in $GRAB_{eCB2.0}$ signal that was detected at 0 sec and reached an initial inflection time point within ≈1.33 min and an EC_{50} = 82 nM, which is less potent than CP's potency at CB_1R (e.g., EC_{50} = 1-3 nM as determined by inhibition of cAMP production) (**Figures 2D-E**).[109-111] As expected, SR1 induced a rapid and concentration-dependent decrease in $GRAB_{eCB2.0}$ signal that was first detected at 0 sec and reached a plateau below basal levels starting at 30 nM for at least 5 min (**Figures 2G**). The IC_{50} for SR1 measured between 4-5 min was 3.3 nM, a value that mirrors SR1's potency at CB_1R (IC_{50} = 5.6-7.8 nM as determined by SR1's inhibition of CP-induced decrease of cAMP levels)

(**Figures 2E**).[109,111-113] Pre-treatment of HEK293 cells with SR1 (300 nM, 20 min) followed by treatment with 2-AG, AEA and CP significantly reduced $GRAB_{eCB2.0}$ activation (**Figures 2H**). **Figure 2H** also shows that 2-AG, AEA and CP failed to elicit increases in fluorescent signals in HEK293 cell expressing the mut-$GRAB_{eCB2.0}$, which has a similar expression profile as $GRAB_{eCB2.0}$ as determined by fluorescence confocal microscopy (**Figure 1B**). Thus, mut-$GRAB_{eCB2.0,}$ which has a phenylalanine 177 to alanine mutation in the region within the orthosteric binding pocket to impair ligand binding, represents a valid negative control.[114,115] As previously reported, the products of 2-AG hydrolysis, arachidonic acid, and glycerol, did not influence the $GRAB_{eCB2.0}$ signal (**Figure 2I**).[93] Together, these results provide strong support for use of this high throughput experimental approach to study the pharmacology and dynamics of changes in $GRAB_{eCB2.0}$ fluorescence when expressed by cells in culture, and show that: 1] Pronounced increases and decreases in $GRAB_{eCB2.0}$ signal are reproducibly detected using a 96 well plate-reader format and promptly spiking agents in media, 2] 2-AG and SR1 modulate $GRAB_{eCB2.0}$ signal with EC_{50}s comparable to their potencies at the CB_1R, and 3] AEA and CP also increase $GRAB_{eCB2.0}$ signal, although with 2-10-fold lower potency than at CB_1R.

The EC_{50} values of 2-AG and AEA for $GRAB_{eCB2.0}$ activation measured here are lower than their previously reported values in cell culture model systems (i.e., 2-AG = 3.1-9.0 μM and AEA = 0.3-0.8 μM), which is likely due to our inclusion of BSA in the buffer to facilitate solubility and interaction with $GRAB_{eCB2.0}$.[93,116] To confirm the effect of BSA on $GRAB_{eCB2.0}$ sensitivity to 2-AG, we tested how BSA affected the 2-AG-induced increase in $GRAB_{eCB2.0}$ signal. **Figure 3A-D** shows that increasing concentrations of BSA alone

did not influence baseline $GRAB_{eCB2.0}$ signal, yet BSA (0.1 mg/ml) increased the 2-AG (10 nM and 100 nM) responses by 7.3- and 4-fold, respectively, when measured 10 min following treatment. BSA (0.1 mg/ml) had a lesser effect on the 1 μM and 10 μM 2-AG-induced increase in $GRAB_{eCB2.0}$ signal, enhancing the $\Delta F/F_0$ by 5% and 7% after 10 min treatment, respectively; likely because these are close to saturating concentrations at $GRAB_{eCB2.0}$ (**Figure 3C-D**). This confirms that BSA increases the 2-AG's availability at the $GRAB_{eCB2.0}$ sensor and its ability to detect mid-to-low nanomolar concentrations of 2-AG.

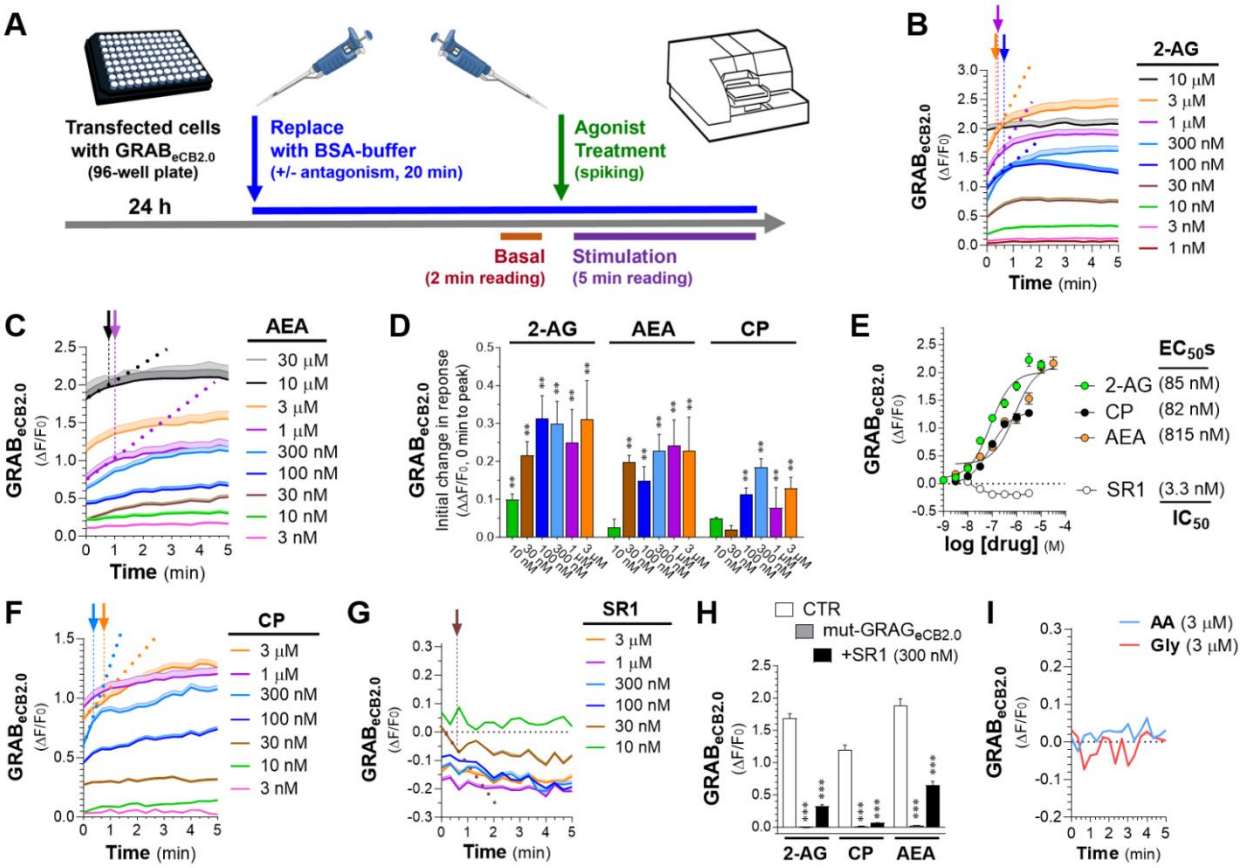

Figure 2.2: A] Schematic of high-throughput fluorescent plate reader assay: HEK293 cells were plated in a 96-well plate and transfected with *eCB2.0* DNA plasmid; 24 h post transfection, growth media was replaced with imaging PBS buffer and incubated for 20 min. For the last 2 min of this incubation, the plate was placed in the fluorescent plate reader and a basal fluorescent signal was measured. Treatments were added immediately after the basal reading and the pate was reinserted in the plate reader and fluorescent signal was recorded for 5 min. **B, C, F, G** and **I]** Kinetics of GRAB$_{eCB2.0}$ activation ($\Delta F/F_0$) following treatment with increasing concentrations of 2-AG (B), AEA (C), CP (F), SR1 (G) and arachidonic acid (**AA**) and glycerol (**Gly**) (I). Arrows represent inflection points and dotted lines represent initial change in response (slope between t=0 and time at inflection). **D]** Initial change in $\Delta F/F_0$ response elicited by increasing concentration of 2-AG, AEA, or CP shown in (B, C, and F). **E]** Concentration dependent responses and EC$_{50}$s of 2-AG, AEA, and CP at inducing GRAB$_{eCB2.0}$ fluorescent signal and of SR1 at reducing GRAB$_{eCB2.0}$ fluorescent signal as determined by averaging $\Delta F/F_0$ between 4-5 min. **H]** 2-AG (1 μM), CP (1 μM), and AEA (10 μM)-induced increases in GRAB$_{eCB2.0}$ fluorescent signal was reduced by SR1 (300 nM) and absent in HEK293 cells expressing mut-GRAB$_{eCB2.0}$. Data represents mean $\Delta F/F_0$ between 4-5 min. Shaded areas on time-course plots and error bars on histograms represent s.e.m. Statistics: (D) **P<0.01 significantly different from basal (Two-Way ANOVA followed by Dunnett's). (H) ***P<0.001 significantly different from corresponding CTR treatment (Two-way ANOVA followed by Dunnett's). n= 9-50 independent experiments performed in triplicate.

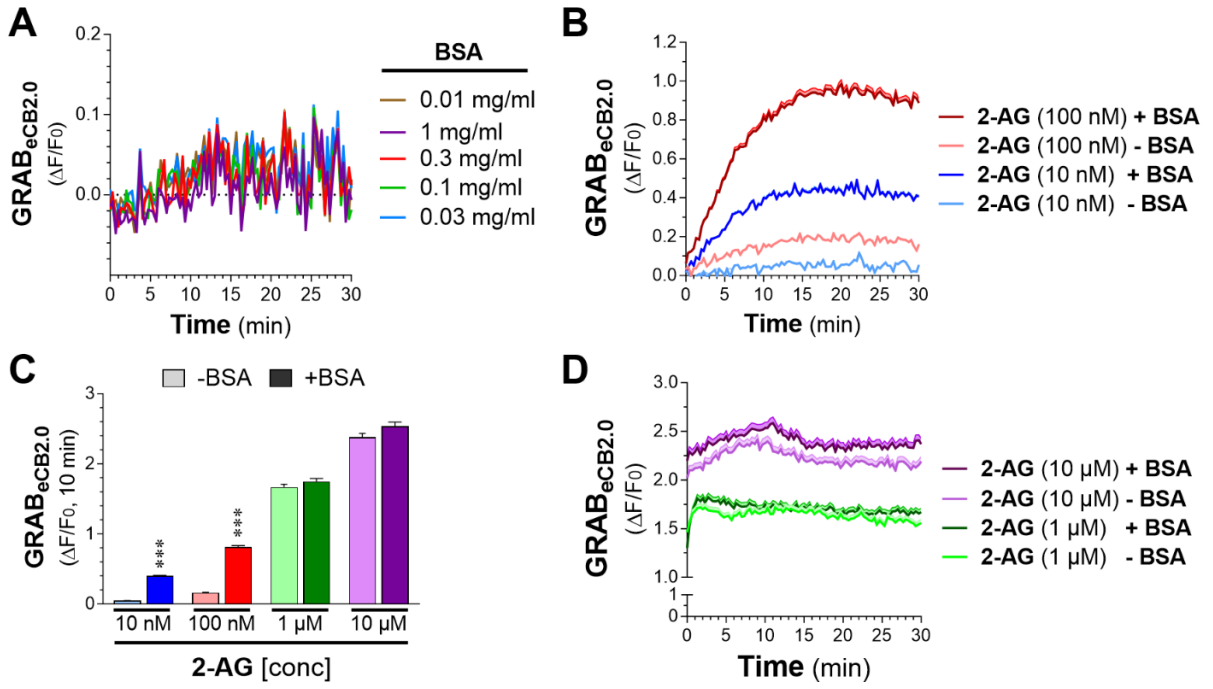

Figure 2.3: BSA Enhances 2-AG-induced activation of $GRAB_{eCB2.0}$. **A]** Effect of increasing concentrations of BSA on $GRAB_{eCB2.0}$ activation ($\Delta F/F_0$). **B and D]** Kinetics of $GRAB_{eCB2.0}$ activation ($\Delta F/F_0$) following treatment with increasing concentrations of 2-AG diluted in PBS alone (-BSA) or in 0.1 mg/ml BSA (+BSA). **C]** Effect of BSA (0.1 mg/ml) on 2-AG-induced increases in $GRAB_{eCB2.0}$ fluorescent signal ($\Delta F/F_0$ after 10 min of treatment). Statistics: ***P<0.001 significantly different (Two-Way ANOVA followed by Sidak's). n= 3 independent experiments. Error bars represent s.e.m.

Pharmacological activity of 2-AG analogues at $GRAB_{eCB2.0}$.

We leveraged the high-throughput approach to determine whether 2-LG and 2-OG, which are produced by cells concomitantly to 2-AG, change $GRAB_{eCB2.0}$ signals when expressed in HEK293 cells.[89,90] Specifically, although 2-LG (18:2) and 2-OG (18:1) are lipid analogues of 2-AG (20:4) and are produced by the same biosynthetic and metabolic pathways as 2-AG, they are likely to activate CB_1R signaling with much lower potency and efficacy than 2-AG. For example, 2-LG partially activates CB_1R (EC_{50}s = 16.6 µM for arrestin recruitment) or antagonizes CB_1R depending on the model system, while there is still no evidence that 2-OG might also activate CB_1R.[89,90] **Figures 4A-B** show that both

2-LG and 2-OG induced a concentration-dependent increase in $GRAB_{eCB2.0}$ signal that was detected at 0 sec and that these responses rapidly reached their initial inflection time points within 1 min. Thus, 2-LG and 2-OG activated $GRAB_{eCB2.0}$ with increasingly rapid onset and EC_{50}s = 0.63 and 0.87 μM, respectively, indicating that 2-LG and 2-OG have higher potency when activating the $GRAB_{eCB2.0}$ sensor compared to their activation of CB_1R (**Figures 4C-D**). We next tested 1-arachidonoylglycerol (**1-AG**, 20:4), which is a product of a non-enzymatic isomerization of 2-AG that is not endogenously produced by mammalian cells, but is commonly used to study the structure activity relationship of monoacylglycerols at CB_1R as its acyl chain length and saturation match that of 2-AG.[66,117,118] We found that 1-AG induced a concentration-dependent increase in $GRAB_{eCB2.0}$ signal that was detected at 0 sec, reached its initial inflection timepoint within 1 min and had an EC_{50} = 1.8 μM, which mirrors its potency at CB_1R (EC_{50} = 1.45 μM for inhibiting cAMP production) (**Figures 4D-E**). The responses to these three monoacylglycerols were blocked by pretreatment with SR1 (300 nM) and absent in cells expressing the mut-$GRAB_{eCB2.0}$ (**Figure 4F**). Thus, 1-AG, 2-LG, and 2-OG increase $GRAB_{eCB2.0}$ signal (rank order of potency: 2-LG > 2-OG > 1-AG; maximum efficacy: 1-AG > 2-LG > 2-OG). Notably, all three lipid analogues had lower potencies than 2-AG and AEA, indicating that the $GRAB_{eCB2.0}$ has greater sensitivity for these two eCBs compared to similar monoacylglycerol lipids.

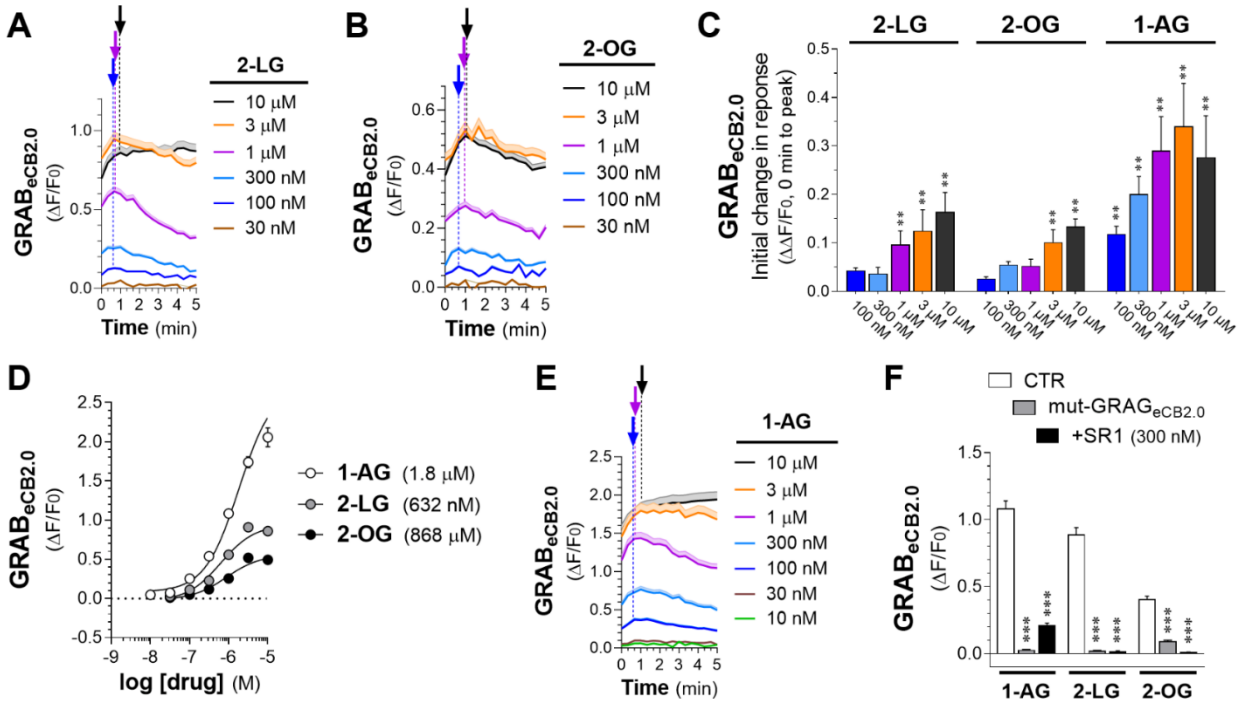

Figure 2.4: 2-LG, 2-OG, and 1-AG activate $GRAB_{eCB2.0}$. HEK293 cells were transfected with *eCB2.0* DNA plasmid and changes in fluorescent signal measured by high-throughput fluorescence assay. **A, B, E]** Kinetics of $GRAB_{eCB2.0}$ activation ($\Delta F/F_0$) following treatment with increasing concentrations of 2-LG (A), 2-OG (B), and 1-AG (E). Shaded areas in time courses and error bars represent s.e.m. Arrows represent inflection points and dotted lines represent initial change in response (slope between t=0 and time at inflection). **C]** Initial response (slope between time = 0 and inflection point) of $\Delta F/F_0$ response. **D]** Concentration dependent responses and EC_{50}s of 2-LG, 2-OG, 1-AG at inducing $GRAB_{eCB2.0}$ fluorescent signal as determined by averaging $\Delta F/F_0$ between 4-5 min. **F]** 2-LG (1 μM), 2-OG (1 μM), and 1-AG (1 μM)-stimulated increases in $GRAB_{eCB2.0}$ fluorescent signal are reduced by SR1 (300 nM) and absent in HEK293 cells expressing mut-$GRAB_{eCB2.0}$. Statistics: (C) **P<0.01 significantly different from basal (Two-way ANOVA followed by Dunnett's). (D) ***P<0.001 significantly different from corresponding CTR treatment (Two-Way ANOVA followed by Dunnett's). n= 3-11 independent experiments performed in triplicate.

Determining THC and CBD's pharmacological activity at $GRAB_{eCB2.0}$.

To extend the pharmacological characterization of $GRAB_{eCB2.0}$ using the high-throughput assay, we tested Δ^9-THC, the principal psychoactive ingredient in *Cannabis* that activates CB_1R as a high-affinity partial agonist,[109] and Δ^8-THC, which activates

CB_1R with a comparable pharmacology as Δ^9-THC but represents a minor product of most *Cannabis* strains and remains poorly characterized.[119] Δ^9-THC increased $GRAB_{eCB2.0}$ signal in a concentration-dependent manner that was detected at 0 sec starting at 1 and 3 μM, and these responses reached their initial inflection points within 1 min (**Figure 5A**). Of note, higher concentrations of Δ^9-THC, i.e., 10 and 30 μM, triggered a response that continuously increased for at least 5 min without apparent inflection (**Figure 5A**). **Figure 5B** shows that Δ^8-THC induced a concentration-dependent increase in $GRAB_{eCB2.0}$ signal that was detected at 0 sec starting at 1 μM, and that all higher concentrations continuously increased for at least 5 min without inflection. Δ^9-THC and Δ^8-THC activate $GRAB_{eCB2.0}$ with comparable EC_{50}s as calculated between 4-5 min (1.6 μM and 2 μM, respectively; **Figure 5C**). These 2 responses were blocked by pretreatment with SR1 (300 nM) and absent in cells expressing the mut-$GRAB_{eCB2.0}$ (**Figure 5D**). Thus, Δ^9-THC and Δ^8-THC similarly increase $GRAB_{eCB2.0}$ signal, although with a 10-100-fold lower potency than their activation of CB_1R, and most of these responses at micromolar concentrations continuously increase for at least 5 min.

CBD acts as a NAM of CB_1R.[87,120] Accordingly, we found that CBD, at up to 3 μM, did not significantly modulate basal $GRAB_{eCB2.0}$ signal but did significantly reduce the 2-AG-induced increase in $GRAB_{eCB2.0}$ signal by 26% at 1 μM and with an IC_{50} = 9.7 nM, values that are similar to CBD's activity at CB_1R (**Figure 5E-G**). Thus, we calculated the Shild plot of this response and found a slop of 0.33, as expected for a NAM (**Figure 5H**). These results indicates that $GRAB_{eCB2.0}$ retains the molecular mechanism that mediates the proposed NAM activity of CBD at CB_1R.

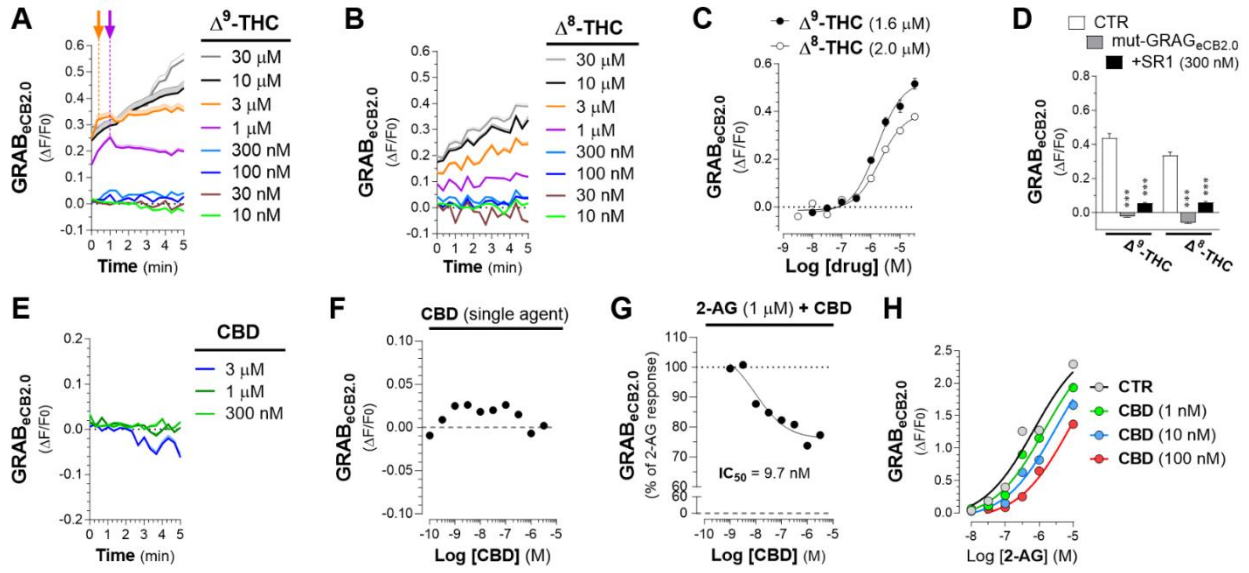

Figure 2.5: Δ^9-THC and Δ^8-THC activate GRAB$_{eCB2.0}$, and CBD act as a negative allosteric modulator. HEK293 cells were transfected with *eCB2.0* DNA plasmid and changes in fluorescent signal measured by high-throughput fluorescence assay. **A-B]** Kinetics of GRAB$_{eCB2.0}$ activation ($\Delta F/F_0$) induced by increasing concentrations of Δ^9-THC (A) or Δ^8-THC (B). Shaded areas in time courses and error bars represent s.e.m. Arrows represent inflection points and dotted lines represent initial change in response (slope between t=0 and time at inflection). **C]** Concentration dependent responses and EC$_{50}$s of Δ^9-THC and Δ^8-THC at inducing GRAB$_{eCB2.0}$ fluorescent signal as determined by averaging $\Delta F/F_0$ between 4-5 min. **D]** Δ^9-THC (10 μM) and Δ^8-THC (10 μM)-stimulated increases in GRAB$_{eCB2.0}$ fluorescent signal are reduced by SR1 (300 nM) and absent in HEK293 cells expressing mut-GRAB$_{eCB2.0}$. **E-F]** CBD (100 pM-10 μM) does not modulate GRAB$_{eCB2.0}$ fluorescent signal (F) and decreased the 2-AG (1 μM)-stimulated increase in GRAB$_{eCB2.0}$ fluorescent signal (IC$_{50}$ of 9.7 nM; G). **H]** Effect of CBD (1, 10, and 100 nM) on 2-AG concentration dependent activation of GRAB$_{eCB2.0}$ ($\Delta F/F_0$). Statistics: (D) ***P<0.001 significantly different from corresponding CTR treatment (Two-way ANOVA followed by Dunnett's). n= 3-7 independent experiments performed in triplicate.

Comparing changes in GRAB$_{eCB2.0}$ fluorescent signals.

We sought to compare key pharmacological and dynamic parameters that characterize changes in GRAB$_{eCB2.0}$ signal elicited by the agents that we tested in this study (chemical structures in Supplementary S2.6A). **Figure 6A** shows GRAB$_{eCB2.0}$ activation by each agonist applied at their EC$_{50}$s results in different GRAB$_{eCB2.0}$ activation

dynamics. Specifically, when analyzing the $\Delta\Delta F/F_0$ of these responses between 3-5 min, we found that the responses induced by monoacylglycerols were decaying between 3-5 min and thus, had reached an earlier maximum response whereas the $GRAB_{eCB2.0}$ signals induced by AEA, CP, and Δ^9-THC continuously increased between 3-5 min and thus had not reached a maximum response within this time-period (**Figure 6B**). Analysis of concentration-responses indicated that 2-AG at 3 μM resulted in the most pronounced increase in $GRAB_{eCB2.0}$ signal as measured by area under the curve between 0-5 min, and thus we calculated the relative efficacy of each agent at the concentration that induced their maximal response as compared to the 2-AG response set at 100%. **Figure 6C** shows that the maximal $GRAB_{eCB2.0}$ responses to AEA (30 μM), 1-AG (10 μM), and CP (3 μM) reached 91%, 81% and 71% of the 2-AG response, respectively. **Figure 6C** also shows that the maximal $GRAB_{eCB2.0}$ responses to 2-LG (10 μM) and 2-OG (10 μM) only reached 37% and 17% of the 2-AG response, respectively, and that Δ^9-THC (30 μM) and Δ^8-THC (30 μM) only reached 22% and 16% of the 2-AG response, respectively. Finally, we compared the antagonism of SR1 (100 and 300 nM) for each ligand. **Figure 6D-E** show that the 2-AG (1 μM), CP (1 μM), 2-LG (10 μM), as well as Δ^9-THC (10 μM) and Δ^8-THC (10 μM) were partially antagonized by SR1 100 nM and antagonized by more than 80% with SR1 300 nM. By contrast, 1-AG (10 μM) and 2-OG (10 μM) were strongly antagonized by SR1 at both 100 and 300 nM, and AEA (10 μM) was antagonized by only 65% by both 100 and 300 nM SR1. These results reveal differences in key pharmacological and dynamic parameters that describe changes in $GRAB_{eCB2.0}$ signal elicited by eCBs and CB_1R ligands.

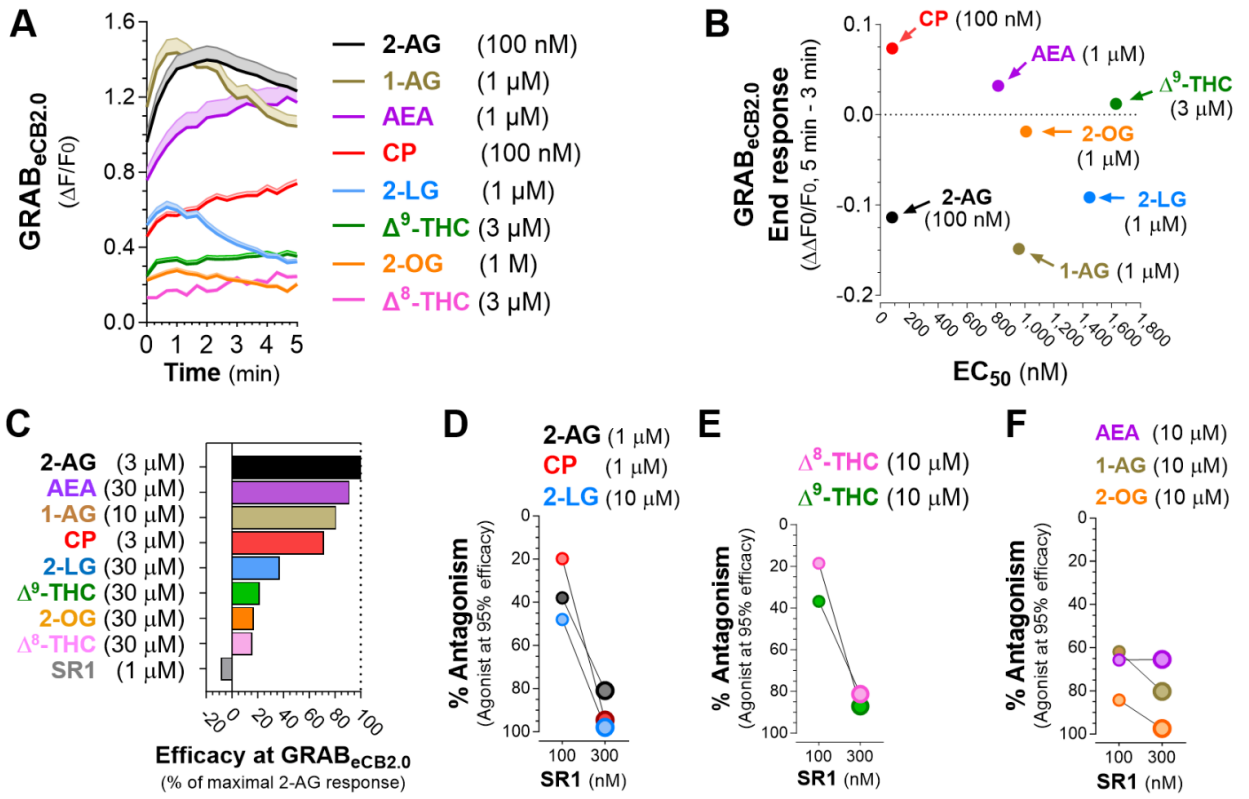

Figure 2.6: Monoacylglycerols have distinct dynamics and pharmacological properties at $GRAB_{eCB2.0}$ compared to THC, CP, and AEA. HEK293 cells were transfected with *eCB2.0* DNA plasmid and changes in fluorescent signal measured by high-throughput fluorescence assay. **A]** Comparison of $GRAB_{eCB2.0}$ activation kinetics elicited by each ligand at a concentration that approaches their respective EC_{50}s. Shaded areas in time courses and error bars represent s.e.m. **B]** Comparison of the EC_{50} of each ligand and their corresponding end response at a concentration that approached their respective EC_{50} and measured between 3-5 min. Y axis positive value represent increase in fluorescent signal (i.e., AEA, CP and D^9-THC) and negative values represent decrease in fluorescent signal (i.e., 2-AG, 1-AG, 2-LG and 2-OG). **C]** Comparison of the maximum increase in $GRAB_{eCB2.0}$ fluorescent signal as expressed by area under the curve and as a percent of 3 μM 2-AG produced by each ligand. **D-F]** Antagonism of each response by SR1 (100 and 300 nM).

Since $GRAB_{eCB2.0}$ activation by 2-AG and its analogues reached a peak maximal response followed by a decay in response and HEK293 cells endogenously express one or more enzymes capable of hydrolyzing eCBs[121], we tested the involvement of enzymatic hydrolysis in this decay. Thus, we treated HEK293 cells with methoxy arachidonoyl

fluorophosphonate (**MAFP**), a broad spectrum inhibitor that targets multiple enzymes that hydrolyze 2-AG, including MAGL, ABHD6, and ABHD12.[122] MAFP (10 nM and 100 nM) potentiated the 2-AG (300 nM)-response by 7% and 29%, respectively (Supplementary Figure S2.6B). Furthermore, MAFP (100 nM) increased the decay time constant (*t*) by 7-fold (Supplementary Figure S2.6C). Together, these results indicate that serine-hydrolases endogenously expressed by HEK293 cells may control the activity of 2-AG at its targets, here $GRAB_{eCB2.0}$.

2.3 DISCUSSION

Similarities and differences in $GRAB_{eCB2.0}$ and CB_1R pharmacology. $GRAB_{eCB2.0}$ was developed by screening for genetic constructs and individual randomized mutations starting with the CB_1R-backbone to improve the change in fluorescent signal in response to 2-AG.[95] The initial pharmacological characterization of $GRAB_{eCB2.0}$ was performed in the absence of BSA in the buffer and resulted in EC_{50}s values that are higher than their EC_{50}s at CB_1R: 2-AG = 3-9 μM, AEA = 0.3-0.8 μM, CP = 20 nM and THC = 2 μM.[93] BSA is known to facilitate the solubility and interaction of CB agents with CB_1R.[116] We found that inclusion of BSA in the buffer improves 2-AG's potency at $GRAB_{eCB2.0}$ to 85 nM, which is comparable to published EC_{50} values at the CB_1R, but didn't affect the activities of AEA, THC, and CP at $GRAB_{eCB2.0}$ compared to published values. This result suggests that BSA might preferentially facilitate the solubility and interaction of select CB agents with CB_1R and $GRAB_{eCB2.0}$, in this case 2-AG.

2-AG interacts with specific amino acids within the orthosteric binding site of CB_1R that are likely conserved in $GRAB_{eCB2.0}$. This is reflected in the similarity of 2-AG's potency at $GRAB_{ecb2.0}$ and its potency at the CB_1R, since the development process likely selected

for a sensor where the binding and activation properties of 2-AG were retained, such as the conservation of amino acids 2-AG may interact with. While there is an overlap between which CB_1R residues are predicted to interact with 2-AG, AEA, CP, and THC (such as F170, F177, W279, and F379 as determined by molecular docking simulations using the crystal structure of agonist-bound hCB_1R), other amino acid interactions may be ligand-specific.[86,123,124] For instance, CP and AEA, but not 2-AG and THC, are predicted to interact with F268. The disparity in potency of AEA and CP at the sensor compared to their potency at the CB_1R indicates that mutating the CB_1R and incorporating the cpEGFP to create $GRAB_{ecb2.0}$ may have impacted the structure of the sensor and subsequent conformation of the ligand binding pocket, resulting in ligand-specific effects on binding and potency that reflect the unique binding properties these agonists have at the native CB_1R. Furthermore, the efficacy of these ligands at $GRAB_{eCB2.0}$ (rank-order of maximal efficacy: 2-AG > AEA > 1-AG > CP >> 2-LG > 2-OG > Δ^9-THC > Δ^8-THC) indicates that $GRAB_{eCB2.0}$ expressed by cells in culture and mouse tissues reliably senses nanomolar changes in 2-AG levels, and micromolar amounts of AEA, eCB analogues, THC and CP. However, due to the differences in potency and maximal efficacy of these ligands, in model systems with a mixture of agonists (i.e. rodents treated with Δ^9-THC) the $GRAB_{eCB2.0}$ may preferentially detect some ligands (2-AG and AEA) over others (Δ^9-THC). Further interrogation of $GRAB_{eCB2.0}$'s response to simultaneous treatment by multiple ligands is needed to decipher the meaning of changes in $GRAB_{eCB2.0}$ signal in these in vivo model systems.

We detected the presence of intracellular $GRAB_{eCB2.0}$ and showed that agonist treatment increases its signal, though to a lesser extent than $GRAB_{eCB2.0}$ at the plasma

membrane. The possibility that $GRAB_{eCB2.0}$ undergoes internalization was indirectly tested by Dong *et al.* in their original publication by quantifying β-arrestin2 binding.[93] Significantly, they found no increase in β-arrestin2 binding when activating $GRAB_{eCB2.0}$ with cannabinoid agonists, in contrast to agonists-induced CB_1R internalization in HEK293 cells that depend on β-arrestin2. This suggests that extracellular agonists slowly cross the plasma membrane and may increase intracellular $GRAB_{eCB2.0}$ signal, though to a lesser extent and with slower kinetics.[125] Therefore, it is unlikely that the sensor will undergo significant internalization, particularly during short incubation times (i.e., 5 min).

$GRAB_{eCB2.0}$ pharmacology relative to abundance of eCB analogues and CB agents. Diacylglycerol lipase (**DAGL**) produces several monoacylglycerols in addition to 2-AG that exhibit significant agonist-like activity at CB_1R, such as 2-LG.[89,90] Furthermore, monoacylglycerol lipase (**MAGL**) and α/β domain containing 6 (**ABHD6**) hydrolyze several MAGs in addition to 2-AG, including 2-LG and 2-OG.[51] However, in the mouse brain, 2-LG is 10 times less abundant than 2-AG while 2-OG is approximately 2-3 times more abundant compared to 2-AG, and in both cases, the mechanism of how 2-LG and 2-OG production is stimulated is not well understood.[126,127] While there is potential that under physiological conditions, $GRAB_{eCB2.0}$ may detect 2-LG and 2-OG, considering that 2-LG and 2-OG activate the $GRAB_{eCB2.0}$ with potencies about 10 times lower than that of 2-AG, we suggest that the activity-dependent increases in $GRAB_{eCB2.0}$ signal measured in cells in culture and mouse tissues that are blocked by DAGL inhibitors and increased by MAGL/ABHD6 inhibitors are more likely to involve change in 2-AG levels than changes in 2-LG and 2-OG levels.

Δ^9-THC increases $GRAB_{eCB2.0}$ signal with an EC_{50} that is ≈100-fold higher than its EC_{50} at CB_1R when measuring inhibition of cAMP production. Since intraperitoneal injections of Δ^9-THC (5 mg/kg) in adult mice results in ≈10 ng/ml of THC in mouse brain (31.8 nM),[128,129] we conclude that $GRAB_{eCB2.0}$ expressed in mouse brain will therefore be able to sense i.p. injections of Δ^9-THC and Δ^8-THC and enable studying their PK profile and how this correlates with changes in behavior, or when either ligand arrives at a particular circuit or brain region in real time.

$GRAB_{eCB2.0}$ plateau versus decay dynamics. When applied at a concentration that approaches their EC_{50} values, CB agents increased $GRAB_{eCB2.0}$ signal with different kinetics: 2-AG, 1-AG, 2-LG, and 2-OG triggered rapid increases in fluorescent signal that were followed by slow decays, whereas AEA, CP, Δ^9-THC, and Δ^8-THC triggered progressive increases in fluorescent signal that did not reach peak response within 5 min. The broad spectrum serine hydrolase inhibitor MAFP reduced this decay in a concentration-dependent manner, indicating that HEK293 cells express one or more hydrolases that metabolize monoacylglycerols,[19,130] and underlie the decay response of 2-AG, 1-AG, 2-LG, and 2-OG. HEK293 cells also lack CYP2C9 and CYP3A4 enzymes that metabolize Δ^9-THC and Δ^8-THC. Thus, Δ^9-THC and Δ^8-THC are likely not enzymatically degraded by HEK293 cells in culture and induced a steadily increasing $GRAB_{eCB2.0}$ signal.

NAM activity of CBD at $GRAB_{eCB2.0}$. Allosteric binding sites are distinct protein domains from orthosteric sites that bind small molecules and either increase or decrease orthosteric site-mediated changes in protein conformations and activities. Early in vitro and in vivo studies showed that CBD reduces CB_1R signaling at concentrations well below

its reported affinity (Ki) to the orthosteric agonist site of CB_1R, providing the initial evidence that CBD acts as a NAM at this receptor.[131-133] Accordingly, in neurons in cell culture, CBD reduces the efficacy and potency of 2-AG and THC at increasing CB_1R signaling and inhibits eCB-mediated synaptic plasticity without influencing basal neurotransmission.[134-136] Mutagenesis of CB_1R indicated that several N-terminal residues of the CB_1R, namely Cys98, Cys107, and Met1, interact with CBD when it occupies the putative allosteric site of the CB_1R that CBD may target, and that this allosteric site overlaps with the orthosteric site which is near the second extracellular loop.[87,137] In silico modeling of CB_1R with an intact N-terminus revealed a potential binding pocket for NAMs of CB_1R in close proximity to its N terminus, one of the longest among class A GPCRs, and molecular docking studies suggest that binding to this site may result in a change in the 3 dimensional structure of the orthosteric binding site and thus in THC's and 2-AG's potencies.[137,138] While these results suggest that CBD inhibits CB_1R signaling by directly interacting with an allosteric binding site on this target, direct demonstration of CBD binding to CB_1R is still needed. We found that CBD does not affect baseline $GRAB_{eCB2.0}$ signal but reduces 2-AG's activity at $GRAB_{eCB2.0}$, a result consistent with the premise that the molecular mechanism involved in mediating CBD's allosteric modulation of CB_1R remains functional in $GRAB_{eCB2.0}$. Accordingly, mutagenesis optimization of CB_1R constructs to generate $GRAB_{eCB2.0}$ did not significantly affect its N-terminus (Supplementary Figure S2.1). Our results suggest that structural and mechanistic comparisons of CBD activity at CB_1R and $GRAB_{eCB2.0}$ might help us better understand that molecular mechanism involved in the allosteric modulation of CB_1R. That is- how

allosteric ligands produce a distinctive receptor conformation with unique signaling and therapeutic value.

In conclusion: We show that 2-AG increases $GRAB_{eCB2.0}$ fluorescent signal as a full agonist and with an EC_{50} similar to its activity at CB_1R, and that $GRAB_{eCB2.0}$ responds to AEA, 2-LG, and 2-OG with EC_{50}s that are higher than their EC_{50}s at CB_1R. Considering the lower amount of AEA, 2-LG, and 2-OG produced by cells, our results suggest that activity-dependent increases in $GRAB_{eCB2.0}$ fluorescent signal measured in cells in culture and mouse tissues will mainly reflect change in 2-AG levels, especially when this response is blocked by inhibitors of 2-AG production and inactivation. We also show that SR1 blocks $GRAB_{eCB2.0}$ fluorescent signal with an IC_{50} similar to its reported potency at CB_1R, and that this leads to levels below baseline fluorescent signal. Thus, $GRAB_{eCB2.0}$ exhibits basal fluorescence and SR1 may act as an inverse-like agonist and represents a useful pharmacological tool to validate $GRAB_{eCB2.0}$ functionality when expressed by various model systems. THC and CP increase $GRAB_{eCB2.0}$ fluorescent signal with EC_{50}s lower than their activity at CB_1R indicating that only high brain concentration of these agents will be detected in cell culture and mouse tissue model systems. CBD reduces the 2-AG-induced increase in $GRAB_{eCB2.0}$ fluorescent signal but not its basal fluorescent signal, suggesting that the molecular mechanism of CBD allosterism present in CB_1R is maintained in $GRAB_{eCB2.0}$. Thus, $GRAB_{eCB2.0}$ provides an opportunity to study how changes in THC and CBD concentration and co-activity at CB_1R might occur in cell culture and mouse tissue model systems. Our results presented here outline the pharmacological profile and activation dynamics of $GRAB_{eCB2.0}$ to improve the interpretation of changes in its fluorescent signal when expressed in various model systems.

Chapter 3.

$P2X_7$ receptor-dependent increase in 2-AG production by neuronal cells in culture: Dynamics and mechanism

3.1 INTRODUCTION

Increase in extracellular ATP concentrations modulates multiple physiological processes, including neurotransmission and neuroinflammation. Specifically, increase in extracellular ATP concentration may result from: 1] neuronal depolarization, which releases ATP through vesicular and channel-dependent mechanisms mediated by connexins and pannexins, or 2] dying cells with disrupted plasma membranes that release intracellular ATP [139,140]. Extracellular ATP then activates P2 receptors that are differentially expressed by neighboring neuronal and immune cells, which include 8 metabotropic receptors and 7 ligand-gated ion channels [141]. $P2X_7Rs$ are calcium-permeable channels and the only P2 receptor subtype activated by high micromolar-to-millimolar concentrations of ATP [142,143]. Activation of $P2X_7Rs$ leads to the opening of its pore and rapid increase in intracellular calcium concentrations ($_i$**[Ca^{2+}]**), changes in plasma membrane fluidity, as well as the activation of multiple additional downstream effectors, such as phospholipases C (**PLC**), PLA_2, PLD, sphingomyelinases, kinases and caspases [144]. Based on this premise, multiple studies have tested the therapeutic value of targeting $P2X_7R$ for the treatment of neurological diseases, including chronic pain [145].

One of the signaling pathways that is also implicated in chronic pain and is regulated by changes in extracellular ATP concentrations is the eCB signaling system. eCB signaling also plays a fundamental role in the control of neurotransmission and

neuroinflammation, and its molecular components have been targeted for the treatment of multiple neurological diseases [146]. For example, eCB levels are increased in rodent models of neuropathic pain [147], eCBs reduce both pronociceptive neurotransmission and the pro-inflammatory phenotype of immune cells [148], and eCB activation of its targeted receptors, such as CB_1R, produces robust analgesia in multiple pain models [19,149]. Furthermore, inhibitors of eCB inactivation, as well as modulators of CB_1R signaling, reduce neuropathic pain in several preclinical mouse models [146,150]. The two best-studied eCBs, AEA and 2-AG, differ in 4 key aspects: 1] they are produced by distinct biosynthetic pathways (N-acyl phosphatidylethanolamine phospholipase D (**NAPE-PLD**) versus PLC and diacylglycerol lipases (**DAGL**), respectively); 2] 2-AG is 10-1000 fold more abundant than AEA in cells; 3] AEA is a potent, partial agonist at CB_1R, whereas 2-AG exhibits lower potency at CB_1R and acts as full agonist; and 4] AEA is mainly inactivated by FAAH whereas 2-AG is differentially inactivated by MAGL and ABHD6 [12,14]. Several important aspects of eCB signaling that remain unexplored include the dynamics of the stimulated production of eCBs, the receptor subtypes and enzymes that control this activity-dependent production, and the dynamics of their on-off responses.

Genetically encoded fluorescent sensors allow for real-time detection of changes in the levels of select endogenously-produced signaling molecules [92]. For example, this technology leverages the high affinity binding of endogenous molecules to specific G protein-coupled receptors (**GPCR**), which stabilizes a conformation to elicit fluorescence of a circularly permutated-green fluorescent protein (**cpGFP**) introduced in the third intracellular loop of the GPCR [95]. $GRAB_{eCB2.0}$ is a recently developed eCB sensor that detects changes in eCB levels with sub second temporal resolution, and its activation has

been demonstrated in cells in culture, mouse brain slices, and *in vivo* during behavior [79,93,96,97,151]. Thus, the spatiotemporal properties of the $GRAB_{eCB2.0}$ provides an opportunity to study the molecular mechanism of eCB signaling at the cellular level.

We previously showed that ATP increases 2-AG production by astrocytes and microglia cells in culture through $P2X_7R$ [152,153]; however the detailed mechanism and the dynamics of this response remains unknown. The mouse neuroblastoma cell line, N2a, expresses multiple subtypes of P2 receptors, as well as the molecular components involved in eCB signaling (e.g., lipases involved in eCB production and inactivation, and CB_1R) and thus represents an ideal model system to study the molecular mechanism that link and control $P2X_7R$-dependent increase in 2-AG production [103,154,155]. Here we validated changes in $GRAB_{eCB2.0}$ signal expressed by N2a cells in culture, and examined the P2 receptor subtype, calcium-dependence, lipases and dynamics involved in the ATP-dependent increases in endogenous 2-AG production by these cells.

3.2 RESULTS

Real time change in $GRAB_{eCB2.0}$ fluorescent signal in N2a cells.

To drive robust $GRAB_{eCB2.0}$ expression, we transfected N2a cells in culture with plasmids containing the chimeric cytomegalovirus-chicken β-actin promoter and *eCB2.0* (**Figure 1a)**. **Figure 1b** shows robust $GRAB_{eCB2.0}$ expression 24 h after transfection as detected by western blot using a CT-CB_1R antibody. $GRAB_{eCB2.0}$ expression was heterogeneous, as expected from transient transfection, and mostly accumulated at the plasma membrane as detected by immunofluorescence using the CT-CB_1R antibody (**Figure 1c**). To measure real time changes in $GRAB_{eCB2.0}$ fluorescence, we used confocal

microscopy (line scanning frequency: 200 Hz, 0.388 FPS) and added pharmacological agents directly in the buffer media on the microscope's stage (**Figure 1a**). **Figure 1d$_{i-ii}$** show that prior to agonist treatment, N2a cells exhibited low, yet clearly detectable, basal fluorescence signal at the plasma membrane, and that 2-AG (1 μM) increased this signal at the 60 sec timepoint. **Figure 1d$_{iii}$** shows that adding the CB_1R antagonist, SR141617 (**SR1**, 2 μM) reduced this response measured after 5 min. Similarly, AEA (10 μM, 60 sec) and the CB_1R agonist, CP55940 (**CP**, 1 μM, 60 sec) increased $GRAB_{eCB2.0}$ signal at the plasma membrane, and these responses were reduced by SR1 (**Figure 1d$_{iv-ix}$**). Note that both the basal and agonist-triggered increase in $GRAB_{eCB2.0}$ fluorescent signal varies in each N2a cell as expected from a heterologous transfection approach (**Figure 1d$_{ii}$**, arrowhead). **Figure 1e** shows the time course of activation and inhibition of these responses, and emphasizes 3 results: 1] 2-AG and CP triggered a 2-fold steeper initial response (slope) and 2-fold greater maximal response (peak) compared to AEA; 2] 2-AG and AEA triggered a 2-fold overall greater response (area under the curve) for compared to CP; 3] Agonist responses were blocked by SR1 treatment with comparable decays (*t*) in their signal (values are in **Table 1**). Thus, $GRAB_{eCB2.0}$ sensors expressed by N2a cells are activated by the CB_1R agonists 2-AG, AEA and CP, and these responses are similarly antagonized by SR1.

Pharmacological profile and dynamics of changes in $GRAB_{eCB2.0}$ fluorescent signal in N2a cells.

We leveraged a fluorescent plate reader assay (96 wells, 3 Hz scanning frequency) to further define the pharmacological profile and dynamics of changes in $GRAB_{eCB2.0}$

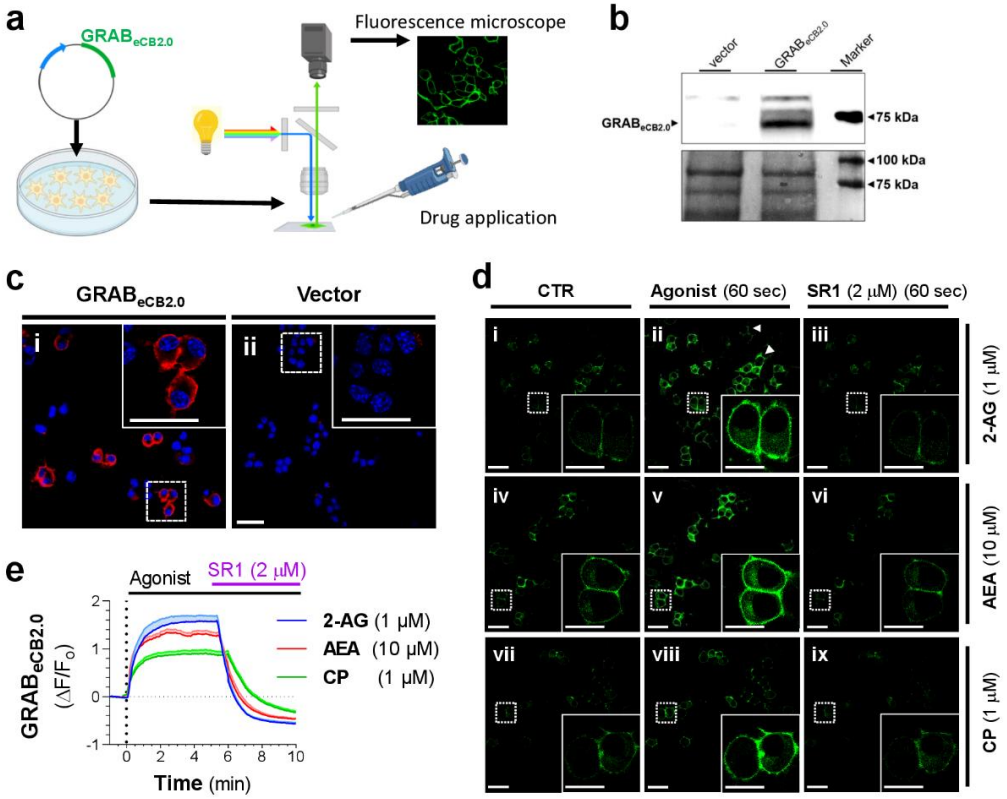

Figure 3.1: CB_1R agonists trigger increases in $GRAB_{eCB2.0}$ fluorescent signal in N2a cells. N2a cells expressing the $GRAB_{eCB2.0}$ were treated with the CB_1R agonists 2-AG, anandamide (**AEA**), or CP55940 (**CP**) followed by the CB_1R antagonist SR141617 (**SR1**), and changes in $GRAB_{eCB2.0}$ fluorescent signal were detected using live-cell confocal microscopy. **a]** Schematic of live-cell imaging workflow. **b-c]** $GRAB_{eCB2.0}$ protein expression as detected by western blot (b) and immunocytochemistry (c) using an antibody against the C-terminus of the CB_1R in N2a cells transfected with $GRAB_{eCB2.0}$ plasmid or empty vector. Scale bars: 40 µm (inset 20 µm). **d]** Effect of CB_1R agonists on $GRAB_{eCB2.0}$ activation and reversibility by SR1 in N2a cells as measured by live-cell confocal microscopy. Activation of $GRAB_{eCB2.0}$ by 2-AG (1 µM): baseline fluorescence (i), 2-AG-induced fluorescence (ii), SR1-induced deactivation (iii). Activation of $GRAB_{eCB2.0}$ by AEA (10 µM): baseline fluorescence (iv), AEA-induced fluorescence (v), SR1-induced deactivation (vi). Activation of $GRAB_{eCB2.0}$ by CP (1 µM): baseline fluorescence (vii), CP-induced fluorescence (viii), SR1-induced deactivation (ix). Baseline fluorescence detected 30 sec prior to agonist treatment. Agonist-induced fluorescence captured after 60 sec of agonist treatment. Reversibility by antagonist detected after 5 min of SR1 (2 µM) treatment. Heterogenous levels of $GRAB_{eCB2.0}$ fluorescence indicated with arrowhead (low signal) and arrow (high signal). Scale bars: 40 µm (inset 40 µm). **e]** Time course of $GRAB_{eCB2.0}$ activation ($\Delta F/F_0$) by CB_1R agonists, and reversibility of this activation by SR1 applied ≈5 min after agonist treatment in a single imaging experiment. N= 10-15 cells per treatment. Shaded area represents s.e.m.

signal in N2a cells. Thus, basal $GRAB_{eCB2.0}$ signal was measured for 1 min, pharmacological agents were added to the media, and approximately 120 sec later, cells were reinserted in the plate reader and fluorescence was measured for an additional 30 min (**Figure 2a**). To facilitate data analysis, we developed a MATLAB R2021a algorithm which averages the fluorescence value measured in each well over time, for multiple experiments and at select timepoints (see the following link for the code: https://github.com/StellaLab/StellaLab.git). **Figures 2b** shows that 2-AG induced concentration-dependent increase in $GRAB_{eCB2.0}$ signal that: 1] was detectable at 0 sec (when cells were reinserted in the plate reader and first fluorescence signal measured); 2] reached a peak response within minutes; and 3] plateaued for up to 30 min. Importantly, glycerol and arachidonic acid (**AA**), hydrolysis products of 2-AG, did not influenced $GRAB_{eCB2.0}$ signal (Supplementary Figure S3.1a-b). AEA also induced concentration-dependent increases in $GRAB_{eCB2.0}$ signal and this response exhibited a comparable kinetic as 2-AG's response (**Figures 2c**).

		CB_1R agonists		
PD parameter	**Units**	**2-AG**	**CP**	**AEA**
Initial response: slope	(x 10^{-2} ΔF/F0/sec)	**3.73**	**2.30**	**4.33**
	(95% CI)	(3.57-3.89)	(2.16-2.44)	(3.97-4.69)
Time to peak	(min)	**4.38**	**3.74**	**4.64**
Maximal response: peak	(ΔF/F0)	**1.79**	**0.90**	**1.69**
	(std. error)	0.074	0.058	0.150
Overall response	(area under the curve)	**453**	**239**	**434**
	(std. error)	12	7	20
Antagonism response: *t*	(sec)	**62.94**	**42.18**	**35.5**
	(95% CI)	(57.71-69.08)	(40.21-44.31)	(33.22-38.03)

Table 1: Parameters of $GRAB_{eCB2.0}$ activation by agonists and reversal by antagonism. N2a cells in culture were transfected with $GRAB_{eCB2.0}$ plasmids and $GRAB_{eCB2.0}$ activated by treating cells with **2-AG** (1 µM), anandamide (**AEA**, 10 µM), or CP55940 (**CP**, 1 µM), and with SR141617 (**SR1**, 2 µM). Changes in fluorescence were detected using live-cell confocal microscopy. Data are shown as a mean of 39-70 cells from 4 independent experiments; error bars represent s.e.m.

To calculate the EC_{50}s of these responses, we averaged $GRAB_{eCB2.0}$ signals during their initial plateau responses (i.e., 4-5 min). **Figures 2d** shows that 2-AG and AEA activate $GRAB_{eCB2.0}$ with EC_{50}s of 81 nM and 58 nM, respectively, as measured after 4-5 min, responses that are similar to their potencies at CB_1R (EC_{50} = 96 and 69 nM for 2-AG and AEA, respectively, as measured by adenylyl cyclase inhibition) [106,118]. CP induced concentration-dependent increases in $GRAB_{eCB2.0}$ signal with EC_{50}s of 193 nM, a response that is ≈100-fold lower than its reported potency at CB_1R (EC_{50} = 1.27-3.11 nM as measured by inhibition of adenylyl cyclase activity) [156,157] (**Figures 2e-f**). SR1 reduced $GRAB_{eCB2.0}$ signal below basal with an IC_{50} of 449 nM, which is approximately 100-fold less potent than its reported IC_{50} at CB_1R (**Figures 2f-g**) (e.g., 5.6 nM when measuring effect of SR1 on CP-induced inhibition of adenylyl cyclase) [111]. Pre-treatment of N2a cells with SR1 blocked $GRAB_{eCB2.0}$ activation induced by 2-AG, AEA, CP (**Figure 2g**). Furthermore; 2-AG, AEA and CP failed to elicit increases in $GRAB_{eCB2.0}$ signal when transfecting N2a cells with mutant $GRAB_{eCB2.0}$ (**mut-$GRAB_{eCB2.0}$**), in which phenylalanine 177 has been mutated to alanine in the region within the orthosteric binding pocket of the CB_1R [114,115] (**Figure 2g**). Importantly, mut-$GRAB_{eCB2.0}$ was expressed at the plasma membrane of N2a cells, further validating the use of this genetic control (Supplementary Figure S3.1c). Thus, changes in $GRAB_{eCB2.0}$ signal expressed by N2a cells in culture are reproducibly detected using a 96 well plate-reader. 2-AG and AEA increase $GRAB_{eCB2.0}$ signal with EC_{50}s comparable to their activities at the CB_1R, and these responses are antagonized by SR1, although with 100-fold lower potency than its activity at CB_1R.

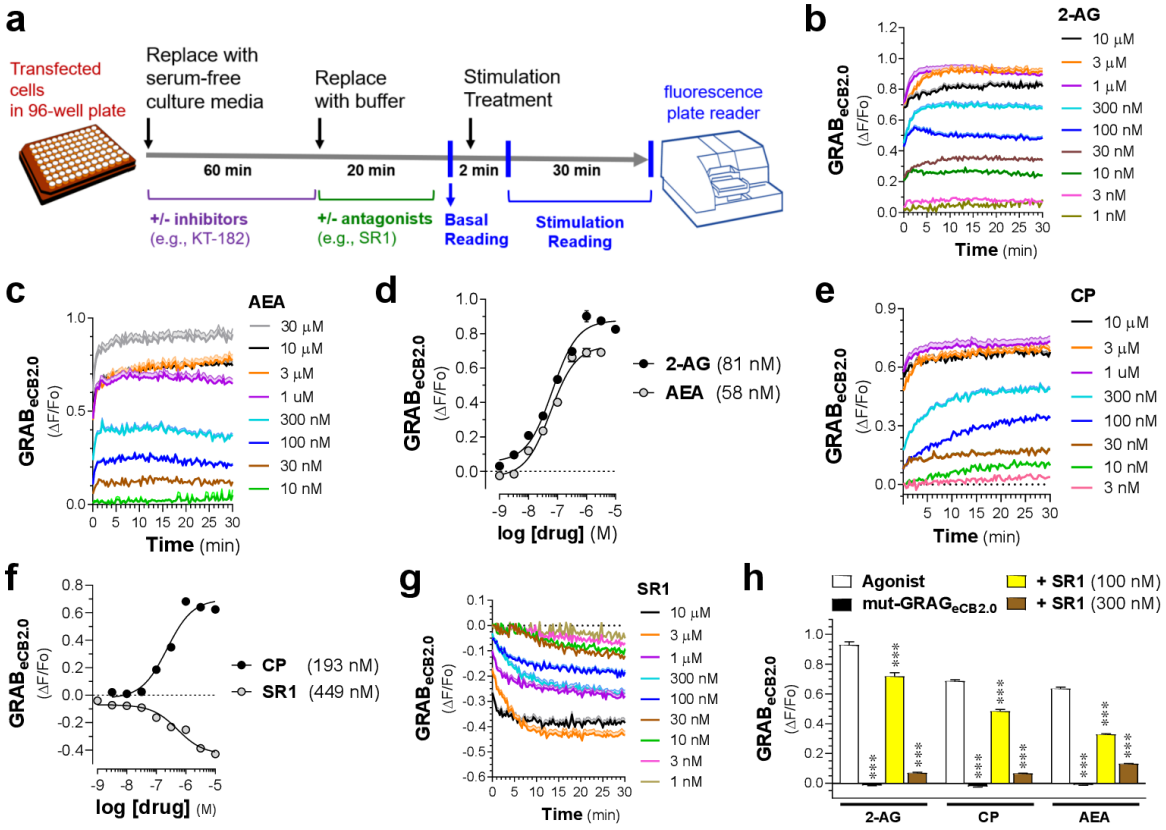

Figure 3.2: **Pharmacological profile of GRAB$_{eCB2.0}$ in N2a cells.** N2a cells expressing GRAB$_{eCB2.0}$ were treated with 2-AG, AEA, CP, and SR1, and changes in GRAB$_{eCB2.0}$ fluorescent signal were detected using a 96 well plate reader. **a]** Protocol for measuring fluorescent changes in GRAB$_{eCB2.0}$-transfected N2a cells using a plate reader. **b-c]** Concentration-dependent increases in fluorescent signal ($\Delta F/F_0$) following treatment with 2-AG (b) or AEA (c) during 30 min treatment. **d]** Concentration-response curve of 2-AG and AEA-induced increases in GRAB$_{eCB2.0}$ fluorescent signal as determined by averaging $\Delta F/F_0$ between 4 and 5 min from time courses in (b) and (c). **e-f]** Effect of CP (e) and SR1 (f) on GRAB$_{eCB2.0}$ fluorescent signal ($\Delta F/F_0$) during 30 min treatment. **g]** Concentration-response curve of CP and SR1-induced changes in GRAB$_{eCB2.0}$ fluorescent signal as determined by averaging $\Delta F/F_0$ between 4 and 5 min for CP from time courses in (e) and from 11-16 min for SR1 from time courses in (f). **h]** Effect of 2-AG (1 µM), CP (1 µM), and AEA (10 µM) on GRAB$_{eCB2.0}$ fluorescent signal in cells pretreated with SR1 (100 nM or 300 nM) or expressing mut-GRAB$_{eCB2.0}$. Determined by averaging $\Delta F/F_0$ between 4- and 5-min. Data are shown as mean of 3-76 independent experiments for 2-AG, 3-10 for AEA, 3-39 for CP, 3-5 for 1-AG, and 4-7 for SR1. Experiments were done in triplicate; shaded areas and error bars represent s.e.m.

ATP stimulates 2-AG production via $P2X_7R$.

To determine if ATP stimulates eCB production in N2a cells, we first measured 2-AG and AEA production by LC-MS (chromatograms, mass spectrums and detection limits are in Supplementary Figure S3.3a-k). **Figure 3a** shows that ATP (300 μM) significantly increased 2-AG levels by 53% after 2 min and this response returned to baseline after 10 min. By contrast, AEA was below the LC-MS detection limit under both basal and ATP (300 μM)-stimulated conditions, indicating that the main eCB produced under these conditions is 2-AG (Supplementary Figure S3.3g-i). **Figure 3b** shows that ATP (300 μM) also increased $GRAB_{eCB2.0}$ signal as measured by real-time fluorescence microscopy, and that this response steadily increased within seconds of treatment and reached its peak response after 8 min ($\Delta F/F_o$ = 0.39). These results show that $GRAB_{eCB2.0}$ reliably detects endogenous production of 2-AG induced by ATP, and that this readout exhibits a more robust and precise dynamic range as compared to LC-MS analysis.

To identify which P2 receptor subtype mediates the ATP-dependent increases in 2-AG levels, we measured changes in $GRAB_{eCB2.0}$ signal using the fluorescence plate reader. **Figure 3c** shows that ATP induced a concentration-dependent increase in $GRAB_{eCB2.0}$ signal characterized by an initial response occurring at 100 μM, a maximal response reached with both 300 μM and 1 mM ATP (0.18-0.2 $\Delta F/F_o$, respectively), and a slow decay. Of note, the 1 mM ATP response was slightly delayed compared to the 300 μM ATP response (**Figure 3c**). We analyzed the initial activation rate induced by ATP as measured between the 0 min, the peak responses, and their rate of decay as measured between the peak response and 30 min (i.e., measurements endpoint). **Figure 3d-e** show that 1] ATP induced a concentration-dependent increase in the initial activation of

$GRAB_{eCB2.0}$ signal and 2] the ATP (1 mM) response is delayed and shows a slower decay compared to the ATP (300 μM) response. Considering that $GRAB_{eCB2.0}$ signal changes in response to exogenous 2-AG applied at low nanomolar (see Figure 2d), we used this concentration-dependent response curve to extrapolate the increase in endogenous concentration of 2-AG induced by ATP (300 μM) and estimated an increase in 2-AG levels of ≈ 9 nM (Supplementary Figure S3.3$_j$).

The high concentration of ATP required to increase 2-AG production suggests the involvement of $P2X_7R$ (**Figure 3f**) [158,159]. Accordingly, the $P2X_7R$ agonist 2,3-O-(4-benzoylbenzoyl)-ATP (**BzATP**) increased $GRAB_{eCB2.0}$ signal in a concentration dependent manner (**Figure 3g**) [158,160,161]. Here, the initial activation and ensuing decay of $GRAB_{eCB2.0}$ signal induced by BzATP were maximal with 300 μM, consistent with involvement of $P2X_7Rs$. Furthermore, the $P2Y_{1/2}$ agonist ADP only increased $GRAB_{eCB2.0}$ signal at 1 mM, a concentration known to activate $P2X_7Rs$ [162], and the $P2Y_{12}$ agonist UTP did not affect $GRAB_{eCB2.0}$ signal, indicating that these P2 receptors are not involved in the ATP-induced increase in $GRAB_{eCB2.0}$ signal (Supplementary Figure S3.3$_{k\text{-}l}$) [163]. Treating N2a cells with BzATP (1 mM) also triggered a delayed initial increase in $GRAB_{eCB2.0}$ signal compared to BzATP (300 μM) (**Figure 3d, e** and **g**). Further confirming the involvement of $P2X_7Rs$, both ATP (300 μM) and BzATP (300 μM) responses were blocked by the $P2X_7R$ antagonist, A74003 (30 μM), without affecting basal $GRAB_{eCB2.0}$ signal (**Figure 3h** and Supplementary Figure S3.3$_m$) [160,164]. Both ATP (300 μM) and BzATP (300 μM) responses were blocked in N2a cells transfected with mut-$GRAB_{eCB2.0}$ and pretreated with SR1 (300 nM) (**Figure 3j**). These results show that ATP stimulates endogenous 2-AG production from N2a via activation of $P2X_7R$.

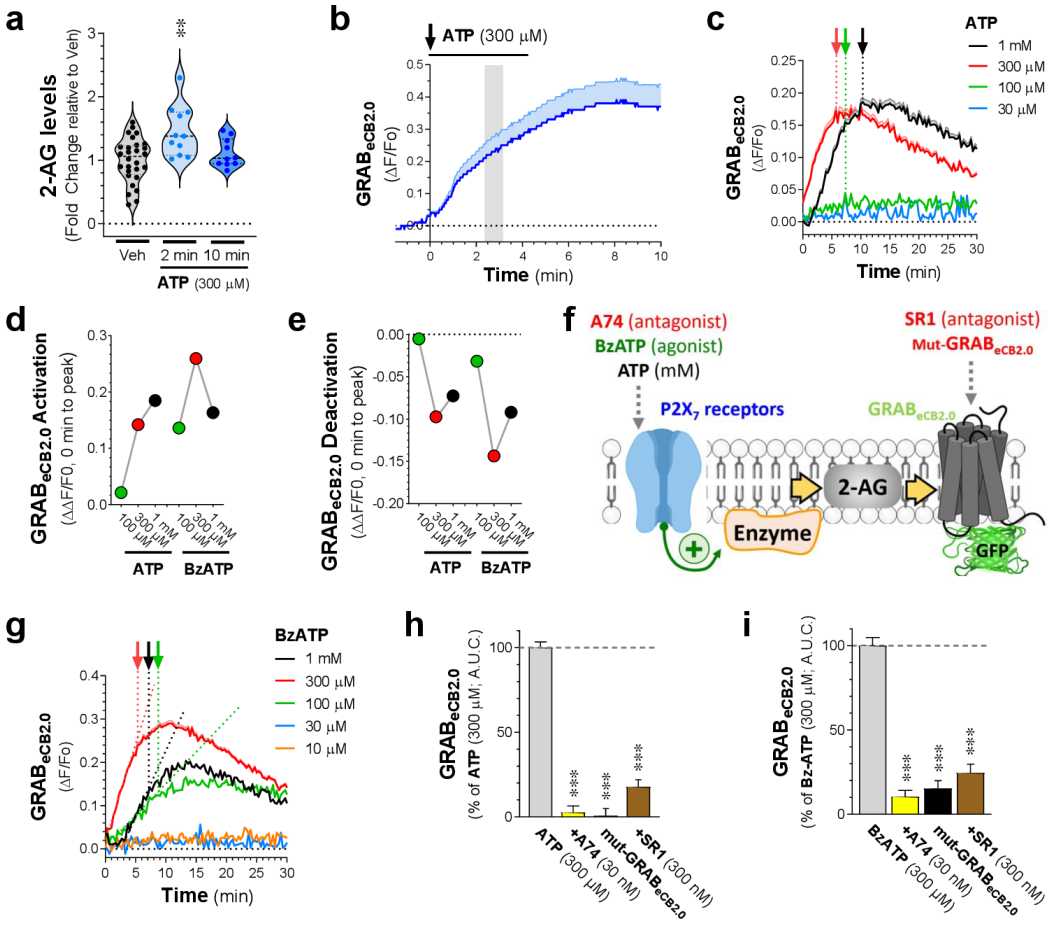

Figure 3.3: ATP increases 2-AG levels in N2a cells by acting at the P2X$_7$ receptor. N2a cells were treated with ATP or BzATP and changes in 2-AG were measured by LC-MS/MS or by GRAB$_{eCB2.0}$ fluorescent signal as detected by live-cell microscopy or a 96 well plate reader. **a]** Effect of ATP (300 µM for 2 and 10 min) on 2-AG levels in un-transfected N2a cells as measured by LC-MS/MS. N=11-30.. **b]** Effect of ATP (300 µM) on GRAB$_{eCB2.0}$ fluorescent signal ($\Delta F/F_0$) as measured by live-cell confocal microscopy. Data is shown as a mean of 39-51 cells from 3-4 independent experiments; shaded area represent s.e.m. **c]** Concentration-dependent effect of ATP on GRAB$_{eCB2.0}$ fluorescent signal ($\Delta F/F_0$) during 30 min treatment. Peak ATP-triggered $\Delta F/F_0$ responses reached at 6 and 10 min for 300 µM and 1 mM respectively. N = 4-23; Shaded area represents s.e.m. **d-e**] Concentration-dependent increase in ATP and BzATP-induced GRAB$_{eCB2.0}$ fluorescence activation (change in $\Delta F/F_0$ from time=0; d) and deactivation (change in $\Delta F/F_0$ from peak to 30 min); e). **f]** Mechanism of ATP- and BzATP-stimulated 2-AG production. **g]** Concentration-dependent effect of BzATP on GRAB$_{eCB2.0}$ fluorescent signal ($\Delta F/F_0$) during 30 min treatment. Peak BzATP-triggered $\Delta F/F_0$ responses reached at 11 min for 300 µM and at 14 min for 100 µM and 1 mM. N = 3-11. **h**] Effect of ATP (300 µM) and BzATP (300 µM) on GRAB$_{eCB2.0}$ fluorescent signal in cells pretreated with SR1 (300 nM), the P2X$_7$R antagonist A74003 (A74, 30 µM), or in cells expressing mut-

$GRAB_{eCB2.0}$. Determined by averaging $\Delta F/F_0$ between 4- and 5-min. N=3-8; error bars represent s.e.m.

Calcium- and PLC-dependence of $P2X_7$-mediated increase in 2-AG production.

Activation of $P2X_7$Rs stimulates multiple calcium-dependent and -independent signaling mechanisms, including increased PLC activity. PLC activity can be stimulated via both the influx of extracellular calcium ($_e$**[Ca^{2+}]**) through its pore and directly through its C-terminus tail that interacts with multiple signaling partners, including PLC [165] (**Figure 4a**). Increased PLC activity generates diacylglycerol (**DAG**), the precursor of 2-AG [17,18]. Absence of $_e[Ca^{2+}]$ in the buffer in combination with EGTA (1 mM) decreased both the ATP (300 μM)- and BzATP (300 μM)-induced increase in $GRAB_{eCB2.0}$ signal by 75 ± 0.38 and 45 ± 0.17, respectively (**Figure 4b-c**). Buffering $_i[Ca^{2+}]$ with BAPTA-AM (30 μM) reduced the overall response of ATP (300 μM)-induced increase in $GRAB_{eCB2.0}$ signal by 25% but did not affect BzATP (300 μM)-induced $GRAB_{eCB2.0}$ signal increase (**Figure 4d-e**). Importantly, buffering $_e[Ca^{2+}]$ with EGTA and $_i[Ca^{2+}]$ with BAPTA did not affect 1] basal $GRAB_{eCB2.0}$ signal and 2] direct activation of $GRAB_{eCB2.0}$ by CP (1 μM), emphasizing the selectivity of these treatments (Supplementary Figures S3.4a-c)These results show that ATP and BzATP-activation of $P2X_7$R and ensuing increase in 2-AG production are partially and differentially dependent on $_e[Ca^{2+}]$ influx and largely independent of $_i[Ca^{2+}]$, most likely because only localized, subcellular increases in $_i[Ca^{2+}]$ close to $P2X_7$R at the plasma membrane, are involved in calcium-dependent increase in 2-AG production.

To test the involvement of PLC, we used the inhibitor U73122, which decreased both the ATP (300 μM)- and BzATP (300 μM)-induced increases in $GRAB_{eCB2.0}$ signal in a concentration-dependent manner, which maximal inhibition of 69 ± 1.2% and X ± 5%, respectively, achieved with 3 μM, a concentration that is known to fully block stimulated

2-AG production in cultured neurons (**Figure 4f-g**) [18]. Treatment with U73122 (3 μM) resulted in a small but significant decrease in the direct activation of $GRAB_{eCB2.0}$ by CP (1 μM) that reached 17.4% at 30 min (Supplementary Figures S3.4d). However, this effect is likely not a concern since this decrease was only 1.5% at 10 min, which corresponds to the approximate time that the ATP (300 μM) and BzATP (300 μM)-stimulated $GRAB_{eCB2.0}$ signal approached their maximum effects. Thus, increased 2-AG production by activation of $P2X_7R$ is dependent on PLC activity.

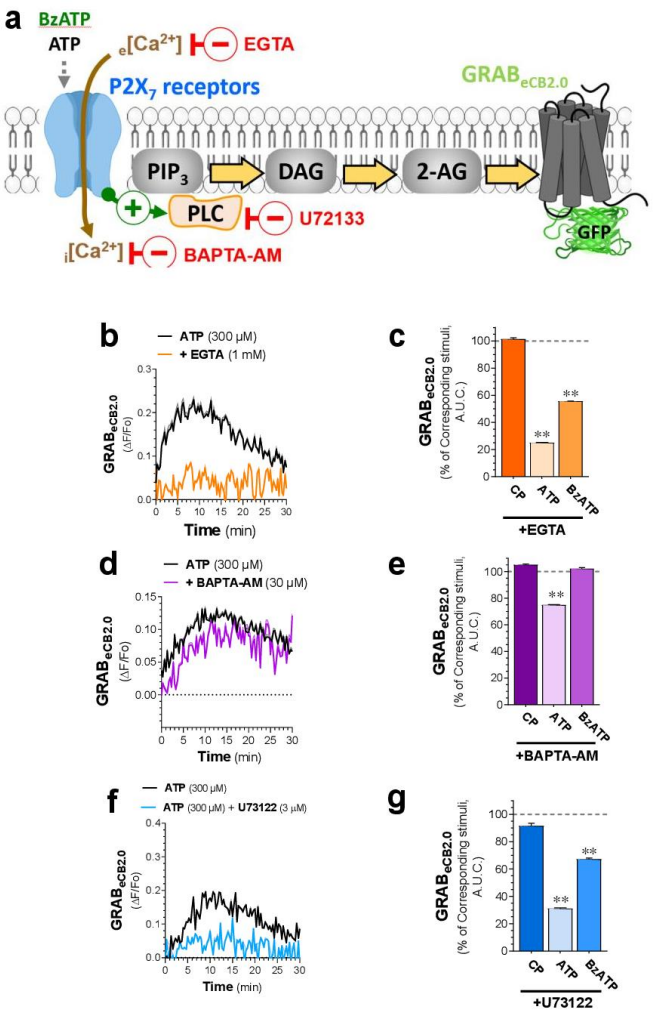

Figure 3.4: $P2X_7R$ agonists stimulate N2a 2-AG production through an extracellular calcium and PLC dependent mechanism. Role of calcium and PLC in $P2X_7R$-dependent 2-AG synthesis tested in N2a cells expressing $GRAB_{eCB2.0}$. Cells were treated with ATP or BzATP in combination with EGTA, BAPTA-AM, or the PLC inhibitor U73122. Changes in $GRAB_{eCB2.0}$ fluorescent signal ($\Delta F/F_0$) over the course of 30 min detected with a 96 well plate reader. **a]** Mechanism of $P2X_7R$-dependent 2-AG production. **b]** Effect of EGTA (1 mM) on the time course of ATP (300 μM) stimulated increase in $GRAB_{eCB2.0}$ fluorescent signal. **d]** Effect of BAPTA-AM (30 μM) on the time course of ATP (300 μM) stimulated increase in $GRAB_{eCB2.0}$ fluorescent signal. **f]** Effect of U73122 (3 μM) on the time course of ATP (300 μM) stimulated increase in $GRAB_{eCB2.0}$ fluorescent signal. N= 3-6 independent experiments. Shaded area represents s.e.m.

DAGL$_\beta$-dependence and ABHD6-independence of P2X$_7$-mediated increase in 2-AG production.

DAGL activity is stimulated by calcium, which hydrolyzes DAG at the *sn*-1 position to generate 2-AG [166]. To test the involvement of DAGL in the P2X$_7$-dependent increase in 2-AG production, we used the inhibitor DO34 (**Figure 5a**) [167]. N2a cells have been reported to express DAGL [103]. We first confirmed this DAGL activity in N2a cells using gel-based activity-based protein profiling (**ABPP**) and leveraged this readout to measure DO34's potency at inhibiting this activity [168]. **Figure 5b-c** show that N2a cells express robust DAGLβ activity but no detectable DAGLα activity when compared to mouse cortical membrane proteome (Supplementary Figures S3.5a), and that DO34 inhibited DAGL$_\beta$ with an IC$_{50}$ = 8.1 nM and reduced DAGL$_\beta$ activity by 88% at 30 nM. ABPP analysis confirmed previous studies showing that N2a cells do not have detectable MAGL activity (Supplementary Figures S3.5b) and express ABHD6 activity, and revealed that ABHD6 was also inhibited by DO34 with an IC$_{50}$ = 8.1 nM and by 54% [46,168,169]. **Figures 5d-e** show that DO34 (10 nM) inhibited both the ATP (300 μM) and BzATP (300 μM) by ≈60% and 75%, respectively. Notably, treatment with DO34 decreased GRABeCB$_{2.0}$ signal below basal ≈8 min following P2X$_7$R by ATP and Bz-ATP (**Figure 5d-e)**. This response is most likely due to the P2X$_7$R's ability to change plasma membrane fluidity following prolonged activation [170] as DO34 by itself did not affect GRABeCB$_{2.0}$ signal (Supplementary Figures S3.6a) (see discussion).

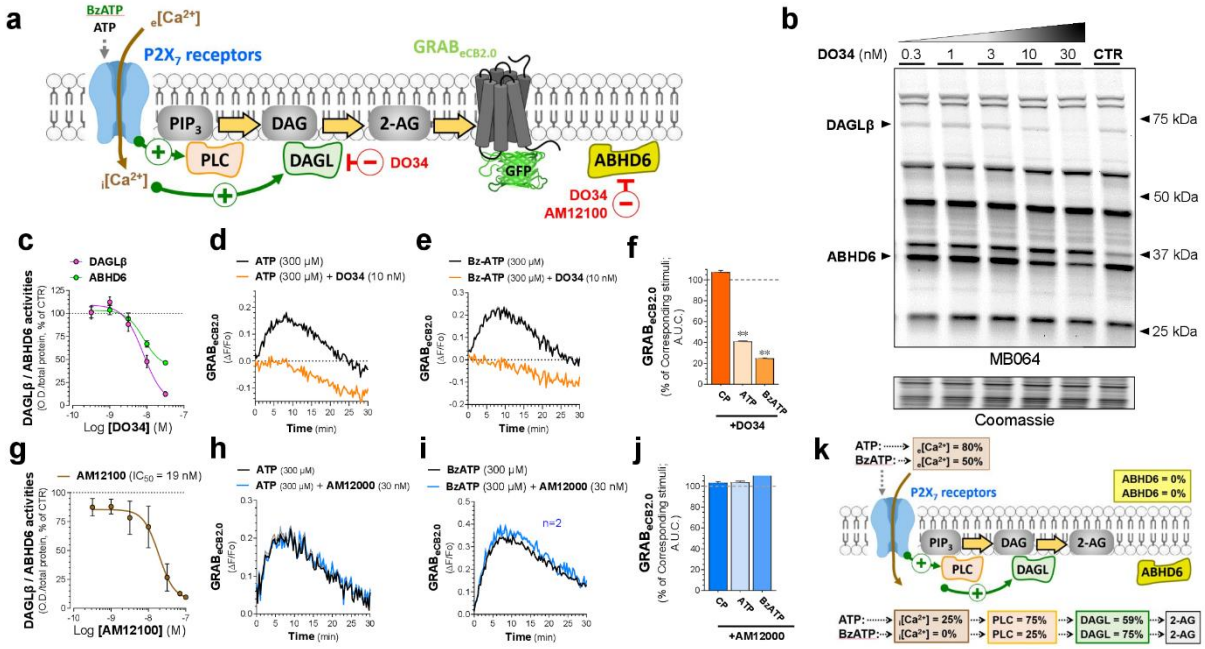

Figure 3.5: DAGLβ activity, but not ABHD6, controls P2X$_7$R-dependent 2-AG synthesis in N2a cells. Mechanism of 2-AG synthesis determined by measuring DAGLβ, ABHD6, and related enzyme activities in N2a cells by gel-based ABPP and by testing the effect of the DAGLβ inhibitor DO34 and ABHD6 inhibitor AM12100 on ATP (300 μM) and BzATP (300 μM)-stimulated increase in GRAB$_{eCB2.0}$ fluorescence. **a]** Mechanism of DAGLβ-dependent 2-AG production following P2X$_7$R activation. **b]** Effect of DO34 (10 nM, 30 min) treatment on activity of endogenously expressed serine hydrolases, including DAGLβ and ABHD6, in the membrane proteome from un-transfected N2a cells. Enzyme activity was detected using gel-based ABPP with the MB064 activity-based probe (2 μM, 15 min). **c]** Potency of DO34 inhibition of DAGLβ and ABHD6 activity as quantified from gel based ABPP in (b). N=4-7 independent experiments. Error bars represent S.E.M. **d-e]** Effect of DO34 (10 nM, 30 min) on the time course of ATP- and BzATP- induced increase in GRAB$_{eCB2.0}$ fluorescent signal ($\Delta F/F_0$). N=6 independent experiments. Shaded area represents S.E.M. **f]** Potency of AM12100 inhibition of ABHD6 activity as quantified from gel based ABPP. N=3-5 independent experiments. Error bars represent S.E.M. **g-h]** Effect of AM12100 (30 nM, 60 min) on the time course of ATP- and BzATP- induced increase in GRAB$_{eCB2.0}$ fluorescent signal ($\Delta F/F_0$). N=4 independent experiments. Shaded area represents s.e.m.

ABHD6 is a multifunctional enzyme that produces 2-AG from DAG under basal non-activated cells [168], and by contrast hydrolysis of 2-AG in stimulated cells [46]. To test if ABHD6 controls the P2X$_7$R-dependent increase in 2-AG production in N2a cells, we used

its recently develop inhibitor, AM12100 (**Figure 5a**) [167,171]. Accordingly, ABPP analysis of N2a treated cells showed that AM12100 inhibited ABHD6 activity by 90% and an IC_{50} = 19 nM without affecting DAGLβ activity (**Figure 5f** and Supplementary Figure S3.5d-e). **Figures 5g-h** show that AM12100 (30 nM) did not affect the ATP (300 μM)- and BzATP (300 μM)-induced increase in $GRAB_{eCB2.0}$ signal. Together, these results show that activity-dependent, $P2X_7R$-induced, increase in 2-AG production by N2a cells involves DAGLβ activity and is not controlled by ABHD6.

3.3 DISCUSSION

Pharmacological profile of $GRAB_{eCB2.0}$ sensors expressed by N2a cells: We found that nanomolar concentrations of 2-AG and AEA increase $GRAB_{eCB2.0}$ signal in N2a cells within seconds and with potencies comparable to their potencies at native CB_1R. The cannabinoid ligands, CP and SR1, increase and decrease $GRAB_{eCB2.0}$ signal, respectively, although with lower potencies compared to their potencies at the native CB_1R [109]. We recently reported the pharmacological profile of $GRAB_{eCB2.0}$ sensor expressed by HEK293 cells, and below note several key similarities and differences [151]. While 2-AG induced comparable increases in $GRAB_{eCB2.0}$ signal in both N2a and HEK293 cells, the EC_{50} of AEA's induced-increase in $GRAB_{eCB2.0}$ signal in N2a was 58 nM compared to 815 nM in HEK293 cells. Differences in these values might be due to differential expression of endogenous AEA inactivating enzymes since AEA can be hydrolyzed or oxidized by multiple mechanisms [172]. The EC_{50} of CP induced-increase in $GRAB_{eCB2.0}$ signal in N2a was 193 nM compared to 82 nM in HEK293 cells, and CP induced a partial agonist response compared to the 2-AG response, which contrasts with the full agonist activity of CP at CB_1Rs [156,173]. Remarkably, the IC_{50} of SR-1's induced-

decrease in $GRAB_{eCB2.0}$ signal in N2a was 449 nM compared to 3.3 nM in HEK293 cells, most likely because of the presence and absence of endogenous CB_1R expression in these cell lines, respectively [174]. Together, these results emphasize the need to characterize the pharmacological profile of $GRAB_{eCB2.0}$ sensor activity in each model system as it may vary depending on the expression profile of eCB hydrolyzing enzymes, fatty acid binding proteins, CB_1Rs and its interacting proteins [31].

The dynamic range, spatial and temporal resolution of measuring changes in 2-AG levels in N2a cells as detected by the $GRAB_{eCB2.0}$ sensor is greatly improved compared to LC-MS analysis because $GRAB_{eCB2.0}$ detects real-time 2-AG changes predominantly localized to the plasma membrane whereas LC-MS measures total 2-AG content in entire cells (i.e., plasma membranes and intracellular organelles) and has limited throughput capabilities. While $GRAB_{eCB2.0}$ sensor detects nanomolar concentrations of AEA, LC-MS analysis showed that N2a cells under basal and ATP-stimulated conditions did not produce detectable AEA, indicating that the low levels of this eCB is unlikely to contribute to $P2X_7R$-mediated increase in $GRAB_{eCB2.0}$ signal. This conclusion is further strengthened by the PLC- and DAGL-dependence of $P2X_7R$-mediated increase in $GRAB_{eCB2.0}$ signal, lipases that do not produce AEA.

Calcium- and PLC-dependence of $P2X_7R$ mediated increase in 2-AG production: We show that the $P2X_7R$ agonist, BzATP, increases $GRAB_{eCB2.0}$ signal, and this response is blocked by the selective $P2X_7R$ antagonist, A74. Furthermore, the $P2Y_{1,2}$ & $P2Y_{12}$ agonists, ADP and UTP, respectively, do not increase $GRAB_{eCB2.0}$ signal, although these receptors subtypes are known to regulate PLC activity [175]. These results show that only activation of $P2X_7R$ and not $P2Y_{1,2}$ & $P2Y_{12}$ agonists increases 2-AG production in N2a

cells. It should be emphasized that we used un-differentiated N2a cells in culture as model system in this study, and thus changes in $GRAB_{eCB2.0}$ signal are likely to reflect 2-AG autocrine signaling as opposed to paracrine signaling.

The ATP versus BzATP activation of $P2X_7R$ and ensuing increase in 2-AG exhibited remarkable differences in their sensitivities to $_e[Ca^{2+}]$: while the ATP response was reduced by 75 ± 5% by extracellular EGTA, the BzATP response was reduced by only 45 ± 5% under these conditions. It is known that $P2X_7R$ activation increases of both calcium-dependent and calcium-independent signaling pathways, and their relative involvement varies when using ATP versus BzATP [176]. Examples include difference in the potency and kinetics of $P2X_7R$ activation: ATP activates $P2X_7R$ relatively slowly, taking several seconds to minutes to fully activate the receptor; whereas BzATP is more potent and activates $P2X_7R$ faster, with a time course of a few seconds or less [144]. Thus, such pharmacological and dynamics variations will differentially activate calcium-dependent and calcium-independent signaling pathways, most of which depend on the intracellular C-terminus portion of $P2X_7R$ [177]. Specifically, the C-terminus portion of $P2X_7R$ constitutes ≈40% of this protein and more than 50 proteins physically interact with $P2X_7R$, including many intracellular signaling proteins [144]. For example, $P2X_7R$ activation by ATP induces the release of interleukin-1 β whereas Bz-ATP induces the releases of both IL-1β and tumor necrosis factor α [178,179]. We found that $P2X_7R$-mediated increase in 2-AG was not affected by buffering $_i[Ca^{2+}]$ with BAPTA-AM, here suggesting that the calcium-dependent enzymes that are activated by the influx of $_e[Ca^{2+}]$ and are involved in a portion of 2-AG production are likely localized in the intracellular space near $P2X_7R$ and only activated by local increase in $_i[Ca^{2+}]$ that result from $P2X_7R$ activation and are not affected by BAPTA-

AM. Thus, our study provides a new example of differential activation profile and calcium-dependence resulting from $P2X_7R$ activation, here increased 2-AG production.

Testing the involvement of DAGLβ and ABHD6 with DO34 and AM12100: Both DAGLα and β produce 2-AG and here we confirm that N2a cells in culture only express DAGLβ activity [168,180]. Treatment of N2a cells with DO34 (10 nM) inhibited DAGLβ activity by 55% and fully block both the ATP and BzATP-induced increase in 2-AG production, suggesting that this enzyme represents the principal rate limiting step in 2-AG production. Remarkably, when treating N2a cells with DO34, both the ATP- and BzATP-induced increase in $GRAB_{eCB2.0}$ signal was followed by a decay that reached values below basal activity (Figure 5d-e). A mechanism that might be responsible for a decrease in $GRAB_{eCB2.0}$ signal below basal activity includes the delayed $P2X_7R$ induced change in plasma membrane fluidity that is enhanced when DAGL is inhibited, disrupting $GRAB_{eCB2.0}$ activity itself. [181-183]. Furthermore, prolonged $P2X_7R$ activation results in the formation of a non-selective membrane pore that is permeable to molecules up to 900 Da, and this pore formation is dependent on membrane lipids since its formation is promoted by phosphatidylglycerol but inhibited by cholesterol [184]. Thus, the combination of DAGL inhibition, which may alter the membrane lipid composition, and a 30 min exposure $P2X_7R$ agonists could result in this pore formation resulting in general plasma membrane and cellular disruption, thereby affecting $GRAB_{eCB2.0}$ activity.

We discovered that DO34 inhibits ABHD6 with the same potency as DAGL but with a lower efficacy (i.e., 33% at 10 nM). Thus, we tested AM12100, which inhibited ABHD6 by 74% at 30 nM and found no effect on both the ATP- and Bz-ATP induced increase in $GRAB_{eCB2.0}$ signal, showing that ABHD6 is not involved in either 2-AG production under

basal conditions, or in hydrolyzing 2-AG under stimulated conditions. The absence of ABHD6 involvement may be due to ABHD6 expression not overlapping with the subcellular compartment that expresses the enzymatic machinery involved in the $P2X_7R$-induced increase in 2-AG production.

Pathological relevance. The high concentrations of ATP (≥ 100 nM) required to activate the $P2X_7R$ can be released by damaged or dying cells as a result of various types of insults, including chronic inflammatory and neuropathic pain [185,186]. Thus, decreases in $P2X_7R$ signaling may have therapeutic benefits. For example, $P2X_7R$ expression is upregulated in peripheral nerve tissue samples from patients experiencing chronic neuropathic pain, and $P2X_7R$ inhibition or knock-down demonstrates significant therapeutic efficacy in preclinical models of neuropathic pain and spinal cord injury [182,185,187]. Many studies have shown that pharmacological enhancement of 2-AG-CB_1R signaling, for example by using positive allosteric modulators of CB_1R, produce analgesia in multiple rodent pain models in a CB_1R-dependent mechanism. Our study provides the first evidence that activation of $P2X_7R$ results in increasing 2-AG production within seconds, demonstrating a mechanistic link between these two signaling pathway that might be targeted for therapeutic benefit, including for the treatment of chronic pain.

Conclusions: Activation of $P2X_7R$ expressed by N2a cells in culture increases 2-AG production with seconds. This mechanism depends partially on ${}_e[Ca^{2+}]$ and PLC, fully on DAGL and not on ${}_i[Ca^{2+}]$ and ABHD6, suggesting a subcellularly-localized molecular machinery. Thus, our study outlines a novel molecular mechanism involved in increased 2-AG production that can be targeted for the treatment of neurological diseases such as neuropathic pain.

Chapter 4.

Metabotropic-dependent increases in autocrine and paracrine 2-AG signaling measured in cells in co-culture

4.1 INTRODUCTION

Endocannabinoid (eCBs) are lipophilic signaling molecules that are produced in an activity-dependent manner and can modulate intracellular signaling pathways throughout the body[12]. In the brain, the most abundant eCB is 2-arachidonoyl glycerol (2-AG), which can target multiple proteins, including acting as an agonist of the G-protein coupled cannabinoid CB_1 and CB_2 receptors (CB_1R and CB_2R, respectively). As a pleiotropic signaling molecule, 2-AG has been implicated in diverse physiological processes, including neurotransmission and neuroinflammation, as well as pathological conditions such as neuropathic pain[14]. The earliest evidence of the role of the eCB system in pain comes from the use of cannabis and phyto-cannabinoids, such as Δ^9-THC, as an analgesic for chronic pain, likely due to a cumulative effect of targeting multiple receptors, including the CB_1R, CB_2R, and glycine receptors[188]. These receptors are expressed in multiple cells involved in inflammation and pain processing, including in sensory neurons and non-neuronal cell-types such as microglia, and can be targeted by 2-AG[189-191]. Thus, enhancing endogenous 2-AG signaling at these targets has a potential therapeutic benefit in conditions such as neuropathic pain.

Several lines of preclinical evidence demonstrate that increased 2-AG signaling has a potential therapeutic benefit in pain relief. In multiple rodent models of pain, administration of exogenous 2-AG or pharmacological inhibition of 2-AG degradation has an anti-allodynic effects and attenuates hyperalgesia[192-194]. Furthermore, clinical and

preclinical studies indicate that neuropathic pain is correlated with elevated 2-AG levels[195]. Both 2-AG and 2-AG targets, such as the CB_1R, are found in multiple regions involved in pain processing, including the dorsal root ganglia spinal cord, periaqueductal grey[196]. However, how this neuronal 2-AG is regulated in a pain state, and the role played by this 2-AG remains unclear. For instance, inflammatory mediators that are involved in peripheral and central sensitization and contribute to hyperalgesia can increase 2-AG levels. But the mechanism of this 2-AG production in neurons is yet to be described.

One of the inflammatory mediators in involved in peripheral sensitization that that can increase 2-AG levels is bradykinin[197-199]. Bradykinin (BK) is a peptide signaling molecule that can induce pain by activating two metabotropic G-protein coupled receptors (the B_1 and B_2 receptor)[200]. In an overexpression mixed co-culture model system, BK stimulated 2-AG production by acting at the B_2R[198]. Furthermore, in dorsal root ganglia primary culture, co-treatment of the cells with BK combined with another inflammatory mediator, ATP, increased 2-AG levels[199]. While this indicates that neuronal BK signaling can regulate 2-AG levels, the precise mechanism of how BK-triggers increases in neuronal 2-AG levels, and the role of this signaling, is yet to be explored. Here we describe the mechanism of BK-stimulated 2-AG production in a neuronal model and show that this 2-AG can act as an autocrine and paracrine signaling molecule in a mixed culture model.

4.2 RESULTS

Bradykinin stimulates 2-AG production in N2a cells

To test how bradykinin regulates 2-AG levels in neurons, we employed a genetically encoded eCB sensor, $GRAB_{eCB2.0}$, to measure changes in eCB levels in neuro2a (N2a) cells. Briefly, the cells were transfected with *eCB2.0* DNA, and changes in

fluorescent signal were measured using live-cell confocal microscopy. Figure 1A shows that baseline $GRAB_{eCB2.0}$ fluorescent signal was low but detectable and BK (1 µM, 2 min) increased this signal predominantly at the plasma membrane, followed by a decrease when measured ten min after the onset of BK. Plotting the time course of the change in $GRAB_{eCB2.0}$ fluorescent signal following BK-treatment demonstrated that the BK-triggered transient increase in $GRAB_{eCB2.0}$ signal reached a maximum $\Delta F/F_0$ of 0.64 at approximately 2.5 min, before decaying by 55% after 10 min of treatment. To test the effect of multiple inflammatory mediators on the $GRAB_{eCB2.0}$ signal, we co-treated N2a cells with BK and ATP (300 µM), which is another inflammatory mediator that can contribute to peripheral hyperalgesia and is known to stimulate 2-AG production in N2a cells by acting at the $P2X_7$ receptor[185]. The $GRAB_{eCB2.0}$ fluorescent signal induced by ATP and BK reached a maximum $\Delta F/F_0$ of 0.56 at approximately 3 min, after which the signal plateaued (Figure 1C).

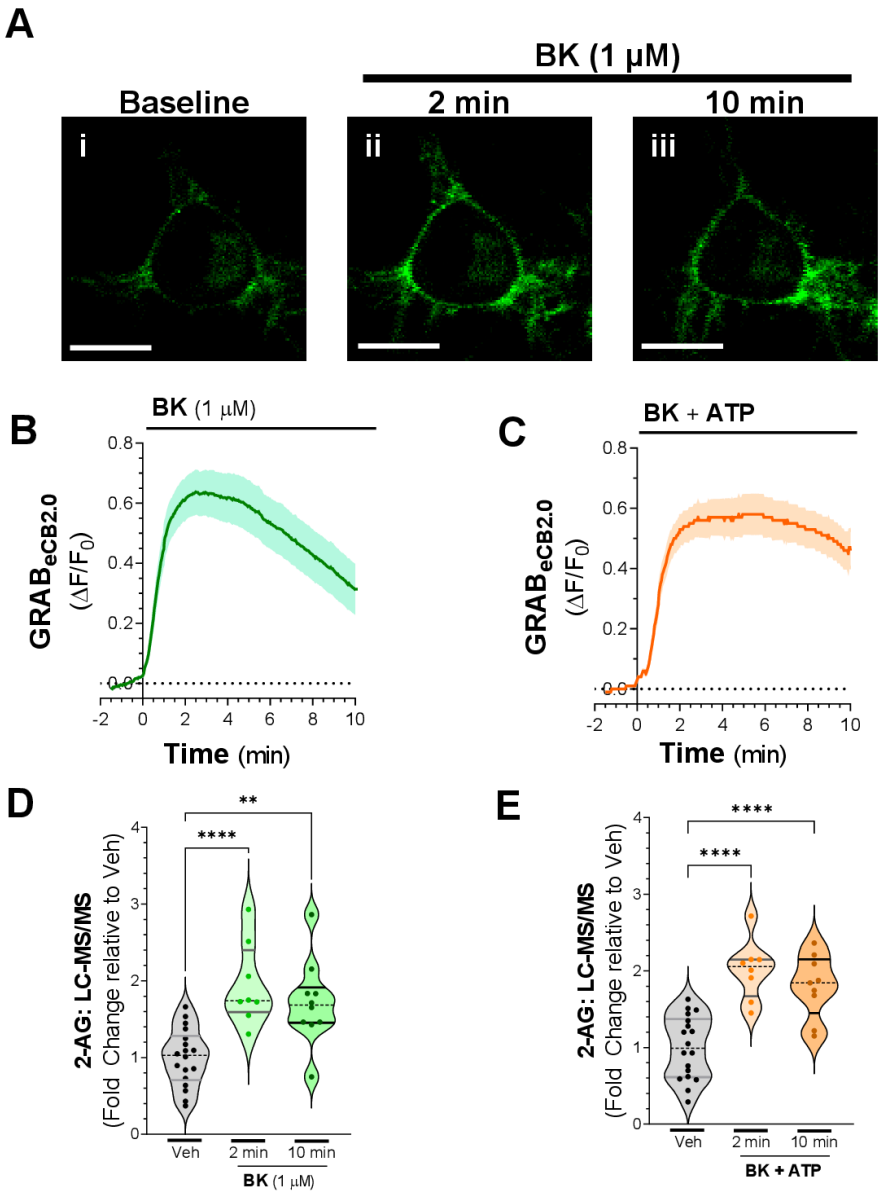

Figure 4.1: Bradykinin stimulates 2-AG production in N2a cells. N2a cells were transfected with $GRAB_{eCB2.0}$ and changes in $GRAB_{eCB2.0}$ fluorescent signal were detected using live-cell confocal microscopy. **a]** Activation of $GRAB_{eCB2.0}$ by BK (1 µM): baseline fluorescence (i), BK-induced fluorescence after 2 min of treatment (ii), BK-induced fluorescence after 10 min of treatment SR1-induced deactivation (iii). Scale bars: 20 µm **b-c]** Time course of $GRAB_{eCB2.0}$ activation ($\Delta F/F_0$) by BK (1 µM; b) or by co-treatment of BK and ATP (300 µM) (c). N = 39-51 cell per treatment from 3 independent experiments. Shaded area represents s.e.m. **d-e]** Effect of BK (1 µM; d) or co-treatment of BK and ATP (300 µM) (e) on 2-AG levels in un-transfected N2a cells after 2 and 10 min of treatment as measured by LC-MS/MS. N=8-18 independent experiments. **P<0.0012 and ****P<0.0001 significantly different from corresponding vehicle (Veh) treatment (One-way ANOVA followed by Tukey's multiple comparisons test).

The utility of the $GRAB_{eCB2.0}$ is characterized by its high spatiotemporal resolution since it can detect changes in eCB levels that occur within seconds with a subcellular resolution. However, the $GRAB_{eCB2.0}$, can be activated by two eCB, 2-AG and AEA, as well as other endogenous lipids such as 2-OG. Therefore, to confirm which $GRAB_{eCB2.0}$ ligand was contributing to the BK-stimulated increase in $GRAB_{eCB2.0}$ signal, we measured the effect of BK as a single agent or in combination with ATP on 2-AG levels using LC-MS/MS, since BK has been shown to increase 2-AG production in multiple cell models. Compared to vehicle treated cells, BK (1 µM) increased 2-AG levels in N2a cells by 95% and 72% at 2 and 10 min, respectively, while the combination treatment of BK (1 µM) and ATP (300 µM) increased 2-AG levels by 101% and 78% at 2 and 10 min, respectively (Figure 1D-E). Thus, BK can stimulate a rapid and transient increase in 2-AG levels in N2a cells that peaks within minutes and is reliably detected using both $GRAB_{eCB2.0}$ and LC-MS/MS.

Mechanism of BK-stimulated 2-AG production

Next, we wanted to determine which receptor and signal-transduction pathway mediated BK-stimulated 2-AG synthesis. To increase our throughput, we employed a $GRAB_{eCB2.0}$ assay using cell plated and transfected in a 96-well plate, followed by detection of changes in $GRAB_{eCB2.0}$ fluorescent signal using a fluorescent plate reader. We validated this approach by testing the effect of increasing concentration of BK on $GRAB_{eCB2.0}$ fluorescent signal. Figure 2A shows that BK resulted in a concentration-dependent increase in $GRAB_{eCB2.0}$ fluorescent signal, with a maximum $\Delta F/F_0$ signal of 0.17 achieved with 1 µM BK. To determine the potency of BK for increasing 2-AG levels, a concentration-response curve using peak $\Delta F/F_0$ was plotted, which returned an EC_{50} of

341 nM (Figure 2B). Notably, the time-to-peak was inversely correlated with the concentration of BK, with the highest concentration of BK, 3 μM, peaking at 1 min while the lowest concentration, 1 nM, peaking at 26 min, and can be described with a non-linear exponential decay function (Figure 2C). Having described the effect of BK as a single agent on changes in changes in $GRAB_{eCB2.0}$ fluorescent signal, we next treated the N2a cells with the combination of BK (1 μM) and ATP (300 μM). This co-treatment resulted in an increase in $GRAB_{eCB2.0}$ fluorescent signal that reached a maximum $\Delta F/F_0$ of 0.41, which was significantly greater than the maximum signals elicited by BK or ATP alone ($\Delta F/F_0$ of 0.16 and 0.23, respectively) (Figure 2D). The maximum signals and the overall magnitude of the effect (as determined by area under the curve) demonstrates that BK (1 μM) and ATP (300 μM) have an additive effect (Figure 2E). Finally, we can estimate the level of 2-AG produced by these stimuli by plotting the $GRAB_{eCB2.0}$ fluorescent signal induced by known concentrations of exogenous 2-AG and fitting a non-linear regression. Thus, BK by itself and in combination with ATP (300) increases 2-AG levels by approximately 7 and 50 nM 2-AG, respectively (Figure 2F). Having validated BK's effect on $GRAB_{eCB2.0}$ fluorescent signal using the plate reader, we proceeded to use this approach to interrogate the mechanism of BK-stimulated 2-AG production.

Bradykinin exerts it biological effect by acting at the B_1 and B_2 receptors (B_1R and B_2R, respectively). Both receptors couple to $G_{\alpha q}$, and activation by BK results in increased intracellular calcium and phospholipase C (PLC) activity[200]. On-demand 2-AG production following activation of a $G_{\alpha q}$-coupled GPCR is well established: 1] activation of a Gαq-coupled receptor increases PLC activity; 2] PLC hydrolyzed PIP2 to produce IP3 and the 2-AG precursor diacylglycerol; 3] DAG is hydrolyzed by the sn-1-specific enzyme

diacylglycerol lipase (DAGL) to produce 2-AG (Figure 3A)[19,20]. N2a can endogenously express B_2R; therefore, we tested the effect of the selective B_2R antagonist HOE 140 on BK-stimulated 2-AG production. HOE 140 (300 nM) inhibited the peak BK-triggered $GRAB_{eCB2.0}$ fluorescent signal by 90% indicating that BK acts at the B_2R in N2a to increase 2-AG levels (Figure 3B). The BK-stimulated fluorescent signal was also reduced by 99% in cells pre-treated with the CB_1R antagonist SR141716 (300 nM) and by 88% in cells expressing the mut-GRABecb2.0, which has a point mutation from phenylalanine 177 to alanine in the ligand-binding pocket that decreases agonist binding (Figure 3B). The PLC inhibitor U73122 (300 nM) did not reduce BK-stimulated $GRAB_{eCB2.0}$ fluorescent signal, but the DAGL inhibitor DO34 (10 nM) decreased the BK-triggered $GRAB_{eCB2.0}$ response by 96% (area under the curve) (Figure 3C-D). Thus, BK-triggered 2-AG production is PLC-independent but mediated by DAGL.

2-AG biosynthesis is activity-dependent and tightly coupled to an increase in intracellular calcium. For instance, increased intracellular calcium and availability of DAG is sufficient for 2-AG synthesis[16]. To determine the role of calcium in BK-triggered 2-AG production, we tested how decreasing extracellular and intracellular calcium using EGTA and BAPTA-AM, respectively, affected BK-stimulated 2-AG production. Figure 3A-B Show that BAPTA-AM (30 µM) and EGTA (1 mM) decreased the overall BK-triggered $GRAB_{eCB2.0}$ response by 66% and 62% (area under curve). Altogether, these data indicate that BK stimulates 2-AG production in N2a cells by acting at the B_2R, but is only partially dependent on increased intracellular calcium and is not dependent on PLC activity. This suggests an alternative mechanism of metabotropic-dependent 2-AG

production that may rely on different lipases in the cell that can generate DAG, since multiple 2-AG biosynthetic pathways have been described[19].

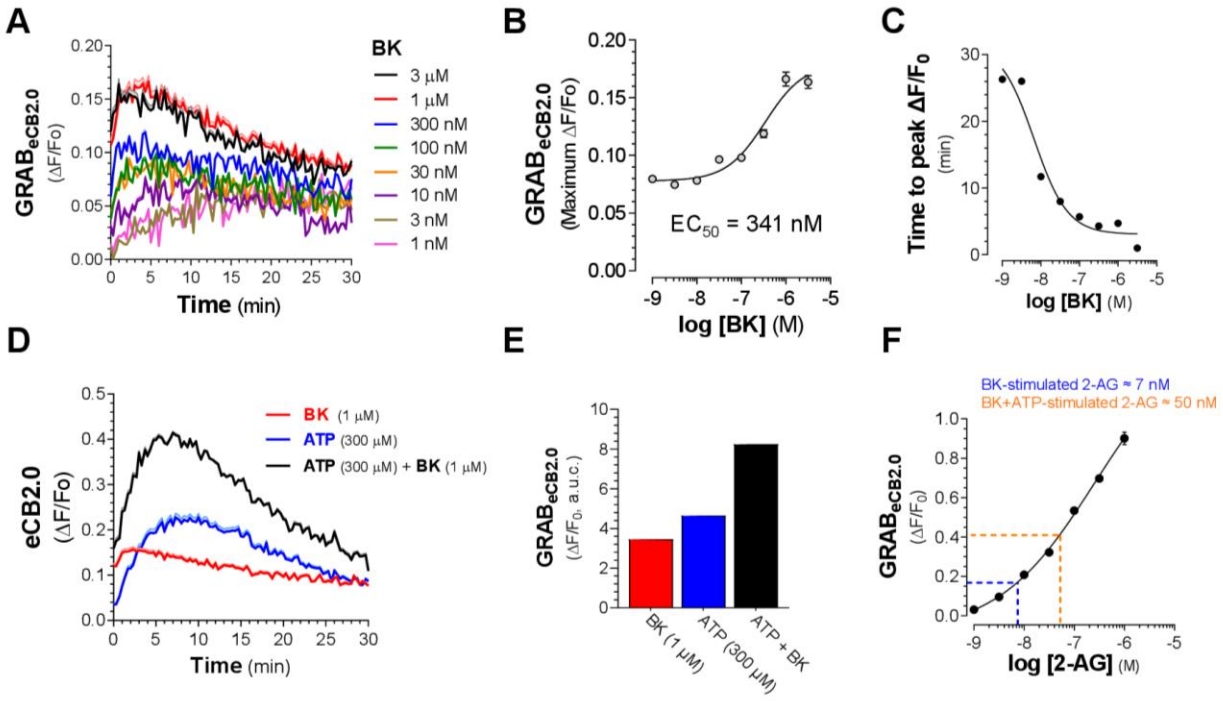

Figure 4.2: Pharmacological Characterization of BK-stimulated 2-AG production. N2a cells were transfected with $GRAB_{eCB2.0}$ and changes in $GRAB_{eCB2.0}$ fluorescent signal were detected using a 96 well plate reader. **a]** Concentration-dependent increases in $GRAB_{eCB2.0}$ fluorescent signal ($\Delta F/F_0$) following treatment with BK (1 μM) over the course of a 30 min treatment. **b]** Concentration-response curve of BK (1 μM)-induced increase in $GRAB_{eCB2.0}$ fluorescent signal (maximum $\Delta F/F_0$) from time courses in (a). **c]** Negative correlation between BK concentration and time-to-peak calculated from results in (a). **d]** Effect of BK (1 μM), ATP (300 μM), or ATP and BK co-treatment on $GRAB_{eCB2.0}$ fluorescent signal ($\Delta F/F_0$) over the course of a 30 min treatment. **e]** Total $GRAB_{eCB2.0}$ fluorescent signal response (area under the curve of data presented in d) for BK (1 μM), ATP (300 μM), or ATP and BK co-treatment. **f]** Interpolation of 2-AG levels resulting from BK (1 μM) or ATP and BK co-treatment using a 2-AG standard curve. All values represent maximum $\Delta F/F_0$.

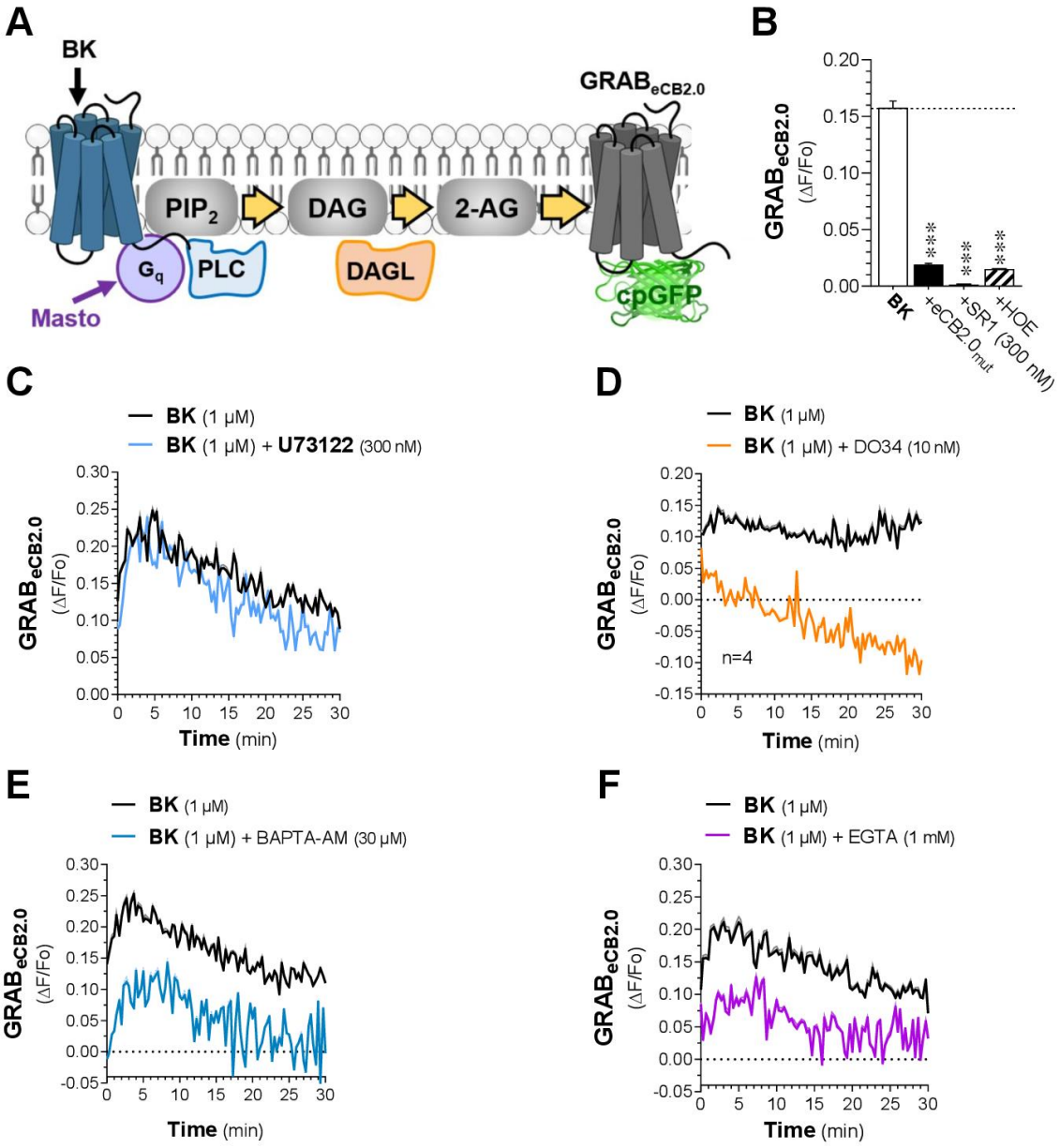

Figure 4.3: BK increases 2-AG levels in N2a cells by acting at the B_2R receptor through a DAGL-dependent mechanism. N2a cells were transfected with GRAB$_{eCB2.0}$ and changes in GRAB$_{eCB2.0}$ fluorescent signal were detected using a 96 well plate reader. **a]** Schematic illustrating the mechanism of BK-dependent 2-AG production. **b**] Effect of BK (1 μM) on GRAB$_{eCB2.0}$ fluorescent signal in cells pretreated with SR1 (300 nM), the B_2R antagonist HOE 140 (HOE, 300 nM), or in cells expressing mut-GRAB$_{eCB2.0}$. Determined by averaging $\Delta F/F_0$ between 4- and 5-min of treatment. error bars represent s.e.m. **c-f]** Effect of U73122 (300 nM; c), DO34 (10 nM; d), BAPTA-AM (30 μM; e), and EGTA (1 mM) on the time course of BK (1 μM)-stimulated increase in GRAB$_{eCB2.0}$ fluorescent signal. N= 3-6 independent experiments. Shaded area represents s.e.m.

2-AG paracrine signaling

The 2-AG stimulated by BK has the potential to act in an autocrine and paracrine manner but expressing GRABeCB2.0 in a single cell type cannot differentiate between these two signaling modalities. Therefore, we developed a mixed cell culture assay that uses HEK293 cells expressing the $GRAB_{eCB2.0}$ as a cell-based reporter system for 2-AG acting as a paracrine signaling molecule (Figure 4A). Briefly, HEK 293 cells were transfected with $GRAB_{eCB2.0}$ and 12 hours after transfection, N2a cells were plated with the HEK 293 cells. Live-cell confocal microscopy was used to measure changes in $GRAB_{eCB2.0}$ signal. Since HEK 293 cells do not exhibit detectable DAGL activity, any activity-dependent 2-AG detected by the sensor in HEK 293 cells will likely be produced in the N2a cells. To validate $GRAB_{eCB2.0}$ activation in this mixed culture model, the cells were treated with 2-AG in order to directly activate the sensor. Figure 4B shows that 2-AG (1 µM)-induced a rapid increase in $GRAB_{eCB2.0}$ fluorescent signal that reached a maximum $\Delta F/F_0$ signal of 2.2, and this increase plateaued within 2 min and remained stable over the 10 min imaging session. Vehicle treated cells did not exhibit any significant increases in fluorescent signal. After confirming the activation of the $GRAB_{eCB2.0}$, we tested if receptor-dependent stimulation of endogenous 2-AG production acted in a paracrine fashion by treating the mixed culture with BK (1 µM) alone or in combination with ATP (300 µM). Both BK and BK+ATP increased the $GRAB_{eCB2.0}$ fluorescent signal in HEK 293 cells in the co-culture experiments, with a maximum $\Delta F/F_0$ signal of 0.12 obtained with BK and 0.48 with the BK and ATP co-treatment (Figure 4C-D). The dynamics of the time-dependent changes in $GRAB_{eCB2.0}$ (fluorescent increase and decay characteristics) mirrored the results in N2a-$GRAB_{eCB2.0}$ cell treated with either BK or BK

and ATP (Figure 1B-C). Notably, Figures 4C-D also show that when these treatments were tested in a culture of HEK 293 cells alone that had been transfected with $GRAB_{eCB2.0}$, BK as a single agent and as co-treatment with ATP produced a small increase in $GRAB_{eCB2.0}$ (maximum $\Delta F/F_0$ = 0.04 and 0.19, respectively) which returned to baseline levels within 2 min and then proceeded to steadily decrease, which indicates that these treatments triggered the production and then degradation of endocannabinoids in the HEK 293 cells. Therefore, the $GRAB_{eCB2.0}$ activation in the mixed co-culture model is a summation of both increased N2a 2-AG production and the transient peak and decay seen in the HEK 293 cells. Despite the increase in co-culture $GRAB_{eCB2.0}$ activation induced by both BK alone and BK in combination with ATP, the magnitude of this activation is dependent on the stimulus. The BK+ATP induced co-culture $GRAB_{eCB2.0}$ signal was ~5-fold greater than the BK-induced $GRAB_{eCB2.0}$ signal (area under curve = 241.5 and 40.3, respectively) (Figure 4E). This indicates that treatment with BK+ATP likely results in greater 2-AG paracrine activity compared to BK alone, potentially due to the differences in the mechanism of 2-AG production and release between the two treatments (Figure 4F). Thus, the extent to which 2-AG participated in paracrine signaling in this mixed co-culture model is dependent on the stimulus.

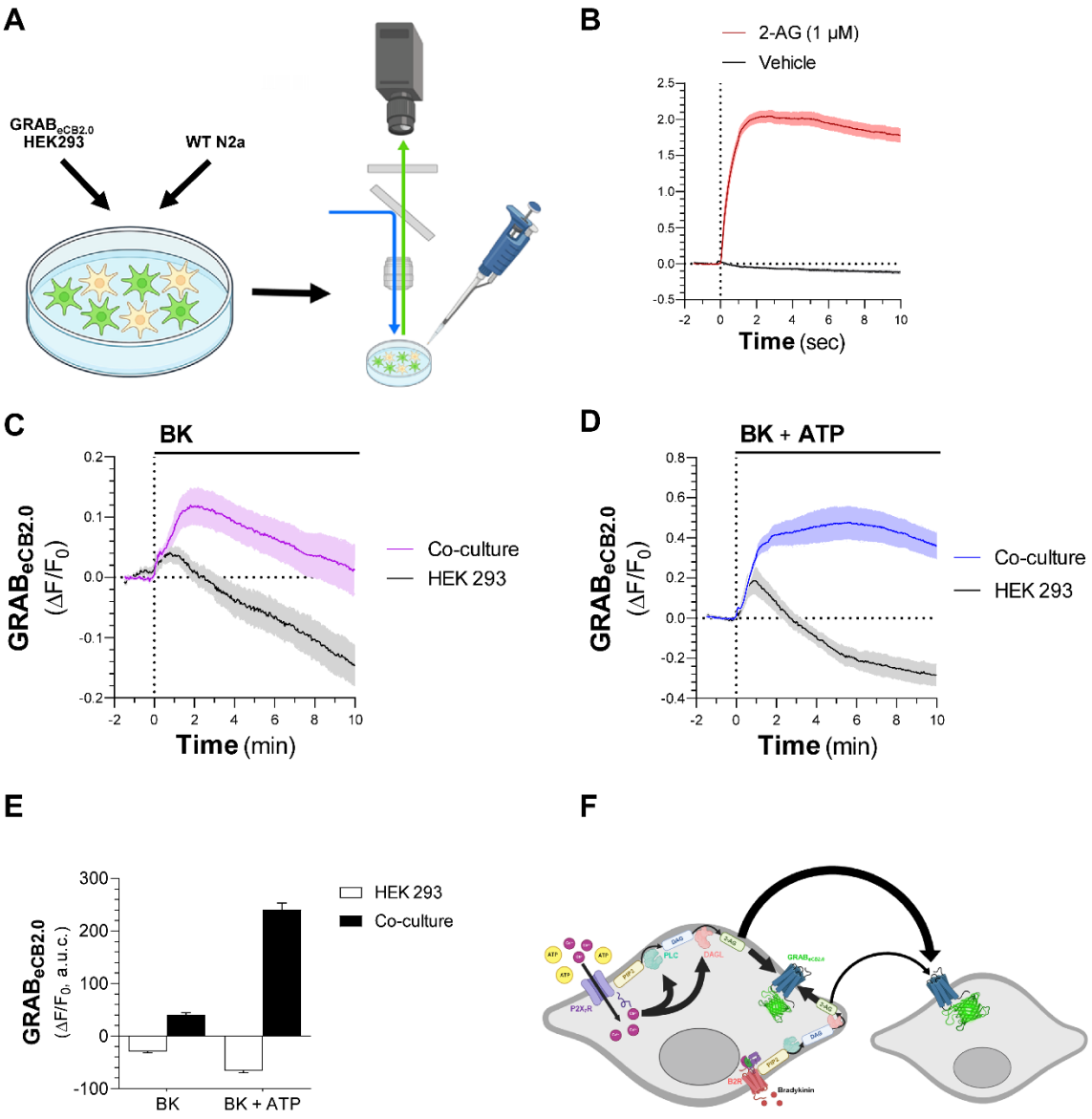

Figure 4.4: 2-AG Paracrine signaling in a mixed co-culture model is stimuli-dependent. HEK 293 cells expressing GRAB$_{eCB2.0}$ were co-cultured with wild-type N2a cells and changes in GRAB$_{eCB2.0}$ fluorescent signal were detected using live-cell confocal microscopy. **a]** Schematic of co-culture protocol for measuring 2-AG paracrine activity. **b]** Validation of GRAB$_{eCB2.0}$ function in co-culture model by direct-activation with 2-AG (1 μM) or vehicle. N= 27-36 cells from 3 independent experiments. Shaded area represents s.e.m. **c-d]** Effect of BK (1 μM) (c) or co-treatment of BK (1 μM) and ATP (300 μM) (d) on the time-course of GRAB$_{eCB2.0}$ fluorescent signal in co-culture or in culture containing only HEK 293-expressing GRAB$_{eCB2.0}$ cells. For co-culture experiments, N= 30-35 cells from 3 independent experiments. For culture containing exclusively HEK 293 cells, N=8-15 cells from single experiment. Shaded area represents s.e.m. **e]** Total GRAB$_{eCB2.0}$ fluorescent signal response (area under the curve) of data presented in Fig 4c-d. **f]** Potential mechanism of stimulus-dependent paracrine activation of GRAB$_{eCB2.0}$.

4.3 DISCUSSION

2-AG signaling is implicated in various physiological processes ranging from short and long-term synaptic plasticity to nociception due to its widespread activity in different cell types and brain regions [19]. 2-AG's pathophysiological role relies on its on-demand production in diverse cell types in the brain and its subsequent action at one or more molecular targets. As a further complexity, 2-AG's diverse signaling role is likely a combination of both paracrine and autocrine signaling in the brain. The earliest description of 2-AG's action in the brain focused on its role as a neurotransmitter. Electrophysiology experiments demonstrated that 2-AG acted as a retrograde neurotransmitter at GABAergic and glutamatergic synapses[36]. This form of paracrine signaling involves activity-dependent or metabotropic-dependent production of 2-AG in a post-synaptic neuron[16]. 2-AG can then travel to the presynaptic neurons where it can activate CB_1R, resulting in decreased pre-synaptic neurotransmitter release[33]. This retrograde signaling can regulates several forms of synaptic plasticity, including DSI\DSE and LTD[33,38]. Since the discovery of 2-AG in retrograde signaling, its actions as a paracrine signaling have expanded to include neuronal-astrocytic and neuronal-microglial crosstalk[43,201].

Neurons and glial cells can express both 2-AG synthesis and catabolic machinery as well as molecular targets, indicating the potential role of autocrine signaling in 2-AG-dependent neuromodulation. For instance, post-synaptic expression of DAGLα (2-AG synthetic enzyme), ABHD6 (2-AG metabolic enzyme), and $GABA_A$ receptor (2-AG target) means that neuronal 2-AG has the capacity to directly act on the neurons it is produced in[58]. Similarly, microglia express DAGLβ (synthesis), ABHD6/MAGL (degradation), and

CB_2R, although the expression of these enzymes can vary based on microglial activation state[202-204]. Therefore, 2-AG produced in a given cell can activate signal transduction pathway through autocrine or paracrine mechanisms. Understanding what molecular mechanisms determine if 2-AG signaling is autocrine, paracrine, or both can further characterize 2-AG's role in the body and the effects of drugs that target 2-AG signaling, such as inhibitors of 2-AG hydrolysis. Here we present a new mixed cell culture model that uses the recently developed eCB sensor as a reporter to measure 2-AG paracrine signaling and show that 2-AG paracrine signaling is stimuli-specific. Further study is needed to determine if ATP alone can trigger a significant level of paracrine 2-AG activity. Since paracrine activation only accounted for about 18% of BK-stimulated 2-AG signaling, it is likely that the paracrine activation observed with the BK and ATP co-treatment is in large part due to ATP. This will help solidify the stimulus-specific model of paracrine signaling.

2-AG is hydrophobic and requires binding proteins, including the fatty-acid binding proteins 3, 5 and 7, to transverse an aqueous environment[205]. Therefore, paracrine 2-AG signaling can be limited by the presence of these 2-AG binding proteins that helps with the transport of 2-AG. This $GRAB_{eCB2.0}$ co-culture reporter system can be used to study the effects of binding proteins in transporting 2-AG to its targets. The results presented here were generated in the presence of 0.1 mg/ml bovine serum albumin, which is a known cannabinoid binding protein[206]. However, other proteins may be involved in 2-AG transport, including the Fatty Acid Binding proteins. This reporter can identify and characterize these binding proteins and allow us to better understand how 2-AG reaches its target

This model can also be used to study 2-AG hydrolysis. The decay in $GRAB_{eCB2.0}$ fluorescent signal in the N2a, HEK 293, and co-culture experiments following treatment with BK or BK and ATP indicates that the 2-AG might be degraded, since enzymatic hydrolysis is the predominant mechanism of terminating 2-AG signaling in the body[19]. Multiple enzymes can hydrolyze 2-AG, including monoacylglycerol lipase, ABHD6, and ABHD12, some of which are endogenously expressed in N2a and HEK 293 cells. The co-culture model can also allow for the use of genetic tools, such as overexpression and knock-out, of one or more of these hydrolyzing enzymes in only one cell type, thus allowing for changes in enzyme expression in either the 2-AG synthesizing cells or the target cells. This can help dissect the different, cell-specific mechanisms by which 2-AG signaling in regulated in the brain. For instance, 2-AG neurotransmission can be regulated by both MAGL, which is a pre-synaptic enzyme located, and ABHD6, a post-synaptic enzyme expressed at the site of 2-AG synthesis, and both enzymes have different effect on 2-AG-dependent synaptic plasticity[19]. This indicates a fine-tuned mechanism for controlling 2-AG signaling that is still not well understood. Furthermore, our results used N2a in an undifferentiated state along with a non-neuronal line in the form of HEK 293 cells. Thus, these results might not reflect synaptic 2-AG signaling mechanisms such as those involved in 2-AG mediated synaptic plasticity. However, this proof-of-concept indicates that this method can be used in higher order models such as neurons in primary culture or mixed primary culture containing neurons and glia in order to study synaptic 2-AG signaling.

Finally, these results provide insight into how inflammatory mediators involved in pain, such as bradykinin and ATP, affect 2-AG signaling in neurons. The release of these

inflammatory mediators can contribute to pain hypersensitivity, which is a result of decreased threshold of sensory neurons (or peripheral sensitization) or increased excitability of neurons in central pain pathways (known as central sensitization)[207,208]. Here, we describe for the first time the mechanism by which bradykinin stimulates 2-AG production in a neuronal model and demonstrate that only a small proportion of this 2-AG travels to other cells in a paracrine fashion. However, when combined with another inflammatory mediator, ATP, the paracrine activity of 2-AG increases. Studies in mice and dorsal root ganglia cultures indicate that this 2-AG can act at TRPV1 receptors to have an anti-nociceptive effect[199]. Furthermore, other 2-AG targets such as CB_1R, which is also expressed along the pain pathways, can decrease the hyperexcitability of neurons, which can potentially limit BK-mediate sensitization. Therefore, 2-AG may be part of a negative feedback loop such that it is stimulated by BK but acts at multiple target proteins to limit BK's effect on the sensitization and excitability of nociceptors. Since increasing endogenous 2-AG can have a therapeutic benefit in conditions like neuropathic pain, understanding where this 2-AG is coming from and the role it is playing can be important in understanding how therapeutics that target the eCB system, like 2-AG hydrolysis inhibitors, exert this therapeutic benefit.

Chapter 5.

Regulation of ABHD6 Activity by a Membrane-Associated Enhancing Factor

5.1 INTRODUCTION

The enzyme α/β hydrolase domain containing 6 (ABHD6) is a multifunctional serine hydrolase that regulates a plethora of biological processes including neurotransmission, metabolism, and inflammation[58]. ABHD6 was first identified as a catabolic enzyme that hydrolyzes the endocannabinoid 2-AG, a lipid neuromodulator that is an agonist at the cannabinoid CB_1 and CB_2R receptors (CB_1R and CB_2R, respectively)[40,46]. Since this initial characterization, ABHD6 is now known to metabolize multiple endogenous substrates throughout the body[51,55]. However, in the central nervous system, ABHD6's regulation of 2-AG levels likely underlies its physiological role. 2-AG acts as a retrograde neurotransmitter and mediates both long and short-term synaptic plasticity, and ABHD6 knock-down and inhibition affects long-term synaptic plasticity in primary neurons in culture[46]. Thus, ABHD6 can regulate 2-AG's activity at its targets, including the CB_1R.

The CB_1R was first discovered as one of the receptors activated by Δ^9-tetrahydrocannabinol, the psychoactive chemical found in cannabis that has been used for thousands of years for its medicinal and recreational effects[1]. Despite the promise of increasing CB_1R signaling for a therapeutic effect, the use of exogenous CB_1R-targeting molecules is limited by their adverse effects, including anxiety and hallucinations[2,4]. Therefore, enhancing 2-AG-signaling at the CB_1R by inhibiting ABHD6 can increase CB_1R signaling in a targeted manner, as it relies on the endogenous, activity-dependent

production of 2-AG[58]. Thus, ABHD6 inhibition is a novel therapeutic strategy for the treatment of devastating neurological disorders.

Since the identification of ABHD6, multiple classes of ABHD6 inhibitors have been developed, including the carbamate WWL70 and the 1,2,3-triazole urea KT-182[169,209]. These inhibitors have subsequently been tested and demonstrate efficacy in multiple rodent models of neurological diseases, including models of epilepsy, neuropathic pain, and migraine[47,49,194]. Despite promising pre-clinical evidence of the efficacy of ABHD6 inhibitors, these inhibitors carry a risk of off-target effects due to their mechanism of action. For instance, although WWL70 and KT-182 have distinct chemical structures, they inhibit ABHD6 in a similar manner: both compounds covalently modify a nucleophilic serine, Ser148, in the active site of ABHD6, irreversibly inhibiting its hydrolysis activity. A majority of the ABHD6 inhibitors developed as of today share this irreversible mechanism of action. The Ser148, along with histidine 306 and aspartate 278, together make up the catalytic triad, which are three amino acid residues in the active site of ABHD6 that are necessary for its hydrolysis activity[51]. The catalytic triad, and specifically the nucleophilic serine, is a conserved feature in all serine hydrolase enzymes, of which there are over a hundred found in humans[73,210]. The targeting of this conserved residue in an irreversible manner carries the risk of potential off-target effects and may limit the clinical use of ABHD6 inhibitors[211]. Efforts to develop novel classes of selective and efficacious ABHD6 inhibitors have been stymied by several factors, including a lack of understanding about 1] ABHD6's structure-function relationship; 2] the mechanisms regulating ABHD6 hydrolysis activity, including its substrate selectivity; and 3] the role and mechanism of its non-hydrolysis activity. Identifying the molecular determinants of ABHD6 activity can help

us understand how to selectively inhibit ABHD6 and the cellular and molecular effects of this inhibition. Here we show that ABHD6 immunoprecipitated from HEK 293 cells exhibits a low level of hydrolysis activity that can be rescued by reintroducing the crude membrane fraction of the HEK 293 cells back to the enzyme. This indicates that a previously undescribed “membrane-enhancing factor” positively regulates ABHD6 activity, and that ABHD6 in different subcellular fractions has different levels of activity that may be result of this regulatory mechanism. Finally, we show that a first-in-class proteolysis-targeting chimera (PROTAC) inhibitor reduces ABHD6 activity in a time-dependent manner.

5.2 RESULTS

Activity of Immunoprecipitated ABHD6

To study the mechanisms regulating ABHD6 activity, HEK 293 cells were transfected with hABHD6 with an N-terminal Myc-tag (Myc-ABHD6). The cells were then lysed, the Myc-ABHD6 was immunoprecipitated using anti-Myc antibody conjugated to agarose beads, and a Coomassie stain was used to confirm the efficiency and purity of the immunoprecipitation (Figure 1A). Figure1B shows that the immunoprecipitated myc-ABHD6 exhibited hydrolysis activity, as determined by measuring the hydrolysis of the fluorogenic substrate 4-Methylumbelliferyl heptanoate (4-MUH) using a fluorescent plate reader, and that this hydrolysis was inhibited by the selective ABHD6 inhibitor KT-182 (1 µM). To determine the efficiency of the pull-down and confirm ABHD6 activity, we used gel-based activity-based protein profiling. A strong band indicating ABHD6 activity in the ABPP and ABHD6 expression in the western blot were present in the input lysate, elution (sample collected immediately after incubation with excess Myc peptide), and Final IP

(multiple elution fractions combined and desalted to remove the Myc peptide), while the flow through (FT; lysate after antibody incubation) was de-enriched in both ABHD6 activity and protein, as expected (Figure 1C). Quantification of ABHD6 activity normalized to its protein level as determined by ABPP and western blotting, respectively, revealed that the immunoprecipitated Myc-ABHD6 (Final IP sample) had 75% less activity than the Myc-ABHD6 in the input. Thus, immunoprecipitated Myc-ABHD6 retained hydrolysis activity, but this activity was significantly decreased compared to Myc-ABHD6 in HEK 293 lysate.

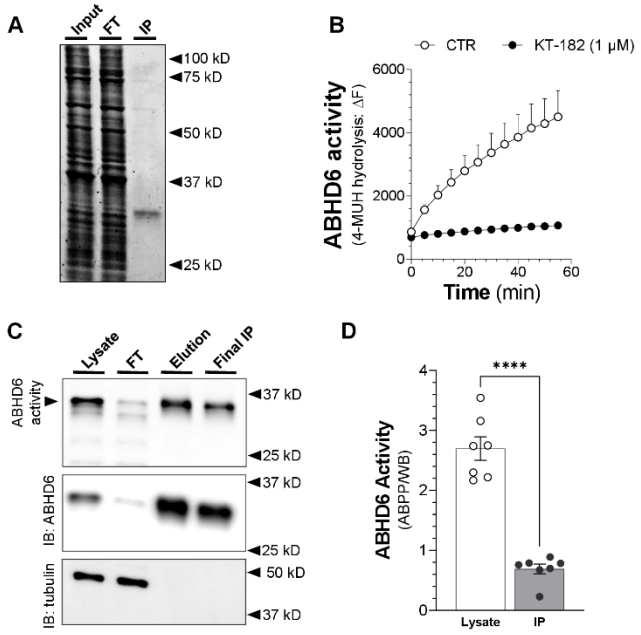

Figure 5.1: Activity of Immunoprecipitated Myc-ABHD6. Myc-ABHD6 was immunoprecipitated from HEK 293 cells with 0.1% triton X-100 and its enzymatic activity was tested using a 4-MUH hydrolysis assay or gel-based ABPP. A] Immunoprecipitated ABHD6 (IP) as detected by Coomassie stain following gel-electrophoresis. B-C] IP Myc-ABHD6 exhibits activity that is inhibited by the selective ABHD6 inhibitor KT-182 (1 μM, 30 min) as measured by hydrolysis of 4-MUH (B) and gel-based ABPP (C). N= 3 independent experiments for 4-MUH assay. Error bars represent s.e.m. D] Quantification of ABHD6 activity normalized to its protein level from the gel based ABPP and western blot experiments in (C). N = 7 independent experiments and error bars represent s.e.m. ****P < 0.0001 significant difference compared to HEK 293 lysate. Significance determined by an un-paired t-test.

Membrane-enhancing factor increases Myc-ABHD6 activity

ABHD6 is a membrane protein with a single transmembrane domain that can localize to the plasma membrane and intracellular membranes, such as in endosomes. Removing ABHD6 from the lipids and proteins residing in the membrane could affect its activity. Therefore, we tested if re-introducing immunoprecipitated Myc-ABHD6 to the crude membrane fraction without any cytosolic and nuclear components (P2 fraction) of un-transfected HEK 293 cells, which have negligible endogenous ABHD6 expression, rescued the loss of activity. The P2 fraction was isolated from HEK 293 cell lysate by first removing nuclei and un-lysed cells with a slow centrifugation step, following an ultracentrifugation step (100,000 x g, 60 min) to pellet the P2 membrane fraction (Figure 2A). Figure 2B shows that the Myc-ABHD6 exhibited a low-intensity band when activity was measured using gel-based ABPP, despite a large signal in the western blot indicating the presence of protein, and that the P2 fraction exhibited multiple faint bands, but no detectable ABHD6 protein expression. However, when the Myc-ABHD6 and P2 fraction were combined, the ABPP signal increased compared to Myc-ABHD6 alone, in spite of a slight decrease in the protein level of ABHD6. To confirm that this membrane enhancing effect of Myc-ABHD6 also increased its hydrolysis of a substrate, and test if this enhanced activity could be inhibited by an ABHD6 inhibitor, we tested the effect of the P2 fraction on immunoprecipitated myc-ABHD6 using the 4-MUH fluorescent assay. Similar to the ABPP results, Myc-ABHD6 alone had a low but detectable level of activity when measuring 4-MUH hydrolysis; however, combining the Myc-ABHD6 and P2 fraction increased the hydrolysis activity by approximately 10-fold, which was reduced by KT-182 by about 91% (Figure 2C). Since the P2 fraction contains both lipids and proteins, we

wanted to determine which of these constituents contributed to the membrane-enhancing effect. Therefore, we depleted the P2 fraction of protein by treating it with proteinase K, followed by heat inactivation of the sample to inactivate the proteinase K. Figure 2C shows that this protein-depleted P2 fraction failed to enhance the activity of Myc-ABHD6, indicating that one or more proteins may underlie this membrane-enhancing effect.

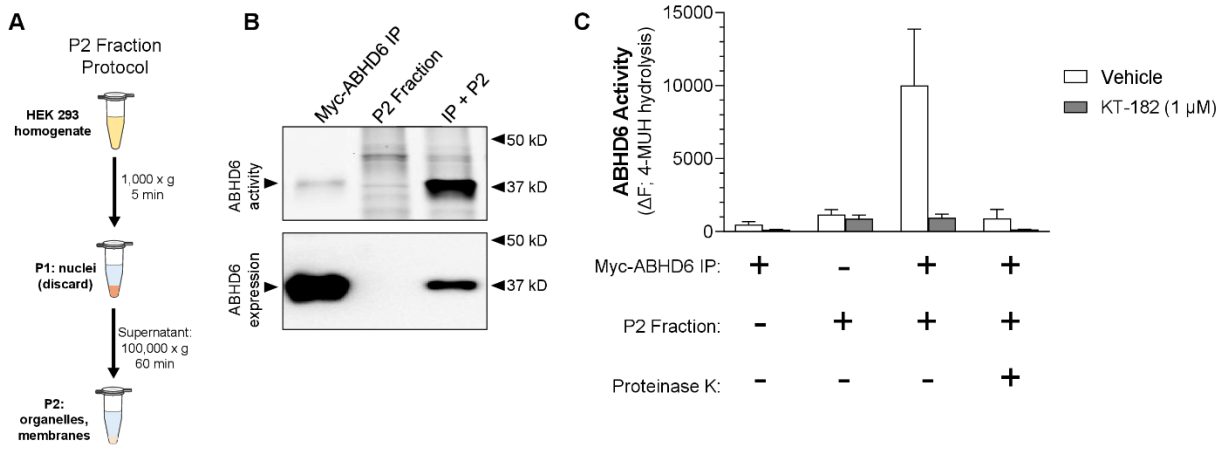

Figure 5.2: Membrane-associated enhancing factor rescues decrease in immunoprecipitated Myc-ABHD6 activity. A] Crude membrane fraction (P2 fraction) from HEK 293 cells was isolated from the cytoplasm and nuclear fraction using differential centrifugation. B] ABHD6 activity and protein expression in IP Myc-ABHD6 sample, P2 fraction, and after IP and P2 were combined as measured by gel based ABPP and western blotting. C] Effect of P2 fraction on IP Myc-ABHD6 enzymatic activity as measured by 4-MUH hydrolysis. Role of protein in the enhancing effect tested by treating P2 fraction with proteinase K for 2 hr followed by heat inactivation of the proteinase K before combining with Myc-ABHD6. N = 4 independent experiments; error bars represent s.e.m.

ABHD6 activity is dependent on subcellular localization

Having determined that the P2 fraction could enhance the activity of Myc-ABHD6 using two separate enzyme activity read-outs, we next questioned whether a specific membrane fraction contributed to this affect since the P2 is a crude fraction containing

the plasma membrane and many organelles. ABHD6 can localize to the plasma membrane and intracellular compartments, and subcellular fractionation assays in BV-2 cells show that ABHD6 hydrolysis activity can be found in mitochondrial and microsomal fractions, with the lowest level in the cytosol as expected since ABHD6 is a membrane protein. However, how this activity correlates to ABHD6 expression levels, and whether ABHD6 activity might be differentially regulated in different membranes has not been studied. First, to confirm the results produced in the BV-2 cells, we used a crude subcellular fractionation protocol (Figure 3A) on lysate from neuro2a (N2a) mouse neuroblastoma cells, which endogenously express ABHD6 and therefore are likely to not exhibit artifacts related to altered trafficking of overexpressed proteins. Figure 3B shows that when the N2a fractions were assayed using gel-based ABPP, the mitochondrial fraction has the greatest amount of activity, followed by the microsomal fraction, and no detectable activity in the cytosolic fraction, which reflects the results from the BV-2 cells. However, the endogenous expression of ABHD6 in the N2a cells was too low to be detected by western blot; therefore, we could not determine whether this activity was a result of differences in protein levels.

To overcome this limitation, we applied the subcellular fractionation protocol to lysate from HEK 293 cells overexpressing Myc-ABHD6 and again used gel-based ABPP to measure ABHD6 activity levels and western blotting to measure ABHD6 protein levels. Figure 3C shows that Myc-ABHD6 activity levels in the three fractions mirrored that of the N2a cells, with the greatest activity in the mitochondrial fraction and no detectable activity in the cytosolic fraction. Furthermore, using a western blotting, we determined that the mitochondrial fraction also had the greatest level of ABHD6 protein expression.

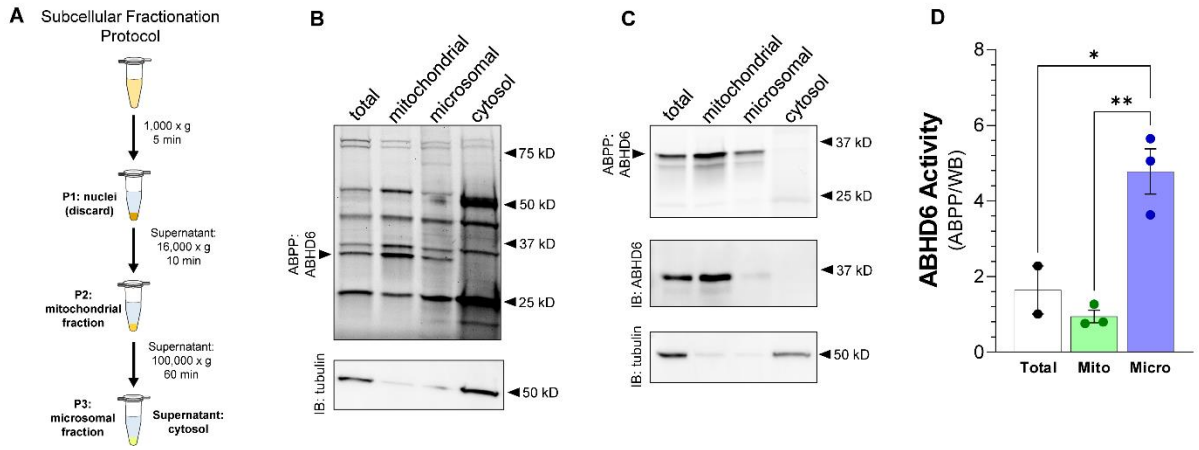

Figure 5.3: ABHD6 activity is dependent on its subcellular localization. Subcellular fractions of wild-type N2a cells of HEK 293 cells transfected with Myc-ABHD6 were isolated by differential centrifugation, and ABHD6 activity and protein levels were detected by gel-based ABPP and western blotting, respectively. A] Crude subcellular fractionation protocol. B] N2a cells exhibit ABHD6 activity in the mitochondrial and microsomal fraction, but not cytosolic fraction, as measured by gel based ABPP. C] Myc-ABHD6 activity and expression in different fractions of HEK 293 cells overexpressing Myc-ABHD6. D] Quantification of ABHD6 activity normalized to its protein level from the gel based ABPP and western blot experiments in (C). N = 2-3 independent experiments and error bars represent s.e.m. *P < 0.0332 and **P < 0.0021 significant difference compared to microsomal fraction. Significance determined using a One-way ANOVA with a Tukey's multiple comparisons test.

However, when the ABHD6 activity was normalized to its protein levels, the microsomal fraction had the greatest amount of activity relative to the amount of protein (Figure 3D). This may indicate that the mitochondrial fraction contains high abundant but low activity ABHD6, while the microsomal fraction has less, but this ABHD6 has greater enzymatic activity. This difference in subcellular ABHD6 activity demonstrates the possibility of a mechanism that can regulate ABHD6 activity in the cell in a subcellular localization-specific manner and may also contribute to the membrane-enhancing effect of the P2 fraction.

Characterization of an ABHD6 PROTAC inhibitor

The membrane-enhancing factor and the differential subcellular activity of ABHD6 indicates an endogenous regulatory mechanism that reversibly modulates ABHD6 activity. Although the identity of the membrane-enhancing factor has not been identified, we wanted to explore the possibility of developing an inhibitor that could also reversibly inhibit ABHD6. To this end, we obtained the novel ABHD6 inhibitor DX-767, developed by Dr. Philippe Diaz, which is designed to reversibly interact with ABHD6, in contrast to most of the present inhibitors which covalently modify the nucleophilic Ser148 in the active site. Aside from being reversible, DX-767 is also designed to be a proteolysis-targeting chimera (PROTAC) drug and has three components: 1] a ligand that binds to ABHD6; 2] a ligand that recruits an E3 ubiquitin ligase; and 3] a linker that connects the two functional group[212]. Thus, DX-767 inhibition relies on the targeted degradation of ABHD6 by the ubiquitin-proteasome system. To test the effect of DX-767 on ABHD6 activity, we treated intact N2a cells with DX-767 (50 µM) for 1, 2, 4, 6, and 8 hours since both the compound entering the cell and the targeted degradation of ABHD6 are likely-dependent processes. Figure 4A-B show that DX-767 resulted in a time-dependent decrease in ABHD6 activity that reached a maximum inhibition of 60% at eight hours of treatment, as measured by gel-based ABPP. Gel-based ABPP was also used to measure the selectivity of DX-767. Figure 4C shows that at eight hours of treatment, the major off-target of DX-767 was fatty acid amide hydrolase (FAAH), which was inhibited by 93%. These results indicate that DX-767 can enter cells and selectively decrease ABHD6 activity in a time-dependent manner but can target other eCB hydrolyzing enzymes such as FAAH. Further study is needed to measure how DX-767 affects ABHD6 protein levels,

identify the maximum level of inhibition that can be achieved with DX-767, test the effect of DX-767 on 2-AG hydrolysis, and eventually develop PROTAC inhibitors with greater selectivity for ABHD6. DX-767 ultimately represents a proof-of-concept for a novel class of ABHD6 inhibitors that can reversibly target ABHD6 for a potential clinical benefit and is an important step in the development of new ABHD6 inhibitors.

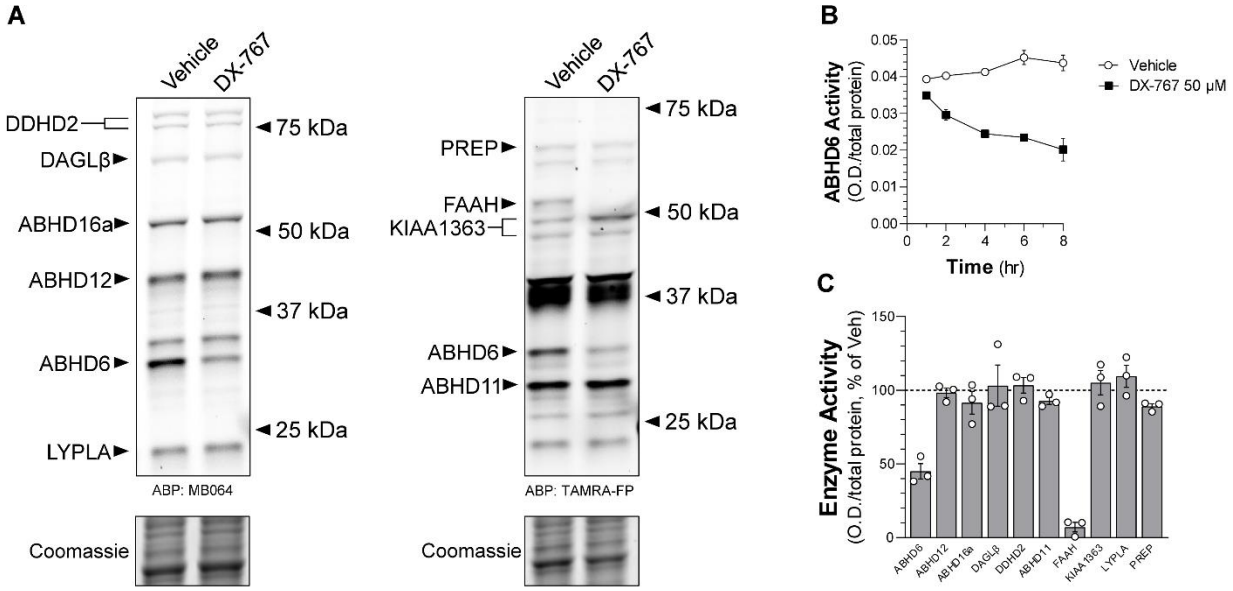

Figure 5.4: The novel ABHD6 PROTAC inhibitor DX-767 inhibits ABHD6 activity in a time-dependent manner. N2a cells were treated in situ with the ABHD6 inhibitor DX-767. ABHD6 activity was measured by isolating the membrane proteome of the cells and using gel-based ABPP. A] Inhibition of ABHD6 by DX-767 (50 μM, 8 hr). B] Quantification of ABHD6 activity measured by gel-based ABPP shown in (A). N= 2-4 independent experiments; error bars represent s.e.m. C] Off-target effects of DX-767 (50 μM, 8 hr). N= 3 independent experiments; error bars represent s.e.m.

5.3 Discussion

ABHD6 has multiple roles in the body, ranging from hydrolysis of 2-AG in the brain to regulating levels of bis(monoacylglycero)phosphates in the liver. How this ABHD6 activity is regulated at a molecular level by interacting proteins and lipids remains unknown. Despite preclinical evidence that ABHD6 inhibitors have a potential therapeutic benefit in

several models of neurological diseases, we still do not understand how and why these inhibitors work. Here, we report the first evidence of a mechanism underlying the positive regulation of ABHD6 activity in the form of a membrane-associated enhancing factor.

Regulation of ABHD6 Activity

Previous evidence of a regulatory mechanism that can affect ABHD6 activity in vivo is limited to the negative regulation of ABHD6 by the protein carnitine-palmitoyltransferase 1C (CPT1C). CPT1C directly interacts with ABHD6, based on FRET and mutational studies, and decreases ABHD6 hydrolysis activity in an overexpression HEK 293t model system and in mouse hypothalamus brain tissue[213]. Furthermore, this negative regulation can be attenuated when brain malonyl-CoA levels decrease, which can occur during fasting. Therefore, CPT1C can enhance 2-AG levels in the hypothalamus by decreasing ABHD6 activity, but not its expression, in response to the nutritional state of the mouse. However, the nature of this interaction and how CPT1C decreases ABHD6 activity in a brain-region-specific manner has not been described. The brain region specific effects of CPT1C, and our data showing a potential mechanism of positive regulation, indicates that there are likely multiple molecular determinants of ABHD6 activity. Identifying these determinants can allow us to: 1] better model ABHD6 for in vitro and cell-based studies; 2] determine if these molecular interactors affect the binding and effect of ABHD6 inhibitors; 3] identify how endogenous interactors can reversibly modulate ABHD6 activity as a starting point to develop novel ABHD6 inhibitors.

Studying the mechanism of ABHD6 activity and its role in signaling has relied on cell model systems. However, the results of these models are not consistent. For instance, ABHD6 inhibition increases glutamate and carbachol-dependent 2-AG

production in neurons in primary culture but does not affect bradykinin-stimulated 2-AG levels in N2a cells[46]. There are several possibilities that underlie this discrepancy: although all three stimuli target metabotropic Gαq-coupled receptors, ABHD6 activity may be stimuli-specific. Another possibility is that N2a ABHD6 expression is too low to regulate 2-AG levels, or that the ABHD6 has less activity. The negative regulation by CPT1C and the positive regulation by the membrane-associated enhancing factor starting points for identifying why ABHD6 activity regulates 2-AG levels in some cell models but not others. Understanding why the effects of ABHD6 inhibition vary so drastically based on cell model system can help us develop and use physiologically relevant model systems to dissect the mechanism of ABHD6-regulated 2-AG and test ABHD6 inhibitors.

Developing ABHD6 Inhibitors: the past, present, and future

Multiple classes of ABHD6 inhibitors have been developed in the past 20 years, all of them targeting the active site of ABHD6 where 2-AG is hydrolyzed, and specifically interacting with Ser148 in the active site. While targeting the nucleophilic serine is an effective strategy to inhibit ABHD6 since it is essential for hydrolysis activity, this serine residue is conserved in the serine hydrolase family and is present in the hundreds of enzymes in this family, potentially limiting the selectivity of these inhibitors. Therefore, novel classes of inhibitors are needed to optimize selectivity for ABHD6 over other serine hydrolases. Reviewing the past development of ABHD6 inhibitors highlights the similar mechanism of action of all the previous inhibitors.

Early evidence of the role of serine hydrolases, and ABHD6 specifically, in the regulation of brain eCB levels relied on non-selective serine hydrolase inhibitors. Examples include methyl arachodonoylfluorophosphanate (MAFP)[214] and phenyl

methylsulfonyl fluoride (PMSF)[215]. Both MAFP and PMSF are irreversible inhibitors and covalently modify the nucleophilic serine found in the active site of all serine hydrolases. The phosphonate-enzyme complex that forms when MAFP with Ser148 resembles the tetrahedral intermediate in the first step of 2-AG hydrolysis, while PMSF results in a sulfonate bound enzyme that is similar the tetrahedral intermediate during the second, saponification step, of 2-AG hydrolysis[216]. while newer inhibitors are more selective, they generally have a similar mechanism of action to MAFP[217].

One of the first classes of selective ABHD6 inhibitors was the carbamate class. Carbamates are characterized by a functional group made up of a carbonyl group, alkoxyl group, and an amino group. This functional group is similar to both amides and esters in that it can interact with and modify Ser148 in ABHD6, while being more proteolytically and chemically stable compared to amides and can pass through cell membranes and potentially the blood brain barrier[218]. Drugs containing the carbamate functional group have been approved for medical use for decades, including as acetylcholinesterase inhibitors (physostigmine), anti-cancer drugs (docetaxel), anticonvulsants (retigabine), and others[218]. The prototypical carbamate ABHD6 inhibitor is WWL70[209] has an anti-inflammatory effect in a mouse model of TBI[219] and can increase 2-AG and decrease prostaglandin formation in LPS-stimulated BV-2 cells[220]. However, the efficacy in the TBI model and in BV-2 cells may not rely on ABHD6 inhibition, since the studies either did not do target validation, or the genetic control could not replicate the effect of WWL70. This demonstrates the need for a more potent and selective ABHD6 inhibitor.

Following the development of WWL70, another ABHD6 inhibitor design effort yielded in compounds with a 1,2,3-triazole urea scaffold. This discovery was precipitated

by the advent of click chemistry in the synthesis of small molecule drugs and allowed for the 1,2,3-triazole moiety to be incorporated into different molecules, resulting in new classes of drugs with a number of clinically relevant effects, including anticancer, antibacterial, and antiviral properties[221]. The 1,2,3-triazole is a synthetic molecule that is metabolically stable and is generally soluble in aqueous solutions due to its hydrogen bonding capacity, setting it apart from inhibitors such as MAFP which consist of lipophilic moieties[221]. The use of 1,2,3-triazole in drug synthesis, along with the observation that *N*-heterocyclic ureas exhibited serine hydrolase inhibition, allowed the Cravatt group to use click chemistry to first synthesize broad-spectrum serine hydrolase inhibitors with by a 1,2,3-triazole urea scaffold[222], followed by optimization of these compounds to generate selective DAGLβ[155] and ABHD6 inhibitors[169]. The 1,2,3-triazole urea ABHD6 inhibitors irreversible and covalently modify the nucleophilic Ser148, similar to FPs and carbamates, but have greater a potency and selectivity compared to the early generations of ABHD6 inhibitors. To date, multiple ABHD6 inhibitors in the 1,2,3-triazole urea class have been developed, including a peripherally restricted ABHD6 inhibitor (KT203), a systemic inhibitor (KT182), and an orally active inhibitor (KT185), all of which are more potent that WWL70 at inhibiting ABHD6, with IC_{50}s of 0.24-15.1 nM for KT182, 0.21-13.6 nM for KT185, and 0.31-3.9 nM for KT203 when tested using a combination of in vitro and in situ competitive ABPP as well as a 2-AG hydrolysis assay. These compounds also exhibit a promising selectivity profile when tested on the mouse brain proteome using competitive gel-based ABPP, with KT182 and KT185 only targeting FAAH, LYPLA1, and LYPLA2 at concentrations about 1000-fold greater than the IC_{50} at ABHD6. Despite this increase in potency and selectivity, the 1,2,3-triazole ureas and carbamates are

irreversible, indicating a shared mechanism of action. To date, only one class of reversible ABHD6 inhibitors has been reported.

The development of reversible ABHD6 inhibitors relied on the premise that a small-molecule analog of 2-AG would be able to bind to the active site but could be hydrolyzed by the enzyme and release rather than forming an inhibitor-enzyme complex like the KT compounds and carbamates. This resulted in the discovery of a class of fatty acid inhibitors which resemble 2-AG's structure in that most of them consist of acyl chains with 1-3 degrees of unsaturation esterified to head groups consisting of oxygenated heterocycles (as opposed to the glycerol in 2-AG)[223]. This effort produced multiple ABHD6 inhibitors, albeit with a lower potency than the 1,2,3-triazole ureas and carbamates. The most potent inhibitor (compound 9) inhibited ABHD6 with an IC_{50} of 0.8 μM when tested in homogenate from cells overexpressing ABHD6, while the remaining lead compounds had IC_{50}s in the low-to-mid μM range[223]. Another concern was that these inhibitors were not selective for ABHD6 and inhibited the AEA hydrolyzing enzyme Fatty Acid Amide Hydrolase (FAAH) and to a lesser extent MAGL[223].

While the carbamate, 1,2,3-triazole ureas, and fatty acid ABHD6 inhibitors were some of the first ABHD6 inhibitors to be developed, since then other classes of ABHD6-targeting molecules have been described, including the 1,2,5-thiadazole carbamate JZP-430, which inhibits ABHD6 and FAAH[224], the N-hydroxysuccinimidyl carbamate MJN110, which inhibits MAGL and ABHD6[225], the glycine sulfonamide LEI-106, which is a dual DAGLα/ABHD6 inhibitor[226], chiral, disubstituted piperidinylureas which are DAGLα/ABHD6 inhibitor[227], and the isoindoline carbamate inhibitor AM12100 which has >100 fold selectivity for ABHD6 over FAAH and MAGL[171,228]. These efforts to develop

ABHD6 inhibitors illustrate the potential for both reversible and irreversible ABHD6 inhibitors with a potential clinical benefit.

Here, we began the process of validation a first-in-class ABHD6 PROTAC inhibitor, DX-767 that relies on targeted protein degradation by the ubiquitin proteasomal system to decrease ABHD6 activity. DX-767 decreased ABHD6 activity in N2a cell in a time-dependent manner, indicating that it can enter the cell to exert its effects on ABHD6 activity, which is an important validation since PROTAC inhibitors can have issues when crossing membranes. Further characterization of DX-767 is needed, including measuring its effects on ABHD6 protein levels, testing it in vivo, and using it to inform a drug discovery effort that can lead to PROTAC inhibitors with greater potency and selectivity. This novel class of inhibitors can also be used to interrogate ABHD6's non-hydrolyzing functions. The discovery that ABHD6 interacts with the GluA1 subunit of the AMPA receptor and can reduce the plasma membrane localization of the AMPA receptor, thereby decreasing excitatory neurotransmission mediated by glutamate's action at the AMPA receptor, indicates that ABHD6 can regulate the trafficking of other proteins. Furthermore, mutation of the Ser148 did not affect ABHD6's role in AMPA receptor trafficking, making this the first demonstration of ABHD6's hydrolysis-independent function in the cell. Studying the mechanism and physiological role of the hydrolysis-independent action can be bolstered by an inhibitor like DX-767, since a PROTAC inhibitor decreased the protein levels of the target rather than just covalently modifying the active site Ser148. Thus, our work demonstrates the potential for a reversible and selective ABHD6 inhibitor that can reduce both hydrolysis-dependent and hydrolysis-independent ABHD6 activity.

Chapter 6.

Conclusion

The endocannabinoid system is a complex signaling system that encompasses at least two major signaling lipids, 2-AG and AEA, multiple/overlapping target proteins, and redundant pathways of synthesis and degradation. Elucidating the eCB system's pathophysiological role and the potential of pharmacologically targeting it for a clinical benefit requires: 1] validated experimental approaches for the sensitive and precise detection of changes in eCB levels; 2] model systems that express the molecular machinery involved in regulating eCB levels; and 3] identifying and characterizing therapeutic targets within the eCB system. For my doctoral thesis, I have worked on each of these points by validating and characterizing a novel eCB sensor, using this sensor to describe the mechanism of how inflammatory mediators ATP and bradykinin (BK) stimulate 2-AG production in a neuronal model, and identifying a novel regulatory mechanism of the 2-AG hydrolyzing enzyme and potential therapeutic target ABHD6.

$GRAB_{eCB2.0}$ Characterization

I found that $GRAB_{eCB2.0}$ can be reliably expressed and activated by multiple ligands in two different cell types, HEK293 and neuro2a (N2a) cells, with maximal efficacy achieved with low µM 2-AG and the sensitivity to detect low nM levels of 2-AG. I also determined that the $GRAB_{eCB2.0}$ sensor can also be used to study the mechanism of endogenous 2-AG production and described distinct ionotropic and metabotropic mechanisms of 2-AG production in N2a cells.

In the process of characterizing the $GRAB_{eCB2.0}$, we are the first to report the difference between the $GRAB_{eCB2.0}$ and LC-MS/MS at detecting endogenous 2-AG in the

same model system. Comparing the sensor and LC-MS/MS side-by side revealed stimulus-specific differences between the two read-outs. In N2a cells, ATP-stimulated 2-AG production had a greater magnitude when measured by the sensor compared to LC-MS/MS. This difference likely reflects how LC-MS/MS is often used with bulk cells or tissue and measures total 2-AG levels at a given time point, while the $GRAB_{eCB2.0}$ can detect fast, transient changes in 2-AG at a cellular or subcellular level, such as at the plasma membrane. Intracellular signal transduction, such as the pathways involved in 2-AG biosynthesis, is tightly regulated in time and space. The $GRAB_{eCB2.0}$ provides an opportunity to study how distinct subcellular pools of 2-AG are regulated and the roles that this compartmentalized 2-AG can play.

The $GRAB_{eCB2.0}$ sensor also exhibits cell-specific pharmacological properties as demonstrated by testing direct activation by multiple CB_1R targeting molecules and their analogs in HEK293 and N2a cells. These differences could reflect how the two cells have unique plasma membrane environments (such as lipids or binding proteins), which may also impact CB_1R activity. CB_1R signaling can be cell-specific: for instance, the CB_1R couples to G-proteins differently in GABAergic cells compared to in glutamatergic cells in the mouse brain, and CB_1R can couple to different G_α proteins, sometimes with opposing downstream effects, depending on the cell type it is expressed in. However, $GRAB_{eCB2.0}$ does not bind to these proteins; thus, the difference in $GRAB_{eCB2.0}$ activation likely due to another factor, such as differences in the lipid environment which may affect $GRAB_{eCB2.0}$ conformation and the ability for ligand binding and activation of the sensor. The cell-specific differences in $GRAB_{eCB2.0}$ activation may point towards a form of CB_1R regulation

that needs further exploration, and it also requires for sensor validation in any new model system it is used in to account for these cell-specific differences.

Stimulation of 2-AG Production by Inflammatory Mediators ATP and bradykinin

Activity-dependent 2-AG production underlies much of 2-AG neuromodulation in the brain. 2-AG biosynthesis in neurons is relatively simple, since increased intracellular calcium and availability of 2-AG precursor, such as DAG, is sufficient for this on-demand 2-AG production. Therein lies the challenge of interrogating 2-AG signaling: intracellular calcium is tightly regulated and can be influenced by many receptor-independent and -dependent mechanisms. While the best described receptor-dependent 2-AG production in neurons is by mGluR1/5 and the M1/M3 muscarinic receptors, other signaling molecules known to increase intracellular calcium levels are the inflammatory mediators ATP and bradykinin (BK).

ATP and BK are involved in peripheral sensitization[229,230]. Following an insult, BK, ATP and other inflammatory transmitters that make up an “inflammatory soup” are released and act at their respective receptors on peripheral nociceptors in sensory ganglia of the spinal cord, such as the dorsal root ganglia. These inflammatory mediators decrease the threshold of these nociceptors, resulting in increased neuronal activity (hyperexcitability) in response to a stimuli, manifesting in hyperalgesia[231,232]. Previous studies have found that ATP alone and in combination with BK can increase 2-AG levels in microglia and cultured dorsal root ganglia, respectively. Furthermore, inhibition of 2-AG hydrolysis has an antinociceptive effect in preclinical models, indicating that 2-AG signaling may serve as a negative feedback loop that can reduce the hyperexcitability of the primary afferent nociceptors and produce analgesic effects. However, the mechanism

of how inflammatory mediators regulate neuronal 2-AG levels has not been characterized. Here I show that both ATP and BK increase 2-AG levels in N2a cells with distinct dynamics, including the magnitude and duration of the increase, and this effect is mediated by ionotropic and metabotropic receptors, respectively. Furthermore, this 2-AG is released extracellularly and can act as a paracrine neurotransmitter, which is a significant finding since there are multiple target proteins and cells in the dorsal root ganglia that 2-AG may act at following its release, including CB_2R receptors on microglia as well as CB_1R and TRPV1 receptors on neurons. Thus, these findings expand the scope of 2-AG signaling in neurons to include ATP and BK and demonstrate that the efficacy of 2-AG hydrolysis inhibitors in preclinical models of inflammatory pain may in part depend on stimulated 2-AG production.

Mechanisms of ABHD6 Regulation

ABHD6 is one of the 2-AG hydrolyzing enzymes expressed in the brain, and a potential therapeutic target to enhance 2-AG signaling for a clinical benefit. Surprisingly, despite efficacy in preclinical models of pain and epilepsy, ABHD6 inhibition did not affect ATP or BK-stimulated 2-AG production in N2a cells. Thus, I sought to explore how ABHD6 activity was regulated to account for the possibility that ABHD6 was not constitutively active in intact cells. Here, I discovered that activity of immunoprecipitated ABHD6 was enhanced when combined with the membrane fraction of HEK293 cells and is likely due to an interacting protein that has not yet been identified. This regulatory mechanism indicates the potential of cell and stimuli-specific changes in ABHD6 activity. For instance, if the membrane-enhancing effect is due to a specific interacting protein, the expression

and trafficking of that protein may determine the levels of ABHD6 activity as well as the binding and inhibition of an ABHD6 inhibitor such as KT-182.

Identifying this membrane-enhancing effect will be essential in determining how ABHD6 functions in the cell and can help account for the discrepancies in ABHD6 activity reported in different in vitro assays, intact cells, and animal models. For instance, in vitro ABPP and hydrolysis assays indicate that ABHD6 hydrolyzes 2-AG; however, in intact N2a cells under basal conditions, ABHD6 can act as a diacylglycerol lipase and can synthesize 2-AG rather than hydrolyze it. In the same way, despite the evidence that the ABHD6 inhibitor WWL70 can enhance glutamate and carbachol-stimulated 2-AG production in intact neurons in primary culture and BV2 cells[46,50], the mechanism of action of ABHD6 inhibitors is inconclusive. In the same way, WWL70 has an anti-inflammatory and analgesic effect in a chronic constriction injury mouse model of neuropathic pain; however, WWL70 does not affect 2-AG levels and instead decreases prostaglandin E_2, indicating that the antinociceptive effect is due to attenuation of inflammatory mediator levels rather than an eCB-mediated effect[220]. This illustrates that although ABHD6 inhibitors demonstrate efficacy in preclinical model systems of epilepsy and pain, the mechanism of action of these inhibitors, and whether increased 2-AG signaling underlies these effects, is not yet known.

Developing novel ABHD6 inhibitors

Understanding the structure and function of ABHD6 can also help us develop novel classes of inhibitors. Currently, all ABHD6 inhibitors targeted the active site and Ser148 specifically. This can cause issues with selectivity since the nucleophilic serine is a conserved residue found in hundreds of serine hydrolases in the body. This potential lack

of selectivity not only can result in off-target adverse events, as was the case of the fatty acid amide hydrolase inhibitor[211], but also limits the use of these inhibitors as research tools to interrogate mechanisms of 2-AG hydrolysis. Potential off-target interactions are particularly concerning since most ABHD6 that have been developed are irreversible. Recent efforts to develop reversible and selective inhibitors for other eCB hydrolyzing enzymes have produced compounds such as the benzylpiperidine derivative-class of MAGL inhibitors, which do not covalently modify the nucleophilic serine and instead interact through hydrogen-bonding in the oxyanion hole in the active site[233]. However, no such inhibitors have been developed for ABHD6. Here, I report the initial characterization of a novel PROTAC ABHD6 inhibitor and has the potential be used for both a research tool and a starting point for developing selective and efficacious ABHD6 inhibitors.

Summary and Future Directions

Multiple model systems have been used to describe eCB signaling, and capturing localized and rapid eCB changes in these models is often technically un-feasible. To this end, the $GRAB_{eCB2.0}$ sensor is a novel tool for measuring eCB levels with high spatial (cellular and subcellular) and temporal (seconds) resolution and can be used to study 2-AG signaling in vivo and in intact cells. The work here used $GRAB_{eCB2.0}$ to describe a novel mechanism of 2-AG biosynthesis in N2a cells. Further work is needed to determine how this mechanism of 2-AG production modulates neurotransmission and inflammation in vivo and identify the role this 2-AG signaling plays in a pathophysiological process such as neuropathic pain. Whether 2-AG levels stimulated by inflammatory mediators play a negative feedback role in the peripheral sensitization of sensory neurons, and if this signaling can be enhanced with an ABHD6 hydrolysis inhibitor also remains to be

determined. Furthermore, the degradative mechanism regulating these 2-AG levels needs to be identified since ABHD6 inhibition did not affect ATP- and BK-stimulated 2-AG production in the N2a cells. N2a cells also express the 2-AG hydrolyzing enzymes ABHD12 and FAAH, and 2-AG can undergo oxidation catalyzed by cyclooxygenase-2 or lipoxygenases as well as phosphorylation by diacylglycerol kinase. Thus, pinpointing which metabolic mechanism is relevant in regulating 2-AG levels can highlight a potential target for enhancing 2-AG signaling. Also, the potential that ABHD6 activity may be differentially regulated may underlie the lack of effect of ABHD6 inhibitors. While this question still needs addressing in intact cells, we discovered a novel mechanism of regulation in vitro in the form of a membrane-associated enhancing factor. Many questions remain unanswered, including the identity of this enhancing factor, how the factor interacts with ABHD6, and if this factor plays a role in ABHD6 activity and regulation of 2-AG neurotransmission in vivo. We are pursuing this direction using proteomics and aim to validate any finding in higher-order model systems. The identification of this membrane-associated enhancing factor emphasizes our limited understand about ABHD6 function and the regulation of 2-AG signaling. Thus, further investigation is needed to fully elucidate the role both ABHD6 and 2-AG play in the body with the goal of developing therapeutics that target 2-AG signaling to provide a therapeutic benefit.

Chapter 7.

Materials and Methods

Chemicals and Reagents:

adenosine triphosphate (Sigma), A740003 (Tocris), 2-arachidonoylglycerol (Cayman), 1-arachodonoylglycerol (Cayman), THC (NIDA Drug Supply Program), CP55940 (Cayman), SR141716 (NIDA Drug Supply Program), arachidonoylethanolamide (Cayman), DO34 (AOBIOUS), AM12100 (gift from Dr. Alexander Makriyannis), U73122 hydrate (Sigma), 1,2-bis(2-aminophenoxy)ethane-N,N,N′,N′-tetraacetate-acetoxymethyl ester (BAPTA-AM; Sigma), goat anti-CB_1R c-terminal antibody (gift from Dr. Ken Mackie; 1:1000 for IF and 1:2,500 for immunoblotting); AlexaFluor 647 conjugated donkey anti-goat (invitrogen; 1:1000); and rabbit anti-actin (1:2,500; Sigma Aldrich); IRDye 800 CW conjugates donkey anti-goat (LI-COR); IRDye 680 RD conjugated goat anti-rabbit (LI-COR).

Cloning:

$GRAB_{eCB2.0}$, mut-$GRAB_{eCB2.0}$, and Myc-hABHD6 DNA were subcloned into an AM/CBA-WPRE-bGH plasmid using the BamHI and EcoRI restriction sites. The plasmid was purified (Purelink HiPure Plasmid Maxiprep Kit, Invitrogen, CA) from transformed Stellar Competent Cells (Takara Bio Inc, Japan). The DNA was sequenced and verified (CLC Sequence Viewer 8) prior to use in transfection.

Cell Culture:

Neuro2a cells (gift from Dr. John Scott) and HEK 293 cells were grown in DMEM (Gibco, supplemented with 10% fetal bovine serum and 1% penicillin/streptomycin) at 37°C and 5% CO_2. To passage cells for experiments, a confluent 10 cm plate of cells was detached

by incubating with 0.25% Trypsin-EDTA for 2-3 minutes at 37°C, adding 4-5 mls of supplemented DMEM and using gentle pipetting to remove any cells still attached, then added to a new plate with fresh supplemented DMEM. Cells were passaged every 3-4 days, and for no more than 25 passages.

Transfection:

All transfections were done by incubating DNA with the transfection reagent polyethylenimine (PEI, 25K linear, Polysciences) in a 1:3 ratio in serum free DMEM, incubating for 20-30 min. The DNA/PEI mixture was then added to cells in a dropwise fashion (or directly into media in eCB2.0 96 well-plate assay) without changing the growth media. Cells were transfected when they were at least 50% confluent and were incubated for 24 hours after transfection before harvesting or using for GRABeCB2.0 assays.

Immunofluorescence:

Glass coverslips (No. 1 thickness; Fisher Scientific) contained in a 6-well plate were coated with poly-D-lysine (50 ng/ml, Sigma, P6407) for 1-2 h at 37°C after which the poly-D-lysine was removed, and coverslips were washed 3 times with sterile water and one time with DMEM. Cells were detached and resuspended in supplemented DMEM as described above, counted using a hemocytometer, plated at a density of 100,000 cells/well, and were transfected after 24 hours with 0.75 µg DNA. 24 hours after transfection, media was removed, and cells were fixed with 4% paraformaldehyde in PBS (Alfa Aeser) for 20 min at room temperature. Following fixation, the cells were washed five times with PBS and permeabilized and blocked with 0.1% saponin (made fresh) and 1% bovine serum albumin (BSA, Sigma) made in PBS for 30 min at room temperature. Cells were incubated in goat anti-CB_1R antibody (1:1000) overnight at 4°C. Cells were

then washed with PBS 6X and incubated in AlexaFluor647 conjugated donkey anti-goat secondary antibody (Invitrogen, 1:1000) for 1 hour at room temperature. Cells were washed with PBS 6X, air dried overnight, and mounted using ProLong Diamond Antifade Mountant with DAPI (ThermoFisher). All antibodies were diluted in 0.1% saponin and 1% BSA made in PBS. Cells were imaged with a Leica SP8X line scanning confocal microscope using a 40X oil objective lens.

Western Blotting:

For detection of CB_1R, $GRAB_{eCB2.0}$, or mut-$GRAB_{eCB2.0}$: N2a or HEK 293 cells were plated as described above at a density of 500,000 cells/well in a 6-well plate 24 hours after plating and were transfected the following day with 0.75 µg DNA. 24 hours after transfection, media was removed, cells were washed three times with ice cold PBS, and in the last wash cells were harvested with a cell scraper and pelleted by centrifuging at 500 x g for 10 minutes. The supernatant was aspirated, and cell pellets were kept at -80°C until further use. To make cell lysate, cells were thawed on ice, resuspended in lysis buffer (25 mM HEPES pH 7.4, 1 mM EDTA, 6 mM $MgCl_2$, and 0.5% CHAPS), Dounce homogenized on ice (20-30 strokes), and incubated on a rotator at 4°C for one hour. Lysate was then centrifuged at 700 x g for 10 min at 4°C, supernatant was collected, and protein concentration of supernatant was determined using a DC Protein Assay. Samples were then mixed with 4X Laemmli Sample Buffer containing 10% β-mercaptoethanol and incubated at 65°C for 5 min. 25 µg of protein were loaded onto a 10% polyacrylamide gel and transferred to PVDF membrane. After transfer, membrane was washed once with tris-buffered saline (TBS) and incubated in blocking buffer (5% BSA in TBS) for 1 hour at room temperature, followed by incubation in primary antibody overnight at 4°C. After

incubation in primary antibody, membranes were washed with TBS with 0.05% TWEEN-20 (TBST) 3 times, 10 min each. Membranes were then incubated in secondary antibody (1:10,000) for 1 hour at room temperature. Blots were then washed with TBST 3 times, 10 min each followed by 3 washes with TBS, 10 min each. Fluorescent signal was detected using a Chemidoc MP (Biorad). Primary antibodies were diluted in blocking buffer. Secondary antibodies were diluted in 1:1 TBS:Odyssey blocking buffer (LI-COR, 927-50000) Primary antibodies: goat anti-CB_1R primary (1:2,500) and rabbit anti-actin (1:2,500; Sigma Aldrich). Secondary antibodies: IRDye 800 CW conjugates donkey anti-goat (Licor) and IRDye 680 RD conjugated goat anti-rabbit (Licor).

Isolating Membrane Proteome:

Neuro2a cells: cells were washed twice by adding ice cold dulbecco's phosphate buffered saline to attached cells and aspirating, then harvested by adding 1 milliliter of ice cold dPBS and detaching cells with a cell scraper and pelleted by centrifuging at 500 x g for 10 minutes. The supernatant was discarded, and pellet was stored at -80°C until further use. To isolate the crude membrane fraction of the cells, the cell pellets were thawed on ice, resuspended in lysis buffer (20 mM Hepes pH 7.2, 2 mM DTT, 10 U/mL Benzonase), dounce homogenized with 20-30 strokes, and centrifuged at 100,000 x g for 45 minutes (Beckman coulter rotor Ti55). The supernatant was discarded, and the pellet was resuspended in buffer (20 mM HEPES pH 7.2 and 2 mM DTT). Mouse brain tissue: cortical tissue from wild-type C57BL/6J mice was collected following decapitation, flash frozen in liquid nitrogen, and stored at -80°C. To prepare membrane proteome, the tissue was thawed on ice, dounce homogenized in ice-cold lysis buffer (20 mM HEPES pH 7.2, 2 mM DTT, 10 U/mL Benzonase) with 20-30 strokes, centrifuged at (2,500×g, 3 min, and

4°C) to pellet debris. The supernatant was then centrifuged at 100,000 x g for 45 minutes (Beckman coulter rotor Ti55). The pellet was resuspended in buffer (20 mM HEPES pH 7.2 and 2 mM DTT). Protein concentration of cell and tissue membrane sample were determined (DC protein assay, Biorad) before aliquoting and flash freezing samples in liquid nitrogen. Samples were stored at -80 until use in gel-based ABPP.

Live-cell imaging:

Glass bottom cell culture plates (MatTek) were coated with poly-D-lysine (50 ng/ml, Sigma) for 1-2 h at 37°C, after which the poly-D-lysine was removed, and coverslips were washed 3 times with sterile water and one time with DMEM. N2a or HEK 293 cells were detached and resuspended in supplemented DMEM as described above, counted using a hemocytometer, plated (250,000 cells per well) and were transfected after 24 hours with 0.75 µg DNA. 24 hours after transfection, for the N2a cells only, the growth media was exchanged for serum free DMEM and cells were incubated at 37°C and 5% CO_2 for 1-2 hours. To image, the serum free DMEM was exchanged for room temperature phosphate-buffered saline containing 1 mM $CaCl_2$ and 0.55 mM $MgCl_2$. For the HEK 293 cells, the growth media was directly exchanged to phosphate-buffered saline. The plates were transferred to a line-scanning, confocal microscope (Leica SP8X) and cells were imaged using a 40X oil objective with the following settings: 485 excitation and 525 emission wavelength, 5% laser power, HyD hybrid detector and a scan speed of 200 lines Hz (0.388 frames per second) with bidirectional scanning. All treatments were made in 1 mg/mL BSA in PBS and added directly to buffer for a final concentration of 0.1 mg/ml BSA. For co-culture experiment: HEK 293 cells were plated at a density of 150,000 cells in a 30 mm plate. The next day, the HEK293 cells were transfected with $GRAB_{eCB2.0}$.12

hours after transfection, the media on the cells was exchange for fresh growth media and 200,000 N2a cells were plated in the same plate. 24 hours after plating the N2a cells, the cells were serum starved for 1 hr, the serum free media was then exchanged for imaging buffer and the plate was placed on the confocal microscope. The cells were imaged for 2 min to establish a baseline. Then treatments were added directly into the buffer and the cells were imaged for another 10 min. All treatments formulated in 0.1 mg/ml bovine serum albumin.

Gel-Based Activity-Based Protein Profiling:

Membrane proteome was thawed on ice and 10 µg of protein was used for assay with volume normalized using 20 mM HEPES. Protein was incubated with activity-based probes, either 250 nM ActivX TAMRA-FP (ThermoFisher Scientific) or 2 µM MB064 (gift from Dr. Mario van der Stelt) for 15 minutes at 37°C. Reaction was quenched with 4X Laemmli Sample Buffer with 10% β-mercaptoethanol (BioRad) and run on a 10% polyacrylamide gel (Biorad). After running for about 1 hour at 150 mV, gel was removed from casing. Fluorescence was detected using a Chemidoc MP (Biorad) using a Cy3, green epifluorescence filter (605/50) for the activity-based probe and Cy5, red epifluorescence filter (695/55) for the protein ladder. The gel was then stained with Coomassie Brilliant Blue (0.1% Coomassie brilliant blue R-250, 25% glacial acetic acid, 40% ethanol) to obtain total protein.

96-well Plate Reader GRAB$_{eCB2.0}$ Detection:

Clear-bottom, black 96-well plates (USA Scientific were coated with poly-D-lysine (50 ng/ml, Sigma) for 1-2h at 37°C, after which the poly-D-lysine was removed, and coverslips were washed 3 times with sterile water and one time with DMEM. N2a cells were

detached and resuspended in supplemented DMEM as described above, counted using a hemocytometer, then plated (20,000 cells per well) and were transfected after 24h with 0.1 µg DNA and 0.3 µg of PEI in 10 µl of serum free DMEM. 24h after transfection, growth media was initially replaced with serum free DMEM for 1h (with or without ABHD6 and DAGL inhibitors), before replacing with PBS supplemented with 1 mM $CaCl_2$ and 0.55 mM $MgCl_2$. Cells were incubated at room temperature for 20 min then a 1 min baseline fluorescence reading was obtained using a fluorescent plate reader using 485 excitation and 525 emission filter settings with a 515 nm cutoff, and a speed of 1 reading every 20 sec. Immediately after baseline reading, treatments (made in 1 mg/mL BSA and PBS) were added to buffer in wells. Approximately 2 min after addition of treatment, the plate was read with same filter settings for 30 min. For cells pre-treated with SR1, SR1 made in PBS was added to cells after media had been replaced with PBS and were incubated for 20 min before baseline reading.

LC-MS/MS Detection of 2-AG:

When N2A cells reached 90-100% confluency, the growth media was removed and replaced with serum free DMEM. Cells were incubated for 1 h at 37°C, after which the media was replaced with PBS supplemented with 1 mM $CaCl_2$ and 0.55 mM $MgCl_2$, incubated at room temperature for about 10 min and then treated for 2- or 10-min. Reaction was quenched by removing buffer and washing three times with ice cold PBS before scraping cells off and centrifuging at 500 x g for 10 min at 4° C to pellet the cells. The buffer was then aspirated, and the pellet resuspended in 20 ml of 0.02% trifluoroacetic acid and 100 ml acetonitrile with 1 picomole of 2-AG-d^5 internal standard (Cayman Chemical) on ice before transferring to 2.5 ml of acetonitrile in a glass vial.

Samples were briefly vortexed and incubated overnight at -20°C. After the overnight incubation, the homogenate was centrifuged at 2,000 x g for 5 min to remove debris, the supernatant was collected and evaporated under nitrogen stream at 35°C and then resuspended in 50 µl of acetonitrile. The samples were capped under nitrogen stream and stored at -80°C until ready for the LC-MS/MS. Chromatographic separation was achieved using a Zorbax C18, 2.1 x 50 mm, 3.5 um reverse-phase column (Agilent). The HPLC output was directed into the electrospray ionization source of a Waters Xevo TQ-S mass spectrometer. Ionization was done in positive mode to detect 2-AG and AEA and in negative mode to detect arachidonic acid. All experiments were done in duplicate; results from each technical replicate were averaged and plotted using GraphPad Prism.

Subcellular Fractionation:

To isolate P2 fraction, wild-type HEK 293 cells were detached and resuspended as described previously and plated at a density of 3,000,000 cells in a 15 cm plate. When the cells reached confluency (48-72 hrs after plating), the growth media was removed, cells were washed twice with ice cold PBS, scraped off in 2 ml of ice cols PBS and transferred to a 15 ml centrifuge tube. The cells were centrifuged at 450 x g for 5 min at 4° C. The supernatant was removed and cells were resuspended in 2.5 ml of lysis buffer (20 mM HEPES pH 7.2, 1 mM $MgCl_2$, 250 mM sucrose, 1 mM DTT, 10 µg/ml aprotinin, 1 µg/ml pepstatin A) and incubated on ice for 15 min. Lysate was then dounce homogenized on ice, slowly passed through a 27.5 gauge syringe 5X slowly, and centrifuged at 1,000 x g for 5 min at 4° C. The pellet (containing nuclear fraction and unlysed cells) was discarded and supernatant was centrifuged at 100,000 x g for 1 hr at 4° C. The supernatant contains the cytosolic fraction and was discarded while the pellet was

resuspended in a buffer containing 25 mM Tris-HCl pH 7.4, 150 mM NaCl, and 2 mM EDTA. The protein concentration of the P2 fraction was determined using (DC protein assay, Biorad) before aliquoting and flash freezing samples in liquid nitrogen. Samples were stored at -80 until use.

To isolate crude mitochondrial and microsomal fractions from N2a cells: 2 confluent 10 cm plates of wild-type N2a cells were first washed twice with ice cold PBS, and in the third wash were scraped off and transferred to a 15 ml tube and centrifuged at 500 x g for 5 min at 4° C. The supernatant was discarded and the pellet was resuspended in lysis buffer (20 mM HEPES pH 7.2, 1 mM $MgCl_2$, 2 mM EDTA, 250 mM sucrose, 1 mM DTT, 10 µg/ml aprotinin, 1 µg/ml pepstatin A, and PhosStop phosphatase inhibitor) and incubated on ice for 15 min. After incubation, the cells were dounce homogenized on ice (about 30 strokes) before being centrifuged at 1,300 x g for 5 min at 4° C to remove un-lysed cells and nuclei. The supernatant was saved, and after saving 100 ul of this “crude lysate” for testing, the remaining supernatant was centrifuged at 16,000 x g for 10 min at 4° C. The pellet was saved and labeled as mitochondrial fraction and resuspended in the lysis buffer. The supernatant was centrifuged at 100,000 x g for 60 min at 4° C. The supernatant contains the cytosolic fraction and the pellet is the microsomal fraction. The microsomal fraction was resuspended in lysis buffer. The protein concentration of all fractions were determined using (DC protein assay, Biorad) before aliquoting and flash freezing samples in liquid nitrogen. Samples were stored at -80 until use in gel-based ABPP and western blotting. The method for isolating crude mitochondrial and microsomal fraction in HEK 293 cells transfected with Myc-hABHD6 was identical to the protocol for

N2a cells except the HEK 293 cells were transfected 24 hrs prior to subcellular fractionation.

Myc-ABHD6 Immunoprecipitation:

HEK 293 cells were detached as described previously and re-plated in a 10 cm plate at a density of 2,000,000 cells/plate. The next day the cells were transfected with Myc-ABHD6 as described above. 24 hrs after transfection, the growth media was removed and the cells were washed 3X with ice cold PBS. The cells were scraped off in the third wash, transferred to a tube, and centrifuged at 1,000 x g for 10 min at 4° C. The supernatant was discarded, the pellet was resuspended in lysis buffer (25 mM Tris-HCl pH 7.4, 150 mM NaCl, 2 mM EDTA, 10 µg/ml aprotinin, 1 µg/ml pepstatin A) and dounce homogenized on ice (30 strokes). Next, triton X-100 was added to the lysate to a final concentration of 1% and the lysate was incubated on a rotator at 4° C for 2 hr. After incubation, the lysate was centrifuged for 16,000 x g for 30 min at 4° C. The supernatant was was then incubated with Pierce anti-c Myc agarose beads (washed prior to use as per manufacturer's instructions and kept in 25 mM Tris-HCl pH 7.4, 150 mM NaCl, 2 mM EDTA until use). 30 ul of supernatant was saved and label "Input." The lysate and bead mixture was incubated on a rotator for 12-16 hours at 4° C. After incubation, beads were washed 3X (beads were pelleted by centrifuging at 12,000 x g for 20 sec, removing the supernatant, and adding 10X bead volume of a wash buffer: 25 mM Tris-HCl pH 7.4, 150 mM NaCl, 2 mM EDTA, and 0.1% triton). Protein was then eluted off the beads by incubating the beads in a 3X bead volume of 0.5 mg/ml c-Myc peptide and incubated for 10 in at 37° C, followed by pelleting the beads (12,000 x g, 20 sec) and saving the elution. Elution step was repeated 3X and all elution were pooled prior to desalting step. To desalt

the elutions and remove the c-Myc peptide, a 10,000 kD concentrator (Pierce) was used. The combined elution were added to a concentrator tube pre-rinsed with wash buffer, and concentrator was centrifuged at 12,000 x g for 2 min. The centrifuging step was repeated until the volume was approximately 1/3 of the original starting volume of the combined elutions. Between centrifugation steps, the elution was pipetted to visibly detect any precipitate formation and wash buffer was added to maintain salt and detergent concentration. The protein concentration of the sample was then determined using (DC protein assay, Biorad) before aliquoting and flash freezing samples in liquid nitrogen until use in gel-based ABPP and 4-MUH hydrolysis assays.

4-MUH ABHD6 activity assay:

To test the activity of immunoprecipitated Myc-ABHD6, in a 96-well, black clear-bottom plate, 0.2 µg of Myc-ABHD6 was incubated with either vehicle of 1 µM KT-182 in a final volume of 95 µl (supplemented with 50 mM Tris pH 7.4 and 1 mM EDTA) at 37° C for 30 min. After incubation, the substrate mM 4-Methylumbelliferyl heptanoate was added for a final concentration of 50 µM was added to each well and the plate was placed in a fluorescent plate reader and read for 1 hr using 355 excitation and 460 emission settings and a speed of 1 reading every 30 sec. To determine the effect of the P2 fraction on IP Myc-ABHD6 activity, the protocol was similar to what is described above with the following changes: 0.2 µg of Myc-ABHD6 was combined with 5 µg of the P2 fraction, with or without 1 µM KT-182 and incubated at 37° C for 30 min.

Data Analysis:

All $GRAB_{eCB2.0}$ fluorescent signals are expressed as $\Delta F/F_0$ as calculated by MATLAB for the high-throughput fluorescence assay or FIJI ImageJ for live cell confocal imaging. For

live cell imaging: changes in $GRAB_{eCB2.0}$ signal were quantified by averaging baseline fluorescence for each cell (F_0: average of fluorescent signal averaged over 30 sec, approximately 30 sec prior to agonist treatment) and calculating relative fold-change in fluorescent signal ($\Delta F/F_0$) by subtracting the signal at every time point measured (to construct a time course) or at a specific time point (i.e. relative change 1 min post-treatment) by F_0 and then dividing by F_0. For the 96-well plate assay: changes in $GRAB_{eCB2.0}$ signal were quantified by averaging baseline fluorescence for each well (F_0: fluorescent signal averaged over 1 min, approximately 2 min prior to start of agonist treatment) and calculating relative fold-change in fluorescent signal ($\Delta F/F_0$) by subtracting the signal at every time point measured (to construct a time F_0. Since every condition was tested in triplicate, the $\Delta F/F_0$ values for all three technical replicates for each condition were averaged to obtain the final $\Delta F/F_0$ used in the analysis. $GRAB_{eCB2.0}$ activation was determined by calculating $\Delta\Delta F/F_0$ between specific time points (i.e., time = 0 and peak signal). This calculation involved first calculating the $\Delta F/F_0$ at each time point, then subtracting the two values. To facilitate a data analysis pipeline, we developed a MATLAB R2021a algorithm that averages the fluorescent signal value of each well over time, for multiple experiments and at select timepoints (see the following link for the code: https://github.com/StellaLab/StellaLab.git). Data are shown as mean + s.e.m. and significance was determined by running a Two-Way ANOVA with Dunnett's Multiple Comparison test using GraphPad Prism.

Chapter 8.

Appendix

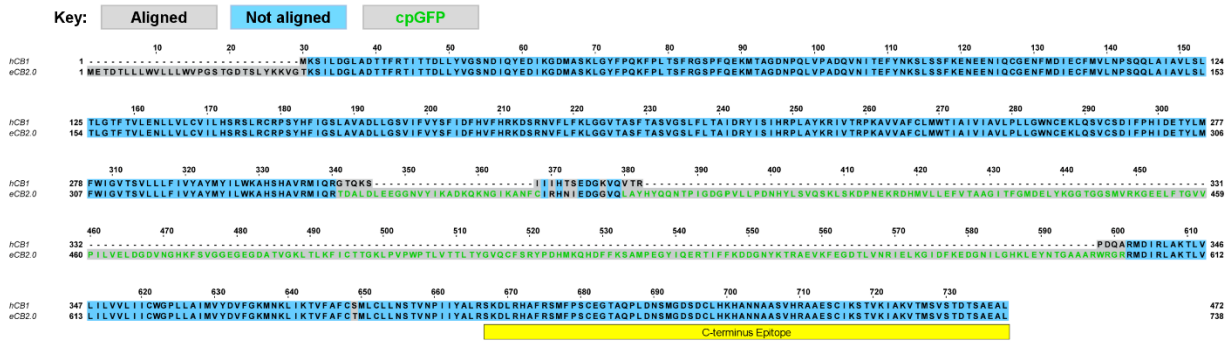

Supp Figure S2.1: sequences of human CB_1R and $GRAB_{eCB2.0.}$ and epitope of the CB_1R antibody directed against the c-terminus used for detecting GRABeCB2.0 expression.

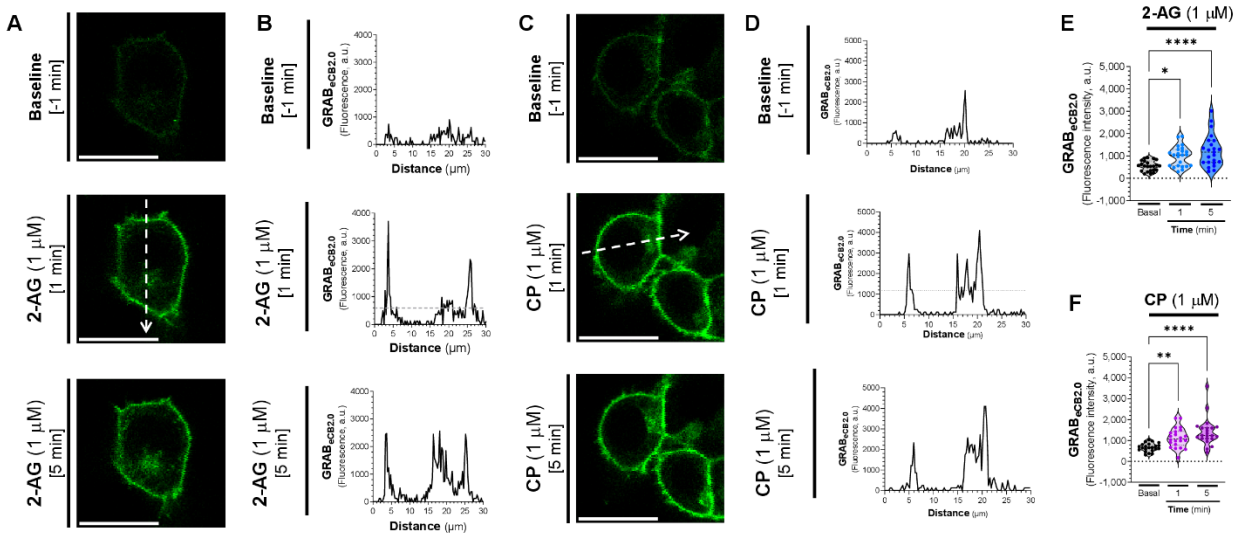

Supp Figure S2.2: Activation of intracellular $GRAB_{eCB2.0}$ by 2-AG and CP.
Intracellular $GRAB_{eCB2.0}$ activation was measured by live-cell confocal microscopy. A] $GRAB_{eCB2.0}$ fluorescent signal at baseline (1 min before treatment with 2-AG) and after addition of 2-AG (1 µM, 1- and 5-min treatment). B] Line scan analysis of 2-AG treated representative cell in (A). C] $GRAB_{eCB2.0}$ fluorescent signal at baseline (1 min before treatment with CP) and after addition of CP (1 µM, 1- and 5-min treatment). D] Line scan analysis of CP-treated representative cell in (A). E-F] Change in $GRAB_{eCB2.0}$ fluorescent signal following 1- and 5- min treatment with 2-AG (1 µM; E) or CP (1 µM; F), as compared to baseline (basal) fluorescent signal. N=22-23 cells from 3 independent experiments. Scale bars= 20 µm. *P<0.0332, **P<0.0021, and ****P<0.0001, significantly different from basal (One-Way ANOVA followed by Tukey's).

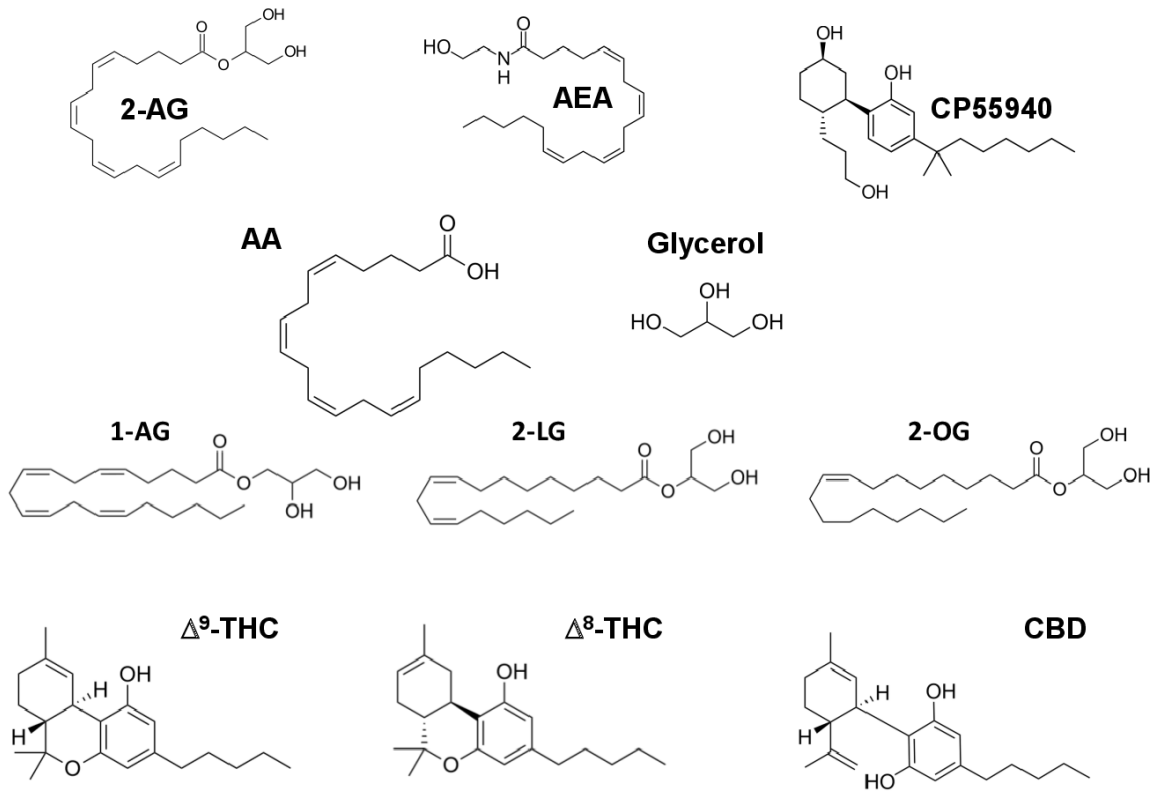

Supp Figure S2.6A: Chemical structures of CB1R agents tested at $GRAB_{eCB2.0}$. The classes of agents tested can be categorized as the following: 1] endocannabinoids: 2-AG and AEA; 2] synthetic cannabinoids: CP55940; 3] products of eCB hydrolysis: arachidonic acid (AA) and glycerol; 4] 2-AG analogs: 1-AG, 2-LG, and 2-OG; and 4] phyto-cannabinoids: Δ8-THC, Δ9-THC, and CBD.

A

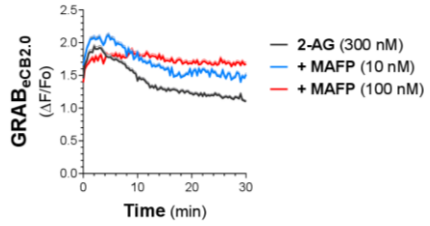

B

		2-AG (300 nM)		
parameter	**Units**	**CTR**	**MAFP** (10 nM)	**MAFP** (100 nM)
Maximal response: peak	($\Delta F/F_o$)	**1.82**	**1.81**	**1.73**
	(std. error)	0.035	0.035	0.034
Overall response	(area under the curve)	**36.37**	**38.97**	**46.83**
	(std. error)			
Decay: *t*	(sec)	**9.3**	**12.97**	**74.58**
	(95% CI)	8.8-9.8	12.2-13.9	65.8-86

Supp Figure S2.6B-C: Effect of MAFP on 2-AG (300 nM)-Triggered $GRAB_{eCB2.0}$ fluorescent signal.

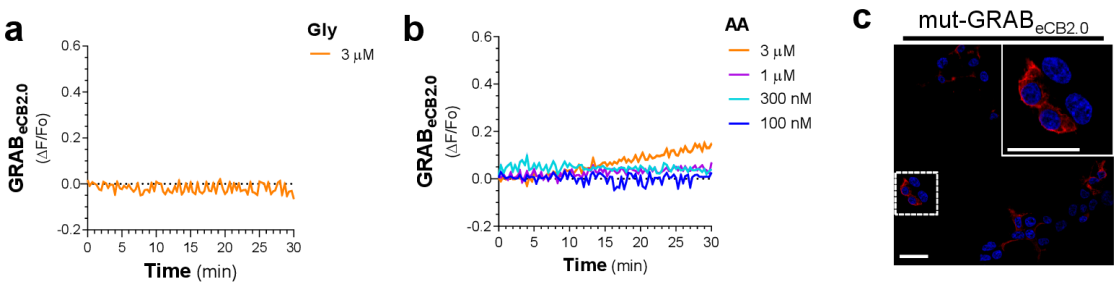

Figure S3.1: Concentration-dependent activation of $GRAB_{eCB2.0}$ by products of 2-AG hydrolysis and expression of mut-$GRAB_{eCB2.0}$. Direct activation of the $GRAB_{eCB2.0}$ in N2a cells by the products of 2-AG hydrolysis arachidonic acid (AA) and glycerol (Gly), as measured by a fluorescent plate reader for 30 min (see Figure 2A). **a-b]** Time courses of changes in $GRAB_{eCB2.0}$ fluorescent signal following treatment with increasing concentrations of Gly (a), and AA (b). Data is shown as a mean of 3-4 independent experiments, with each experiment done in triplicate. Shaded area represents s.e.m. **c]** mut-$GRAB_{eCB2.0}$ expression in N2a cells. N2a cells transiently transfected with mut-$GRAB_{eCB2.0}$ and protein expression was detected using immunocytochemistry with a C-terminus CB_1R antibody. Experiment repeated twice with similar results. Scale bars represents 20 μm.

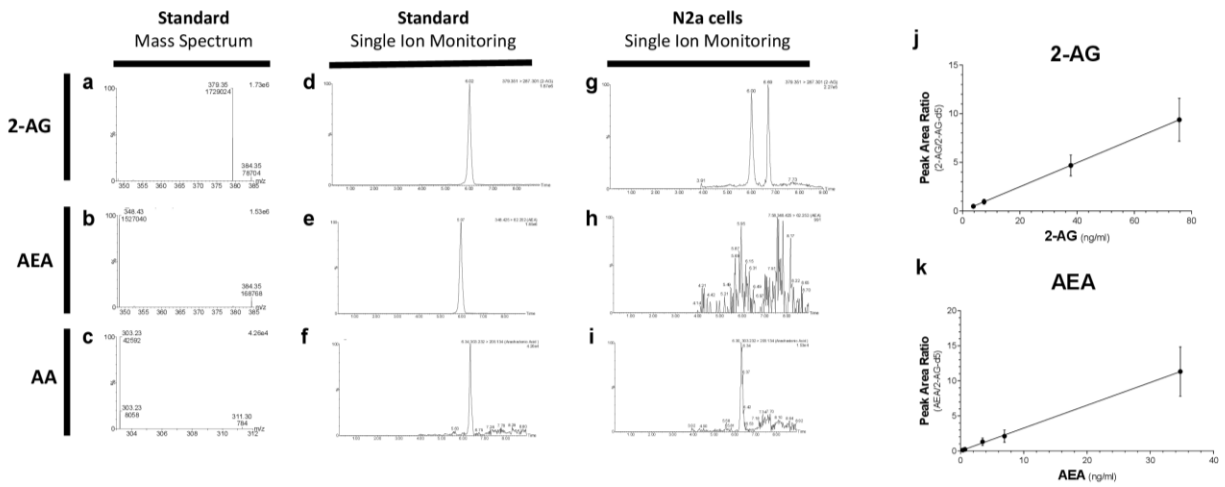

Figure S3.3$_{a-i}$: Measuring 2-AG, AEA, and AA by LC-MS: standards and N2a cell lysate.

a, b, c] Mass spectra of target analyte precursor ions obtained by injecting standards of 2-AG (a, *m/z* 379.35), AEA (b, *m/z* 348.43), and AA (c, *m/z* 303.23) standards containing internal standard of 2-AG-d_5 (*m/z* 384.35). **d, e, f]** Chromatograms of 2-AG (b), AEA (e), and AA (h) standards. Mass spectra and chromatograms of standards were generated by using 1 pmol of 2-AG, 1 pmol of AEA, and 5 pmol AA. **g, h, i]** Chromatograms detecting 2-AG, AA, and AEA in lysate made from vehicle treated N2a cells. Analytes were measured by monitoring the *m/z* transitions from 379.35 to 287.3 for 2-AG, 348.43 to 62.25 for AEA, and 303.23 to 205.13 for AA following collision-induced dissociation. All standard and N2a samples contained 0.2 pmol of 2-AG-d_5 internal standard. The x-axis of chromatograms represents retention time in min. **j-k]** Calibration curves for 2-AG (j) and AEA (k) used to quantify 2-AG content in N2a samples. R^2 = 1.00 for 2-AG calibration curve and 0.9994 for AEA calibration curve. N= 5-13 for 2-AG and AEA. Limit of detection is 0.84 ng/ml for 2-AG and 0.21 ng/ml for AEA. Error bars represent s.d.

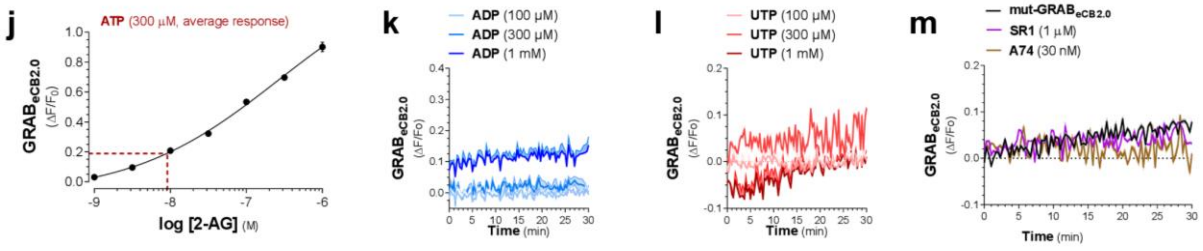

Figure S3.3$_{j-m}$: Interpolation of ATP-stimulated 2-AG levels and effect of purinergic agonists ADP and UTP on GRAB$_{eCB2.0}$ fluorescent signal.

j] Interpolation of 2-AG concentrations of GRAB$_{eCB2.0}$-expressing N2a cells treated with ATP (300 µM) (see Figure 4B), calculated from a non-linear regression using the concentration response curve generated from 2-AG (see Figure 2D) (log(agonist) vs. response -- Variable slope: Hill slope (0.45)). **k-l]** Time courses of changes in GRAB$_{eCB2.0}$ fluorescent signal in N2a cells following treatment with increasing concentrations of ADP (k), and UTP (l). **m]** Effect of SR1 and A74 pretreatment on GRAB$_{eCB2.0}$ fluorescent signal in N2a cells. All GRAB$_{eCB2.0}$ fluorescent signal was measured using a fluorescent plate reader. Data is shown as a mean of 3-6 independent experiments, with each experiment done in triplicate. Shaded area represents s.e.m.

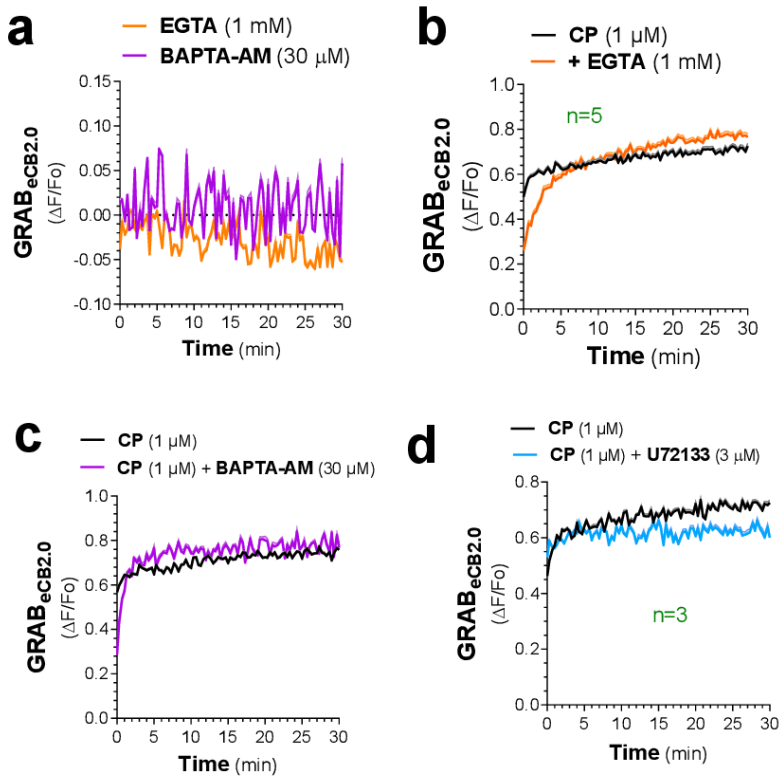

Figure S3.4$_{a-d}$: Effect of EGTA, BAPTA-AM, and U73122 on basal and CP-induced GRAB$_{eCB2.0}$ fluorescent signal.

a] Time courses of basal GRAB$_{eCB2.0}$ fluorescent signal in N2a cells following treatment with EGTA (1 mM) and BAPTA-AM (30 μM). **b-d]** Effect of EGTA (1 mM, b), BAPTA-AM (30 μM, c), and U73122 (3 μM, d) on GRABeCB2.0 activation by CP (1 μM). Data is shown as a mean of 10-13 independent experiments for (a) and 4-8 independent experiments for (b-d), with each experiment done in triplicate. Shaded area represents s.e.m.

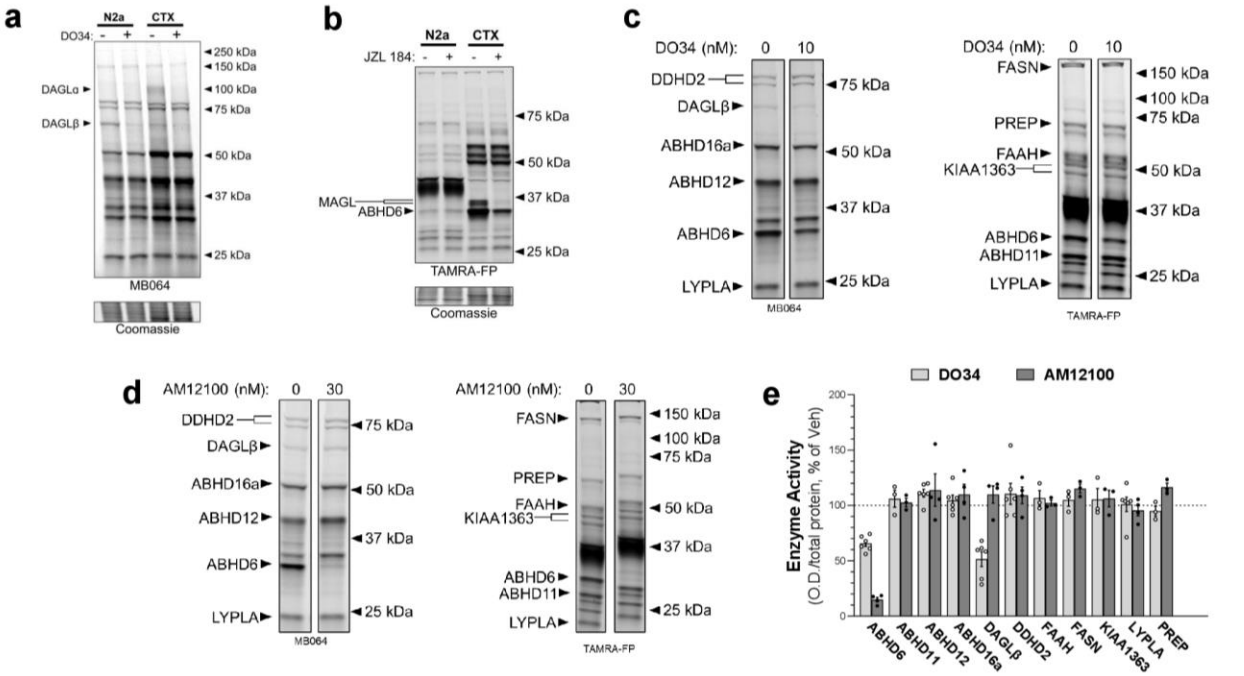

Figure S3.5: <u>N2a cells exhibit DAGLβ and ABHD6 activity, but not DAGLα and MAGL activity.</u>

a] DAGL activity in N2a cells and mouse cortex (CTX, positive control) was measured by gel-based ABPP using the activity-based probe MB064 (2 μM, 15 min). Identity of bands confirmed using DAGL inhibitor DO34 (membrane proteome treated with 10 nM for 30 min). **b]** Activity of 2-AG hydrolyzing enzymes in N2a cells. MAGL and ABHD6 activity in N2a cells and mouse cortex (CTX, positive control) was measured by gel-based ABPP using the activity-based probe TAMRA-FP (500 nM, 15 min). Identity of MAGL bands confirmed using MAGL inhibitor JZL 184 (membrane proteome treated with 10 nM for 30 min). **c]** Selectivity of DO34 (10 nM, 30 min in situ) as measured by gel-based ABPP. Cells were treated in situ with DO34, and enzyme activity was measured in the membrane proteome was treated with the activity-based probes MB064 (2 μM, 15 min, 37°C) or TAMRA-FP (500 nM, 15 min, 37°C). **c-e]** Selectivity of DO34 (c) and AM12100 (d) in N2a membrane proteome as measured by gel-based ABPP. Cells were treated in situ with DO34 (10 nM, 30 min) or AM12100 (30 nM, 60 min), and membrane proteome was treated with activity-based probes MB064 (2 μM, 15 min) or TAMRA-FP (500 nM, 15 min). Quantification of gel-based ABPP results presented in (e) represent the mean from 4-6 independent experiments. Error bars represent s.e.m.

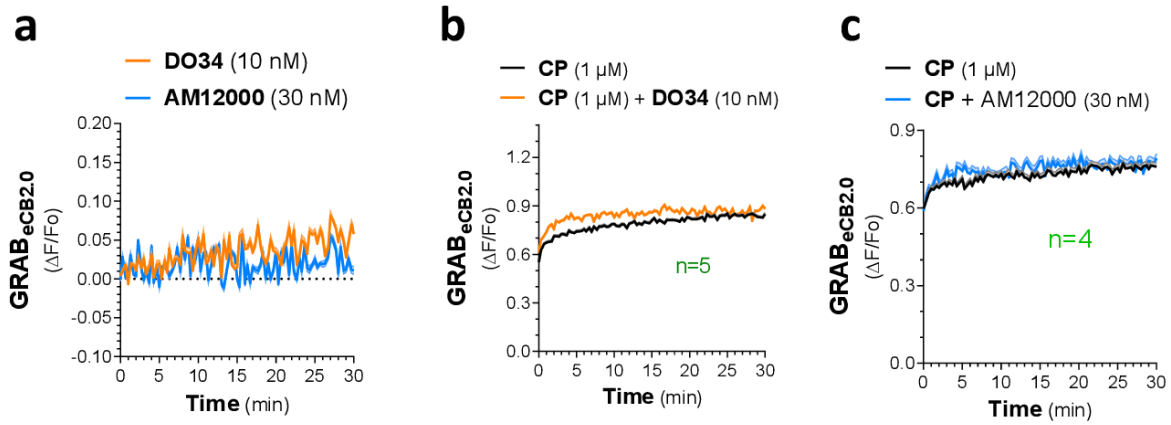

Figure S3.6$_{a-c}$: Effect of DO34 and AM12100 on basal and CP-induced GRAB$_{eCB2.0}$ fluorescent signal.

a] Time courses of basal GRAB$_{eCB2.0}$ fluorescent signal in N2a cells pretreated with DO34 (10 nM) and AM12100 (30 nM). **b-c]** Effect of DO34 (10 nM, b) and AM12100 (30 nM, c) on GRABeCB2.0 activation by CP (1 μM). Data is shown as a mean of 4-5 independent experiments, with each experiment done in triplicate. Shaded area represents s.e.m.

BIBLIOGRAPHY

1 Ben Amar, M. Cannabinoids in medicine: A review of their therapeutic potential. *J Ethnopharmacol* **105**, 1-25, doi:10.1016/j.jep.2006.02.001 (2006).

2 Alexander, S. P. H. Therapeutic potential of cannabis-related drugs. *Progress in Neuro-Psychopharmacology and Biological Psychiatry* **64**, 157-166, doi:https://doi.org/10.1016/j.pnpbp.2015.07.001 (2016).

3 Dos Reis Rosa Franco, G., Smid, S. & Viegas, C. Phytocannabinoids: General Aspects and Pharmacological Potential in Neurodegenerative Diseases. *Curr Neuropharmacol* **19**, 449-464, doi:10.2174/1570159x18666200720172624 (2021).

4 LaFrance, E. M., Stueber, A., Glodosky, N. C., Mauzay, D. & Cuttler, C. Overbaked: assessing and predicting acute adverse reactions to Cannabis. *Journal of Cannabis Research* **2**, 3, doi:10.1186/s42238-019-0013-x (2020).

5 Bow, E. W. & Rimoldi, J. M. The Structure-Function Relationships of Classical Cannabinoids: CB1/CB2 Modulation. *Perspect Medicin Chem* **8**, 17-39, doi:10.4137/pmc.S32171 (2016).

6 Mudge, E. M., Murch, S. J. & Brown, P. N. Chemometric Analysis of Cannabinoids: Chemotaxonomy and Domestication Syndrome. *Sci Rep* **8**, 13090, doi:10.1038/s41598-018-31120-2 (2018).

7 Smith, C. J., Vergara, D., Keegan, B. & Jikomes, N. The phytochemical diversity of commercial Cannabis in the United States. *PLOS ONE* **17**, e0267498, doi:10.1371/journal.pone.0267498 (2022).

8 Badowski, M. E. & Yanful, P. K. Dronabinol oral solution in the management of anorexia and weight loss in AIDS and cancer. *Ther Clin Risk Manag* **14**, 643-651, doi:10.2147/tcrm.S126849 (2018).

9 Ware, M. A., Daeninck, P. & Maida, V. A review of nabilone in the treatment of chemotherapy-induced nausea and vomiting. *Ther Clin Risk Manag* **4**, 99-107, doi:10.2147/tcrm.s1132 (2008).

10 Silva, G. D., Del Guerra, F. B., de Oliveira Lelis, M. & Pinto, L. F. Cannabidiol in the Treatment of Epilepsy: A Focused Review of Evidence and Gaps. *Front Neurol* **11**, 531939, doi:10.3389/fneur.2020.531939 (2020).

11 Manthey, J. *et al.* The impact of legal cannabis availability on cannabis use and health outcomes: A systematic review. *International Journal of Drug Policy* **116**, 104039, doi:https://doi.org/10.1016/j.drugpo.2023.104039 (2023).

12 Lu, H.-C. & Mackie, K. An Introduction to the Endogenous Cannabinoid System. *Biol Psychiatry* **79**, 516-525, doi:10.1016/j.biopsych.2015.07.028 (2016).

13 Buczynski, M. W. & Parsons, L. H. Quantification of brain endocannabinoid levels: methods, interpretations and pitfalls. *Br J Pharmacol* **160**, 423-442, doi:10.1111/j.1476-5381.2010.00787.x (2010).

14 Zou, S. & Kumar, U. Cannabinoid Receptors and the Endocannabinoid System: Signaling and Function in the Central Nervous System. *Int J Mol Sci* **19**, 833, doi:10.3390/ijms19030833 (2018).

15 Hashimotodani, Y. *et al.* Acute inhibition of diacylglycerol lipase blocks endocannabinoid-mediated retrograde signalling: evidence for on-demand biosynthesis of 2-arachidonoylglycerol. *J Physiol* **591**, 4765-4776, doi:10.1113/jphysiol.2013.254474 (2013).

16 Shonesy, B. C., Winder, D. G., Patel, S. & Colbran, R. J. The initiation of synaptic 2-AG mobilization requires both an increased supply of diacylglycerol precursor and increased postsynaptic calcium. *Neuropharmacology* **91**, 57-62, doi:10.1016/j.neuropharm.2014.11.026 (2015).

17 Jung, K.-M. *et al.* Stimulation of Endocannabinoid Formation in Brain Slice Cultures through Activation of Group I Metabotropic Glutamate Receptors. *Mol Pharmacol* **68**, 1196, doi:10.1124/mol.105.013961 (2005).
18 Stella, N., Schweitzer, P. & Piomelli, D. A second endogenous cannabinoid that modulates long-term potentiation. *Nature* **388**, 773-778, doi:10.1038/42015 (1997).
19 Baggelaar, M. P., Maccarrone, M. & van der Stelt, M. 2-Arachidonoylglycerol: A signaling lipid with manifold actions in the brain. *Progress in Lipid Research* **71**, 1-17, doi:https://doi.org/10.1016/j.plipres.2018.05.002 (2018).
20 Hashimotodani, Y. *et al.* Phospholipase Cβ Serves as a Coincidence Detector through Its Ca2+ Dependency for Triggering Retrograde Endocannabinoid Signal. *Neuron* **45**, 257-268, doi:https://doi.org/10.1016/j.neuron.2005.01.004 (2005).
21 Kellogg, R., Mackie, K. & Straiker, A. Cannabinoid CB1 receptor-dependent long-term depression in autaptic excitatory neurons. *J Neurophysiol* **102**, 1160-1171, doi:10.1152/jn.00266.2009 (2009).
22 Robbe, D., Kopf, M., Remaury, A., Bockaert, J. & Manzoni, O. J. Endogenous cannabinoids mediate long-term synaptic depression in the nucleus accumbens. *Proc Natl Acad Sci U S A* **99**, 8384-8388, doi:10.1073/pnas.122149199 (2002).
23 Herkenham, M. *et al.* Characterization and localization of cannabinoid receptors in rat brain: a quantitative in vitro autoradiographic study. *J Neurosci* **11**, 563-583, doi:10.1523/jneurosci.11-02-00563.1991 (1991).
24 Chou, S., Ranganath, T., Fish, K. N., Lewis, D. A. & Sweet, R. A. Cell type specific cannabinoid CB1 receptor distribution across the human and non-human primate cortex. *Scientific Reports* **12**, 9605, doi:10.1038/s41598-022-13724-x (2022).
25 Steindel, F. *et al.* Neuron-type specific cannabinoid-mediated G protein signalling in mouse hippocampus. *Journal of Neurochemistry* **124**, 795-807, doi:https://doi.org/10.1111/jnc.12137 (2013).
26 Robin, L. M. *et al.* Astroglial CB(1) Receptors Determine Synaptic D-Serine Availability to Enable Recognition Memory. *Neuron* **98**, 935-944.e935, doi:10.1016/j.neuron.2018.04.034 (2018).
27 Navarro, G. *et al.* Receptor-heteromer mediated regulation of endocannabinoid signaling in activated microglia. Role of CB1 and CB2 receptors and relevance for Alzheimer's disease and levodopa-induced dyskinesia. *Brain, Behavior, and Immunity* **67**, 139-151, doi:https://doi.org/10.1016/j.bbi.2017.08.015 (2018).
28 Atwood, B. K. & Mackie, K. CB2: a cannabinoid receptor with an identity crisis. *Br J Pharmacol* **160**, 467-479, doi:10.1111/j.1476-5381.2010.00729.x (2010).
29 Li, Y. & Kim, J. Neuronal expression of CB2 cannabinoid receptor mRNAs in the mouse hippocampus. *Neuroscience* **311**, 253-267, doi:10.1016/j.neuroscience.2015.10.041 (2015).
30 Stella, N. Cannabinoid and cannabinoid-like receptors in microglia, astrocytes, and astrocytomas. *Glia* **58**, 1017-1030, doi:10.1002/glia.20983 (2010).
31 Busquets-Garcia, A., Bains, J. & Marsicano, G. CB(1) Receptor Signaling in the Brain: Extracting Specificity from Ubiquity. *Neuropsychopharmacology* **43**, 4-20, doi:10.1038/npp.2017.206 (2018).
32 Morales, P., Bruix, M. & Jiménez, M. A. Structural Insights into β-arrestin/CB1 Receptor Interaction: NMR and CD Studies on Model Peptides. *Int J Mol Sci* **21**, doi:10.3390/ijms21218111 (2020).
33 Kano, M., Ohno-Shosaku, T., Hashimotodani, Y., Uchigashima, M. & Watanabe, M. Endocannabinoid-Mediated Control of Synaptic Transmission. *Physiological Reviews* **89**, 309-380, doi:10.1152/physrev.00019.2008 (2009).

34 Diana, M. A. & Marty, A. Endocannabinoid-mediated short-term synaptic plasticity: depolarization-induced suppression of inhibition (DSI) and depolarization-induced suppression of excitation (DSE). *Br J Pharmacol* **142**, 9-19, doi:10.1038/sj.bjp.0705726 (2004).

35 Ohno-Shosaku, T., Maejima, T. & Kano, M. Endogenous Cannabinoids Mediate Retrograde Signals from Depolarized Postsynaptic Neurons to Presynaptic Terminals. *Neuron* **29**, 729-738, doi:https://doi.org/10.1016/S0896-6273(01)00247-1 (2001).

36 Wilson, R. I. & Nicoll, R. A. Endogenous cannabinoids mediate retrograde signalling at hippocampal synapses. *Nature* **410**, 588-592, doi:10.1038/35069076 (2001).

37 Sigel, E. *et al.* The major central endocannabinoid directly acts at GABA(A) receptors. *Proc Natl Acad Sci U S A* **108**, 18150-18155, doi:10.1073/pnas.1113444108 (2011).

38 Castillo, P. E., Younts, T. J., Chávez, A. E. & Hashimotodani, Y. Endocannabinoid signaling and synaptic function. *Neuron* **76**, 70-81, doi:10.1016/j.neuron.2012.09.020 (2012).

39 Oubraim, S., Wang, R., Hausknecht, K. A., Shen, R. Y. & Haj-Dahmane, S. Tonic Endocannabinoid Signaling Gates Synaptic Plasticity in Dorsal Raphe Nucleus Serotonin Neurons Through Peroxisome Proliferator-Activated Receptors. *Front Pharmacol* **12**, 691219, doi:10.3389/fphar.2021.691219 (2021).

40 Blankman, J. L., Simon, G. M. & Cravatt, B. F. A comprehensive profile of brain enzymes that hydrolyze the endocannabinoid 2-arachidonoylglycerol. *Chem Biol* **14**, 1347-1356, doi:10.1016/j.chembiol.2007.11.006 (2007).

41 Alex, S. *et al.* Monoacylglycerol Lipase Limits the Duration of Endocannabinoid-Mediated Depolarization-Induced Suppression of Excitation in Autaptic Hippocampal Neurons. *Mol Pharmacol* **76**, 1220, doi:10.1124/mol.109.059030 (2009).

42 Long, J. Z., Nomura, D. K. & Cravatt, B. F. Characterization of monoacylglycerol lipase inhibition reveals differences in central and peripheral endocannabinoid metabolism. *Chem Biol* **16**, 744-753, doi:10.1016/j.chembiol.2009.05.009 (2009).

43 Viader, A. *et al.* Metabolic Interplay between Astrocytes and Neurons Regulates Endocannabinoid Action. *Cell Rep* **12**, 798-808, doi:10.1016/j.celrep.2015.06.075 (2015).

44 Schlosburg, J. E. *et al.* Chronic monoacylglycerol lipase blockade causes functional antagonism of the endocannabinoid system. *Nat Neurosci* **13**, 1113-1119, doi:10.1038/nn.2616 (2010).

45 Blankman, J. L., Long, J. Z., Trauger, S. A., Siuzdak, G. & Cravatt, B. F. ABHD12 controls brain lysophosphatidylserine pathways that are deregulated in a murine model of the neurodegenerative disease PHARC. *Proceedings of the National Academy of Sciences* **110**, 1500-1505, doi:10.1073/pnas.1217121110 (2013).

46 Marrs, W. R. *et al.* The serine hydrolase ABHD6 controls the accumulation and efficacy of 2-AG at cannabinoid receptors. *Nat Neurosci* **13**, 951-957, doi:10.1038/nn.2601 (2010).

47 Liktor-Busa, E. *et al.* ABHD6 and MAGL control 2-AG levels in the PAG and allodynia in a CSD-induced periorbital model of headache. *Front Pain Res (Lausanne)* **4**, 1171188, doi:10.3389/fpain.2023.1171188 (2023).

48 Naydenov, A. V. *et al.* ABHD6 blockade exerts antiepileptic activity in PTZ-induced seizures and in spontaneous seizures in R6/2 mice. *Neuron* **83**, 361-371, doi:10.1016/j.neuron.2014.06.030 (2014).

49 Westenbroek, R., Kaplan, J., Viray, K. & Stella, N. The serine hydrolase ABHD6 controls survival and thermally induced seizures in a mouse model of Dravet syndrome. *Neurobiol Dis* **180**, 106099, doi:10.1016/j.nbd.2023.106099 (2023).

50 Muccioli, G. G. *et al.* Identification of a novel endocannabinoid-hydrolyzing enzyme expressed by microglial cells. *J Neurosci* **27**, 2883-2889, doi:10.1523/jneurosci.4830-06.2007 (2007).

51 Navia-Paldanius, D., Savinainen, J. R. & Laitinen, J. T. Biochemical and pharmacological characterization of human α/β-hydrolase domain containing 6 (ABHD6) and 12 (ABHD12). *J Lipid Res* **53**, 2413-2424, doi:10.1194/jlr.M030411 (2012).

52 Kind, L. & Kursula, P. Structural properties and role of the endocannabinoid lipases ABHD6 and ABHD12 in lipid signalling and disease. *Amino Acids* **51**, 151-174, doi:10.1007/s00726-018-2682-8 (2019).

53 Pusch, L. M., Riegler-Berket, L., Oberer, M., Zimmermann, R. & Taschler, U. α/β-Hydrolase Domain-Containing 6 (ABHD6)- A Multifunctional Lipid Hydrolase. *Metabolites* **12**, doi:10.3390/metabo12080761 (2022).

54 Pribasnig, M. A. *et al.* α/β Hydrolase Domain-containing 6 (ABHD6) Degrades the Late Endosomal/Lysosomal Lipid Bis(monoacylglycero)phosphate. *J Biol Chem* **290**, 29869-29881, doi:10.1074/jbc.M115.669168 (2015).

55 Thomas, G. *et al.* The serine hydrolase ABHD6 Is a critical regulator of the metabolic syndrome. *Cell Rep* **5**, 508-520, doi:10.1016/j.celrep.2013.08.047 (2013).

56 Baggelaar, M. P. *et al.* Chemical Proteomics Maps Brain Region Specific Activity of Endocannabinoid Hydrolases. *ACS Chemical Biology* **12**, 852-861, doi:10.1021/acschembio.6b01052 (2017).

57 Shao, L. R., Habela, C. W. & Stafstrom, C. E. Pediatric Epilepsy Mechanisms: Expanding the Paradigm of Excitation/Inhibition Imbalance. *Children (Basel)* **6**, doi:10.3390/children6020023 (2019).

58 Cao, J. K., Kaplan, J. & Stella, N. ABHD6: Its Place in Endocannabinoid Signaling and Beyond. *Trends in pharmacological sciences* **40**, 267-277, doi:10.1016/j.tips.2019.02.002 (2019).

59 Saini, R. K., Prasad, P., Shang, X. & Keum, Y. S. Advances in Lipid Extraction Methods-A Review. *Int J Mol Sci* **22**, doi:10.3390/ijms222413643 (2021).

60 Löfgren, L., Forsberg, G.-B. & Ståhlman, M. The BUME method: a new rapid and simple chloroform-free method for total lipid extraction of animal tissue. *Scientific Reports* **6**, 27688, doi:10.1038/srep27688 (2016).

61 Sachin, P., David, J. R. & Cecilia, J. H. Differential Regulation of the Endocannabinoids Anandamide and 2-Arachidonylglycerol within the Limbic Forebrain by Dopamine Receptor Activity. *Journal of Pharmacology and Experimental Therapeutics* **306**, 880, doi:10.1124/jpet.103.054270 (2003).

62 Fuchs, B., Süß, R., Teuber, K., Eibisch, M. & Schiller, J. Lipid analysis by thin-layer chromatography—A review of the current state. *Journal of Chromatography A* **1218**, 2754-2774, doi:https://doi.org/10.1016/j.chroma.2010.11.066 (2011).

63 Keereetaweep, J. & Chapman, K. D. Lipidomic Analysis of Endocannabinoid Signaling: Targeted Metabolite Identification and Quantification. *Neural Plast* **2016**, 2426398-2426398, doi:10.1155/2016/2426398 (2016).

64 Muccioli, G. G. & Stella, N. An optimized GC-MS method detects nanomolar amounts of anandamide in mouse brain. *Anal Biochem* **373**, 220-228, doi:10.1016/j.ab.2007.09.030 (2008).

65 Zoerner, A. A. *et al.* Quantification of endocannabinoids in biological systems by chromatography and mass spectrometry: A comprehensive review from an analytical and biological perspective. *Biochimica et Biophysica Acta (BBA) - Molecular and Cell Biology of Lipids* **1811**, 706-723, doi:https://doi.org/10.1016/j.bbalip.2011.08.004 (2011).

66 Dócs, K. *et al.* The Ratio of 2-AG to Its Isomer 1-AG as an Intrinsic Fine Tuning Mechanism of CB1 Receptor Activation. *Front Cell Neurosci* **11**, doi:10.3389/fncel.2017.00039 (2017).

67 Aoki, J., Isokawa, M. & Toyoda, M. Space and Time Coherent Mapping for Subcellular Resolution of Imaging Mass Spectrometry. *Cells* **11** (2022).

68 Veloso, A. *et al.* Anatomical Distribution of Lipids in Human Brain Cortex by Imaging Mass Spectrometry. *Journal of The American Society for Mass Spectrometry* **22**, 329-338, doi:10.1007/s13361-010-0024-5 (2011).

69 Jackson, S. N. *et al.* MALDI-Ion Mobility Mass Spectrometry of Lipids in Negative Ion Mode. *Anal Methods* **6**, 5001-5007, doi:10.1039/c4ay00320a (2014).

70 Wang, S. *et al.* Advanced Activity-Based Protein Profiling Application Strategies for Drug Development. *Front Pharmacol* **9**, 353, doi:10.3389/fphar.2018.00353 (2018).

71 Niphakis, M. J. & Cravatt, B. F. Enzyme Inhibitor Discovery by Activity-Based Protein Profiling. *Annual Review of Biochemistry* **83**, 341-377, doi:10.1146/annurev-biochem-060713-035708 (2014).

72 Janssen, A. P. A. *et al.* Development of a Multiplexed Activity-Based Protein Profiling Assay to Evaluate Activity of Endocannabinoid Hydrolase Inhibitors. *ACS Chem Biol* **13**, 2406-2413, doi:10.1021/acschembio.8b00534 (2018).

73 Kidd, D., Liu, Y. & Cravatt, B. F. Profiling Serine Hydrolase Activities in Complex Proteomes. *Biochemistry* **40**, 4005-4015, doi:10.1021/bi002579j (2001).

74 Miralpeix, C. *et al.* Carnitine palmitoyltransferase 1C negatively regulates the endocannabinoid hydrolase ABHD6 in mice, depending on nutritional status. *Br J Pharmacol* **n/a**, doi:https://doi.org/10.1111/bph.15377 (2021).

75 Shields, C. M., Zvonok, N., Zvonok, A. & Makriyannis, A. Biochemical and Proteomic Characterization of Recombinant Human α/β Hydrolase Domain 6. *Sci Rep* **9**, 890, doi:10.1038/s41598-018-36633-4 (2019).

76 Dong, A. *et al.* A fluorescent sensor for spatiotemporally resolved imaging of endocannabinoid dynamics in vivo. *Nat Biotechnol*, doi:10.1038/s41587-021-01074-4 (2021).

77 Singh, S. *et al.* Pharmacological characterization of the endocannabinoid sensor GRAB_{eCB2.0}. *bioRxiv*, 2023.2003.2003.531053, doi:10.1101/2023.03.03.531053 (2023).

78 Farrell, J. S. *et al.* In vivo endocannabinoid dynamics at the timescale of physiological and pathological neural activity. *Neuron* **109**, 2398-2403.e2394, doi:https://doi.org/10.1016/j.neuron.2021.05.026 (2021).

79 Liput, D. J. *et al.* 2-Arachidonoylglycerol mobilization following brief synaptic stimulation in the dorsal lateral striatum requires glutamatergic and cholinergic neurotransmission. *Neuropharmacology* **205**, 108916 (2022).

80 Busquets-Garcia, A., Bains, J. & Marsicano, G. CB 1 receptor signaling in the brain: extracting specificity from ubiquity. *Neuropsychopharmacology* **43**, 4-20 (2018).

81 Lutz, B. Neurobiology of cannabinoid receptor signaling. *Dialogues in Clinical Neuroscience* **22**, 207 (2020).

82 Shen, M. & Thayer, S. A. Đ⁹-Tetrahydrocannabinol acts as a partial agonist to modulate glutamatergic synaptic transmission between rat hippocampal neurons in culture. *Molecular Pharmacology* **55**, 8-13 (1999).

83 Kelley, B. G. & Thayer, S. A. Delta 9-tetrahydrocannabinol antagonizes endocannabinoid modulation of synaptic transmission between hippocampal neurons in culture. *Neuropharmacology* **46**, 709-715 (2004).

84 Straiker, A. & Mackie, K. Depolarization-induced suppression of excitation in murine autaptic hippocampal neurones. *J Physiol* **569**, 501-517 (2005).

85 Roloff, A. M. & Thayer, S. A. Modulation of excitatory synaptic transmission by Δ9-tetrahydrocannabinol switches from agonist to antagonist depending on firing rate. *Molecular Pharmacology* **75**, 892-900 (2009).

86 Shahbazi, F., Grandi, V., Banerjee, A. & Trant, J. F. Cannabinoids and cannabinoid receptors: the story so far. *Iscience* **23**, 101301 (2020).

87 Laprairie, R. B., Bagher, A. M., Kelly, M. E. & Denovan-Wright, E. M. Cannabidiol is a negative allosteric modulator of the cannabinoid CB1 receptor. *Br J Pharmacol* **172**, 4790-4805, doi:10.1111/bph.13250 (2015).

88 Jakowiecki, J. *et al.* Allosteric Modulation of the CB1 Cannabinoid Receptor by Cannabidiol-A Molecular Modeling Study of the N-Terminal Domain and the Allosteric-Orthosteric Coupling. *Molecules* **26**, doi:10.3390/molecules26092456 (2021).

89 Murataeva, N., Straiker, A. & Mackie, K. Parsing the players: 2-arachidonoylglycerol synthesis and degradation in the CNS. *Br J Pharmacol* **171**, 1379-1391, doi:10.1111/bph.12411 (2014).

90 Lu, L., Williams, G. & Doherty, P. 2-Linoleoylglycerol Is a Partial Agonist of the Human Cannabinoid Type 1 Receptor that Can Suppress 2-Arachidonolyglycerol and Anandamide Activity. *Cannabis Cannabinoid Res* **4**, 231-239, doi:10.1089/can.2019.0030 (2019).

91 Tortoriello, G. *et al.* Genetic Manipulation of sn-1-Diacylglycerol Lipase and CB(1) Cannabinoid Receptor Gain-of-Function Uncover Neuronal 2-Linoleoyl Glycerol Signaling in Drosophila melanogaster. *Cannabis Cannabinoid Res* **6**, 119-136, doi:10.1089/can.2020.0010 (2021).

92 Labouesse, M. A. & Patriarchi, T. A versatile GPCR toolkit to track in vivo neuromodulation: not a one-size-fits-all sensor. *Neuropsychopharmacology* **46**, 2043-2047 (2021).

93 Dong, A. *et al.* A fluorescent sensor for spatiotemporally resolved imaging of endocannabinoid dynamics in vivo. *Nature biotechnology*, 1-12 (2021).

94 Patriarchi, T. *et al.* Ultrafast neuronal imaging of dopamine dynamics with designed genetically encoded sensors. *Science* **360**, eaat4422, doi:10.1126/science.aat4422 (2018).

95 Ravotto, L., Duffet, L., Zhou, X., Weber, B. & Patriarchi, T. A bright and colorful future for G-protein coupled receptor sensors. *Frontiers in Cellular Neuroscience* **14**, 67 (2020).

96 Farrell, J. S. *et al.* In vivo endocannabinoid dynamics at the timescale of physiological and pathological neural activity. *Neuron* **109**, 2398-2403. e2394 (2021).

97 Liu, Z. *et al.* Deficiency in endocannabinoid synthase DAGLB contributes to Parkinson's disease and dopaminergic neuron dysfunction. *bioRxiv* (2021).

98 Baggelaar, M. P. *et al.* Highly selective, reversible inhibitor identified by comparative chemoproteomics modulates diacylglycerol lipase activity in neurons. *Journal of the American Chemical Society* **137**, 8851-8857 (2015).

99 Rozenfeld, R. Type I Cannabinoid Receptor Trafficking: All Roads Lead to Lysosome. *Traffic* **12**, 12-18, doi:https://doi.org/10.1111/j.1600-0854.2010.01130.x (2011).

100 Rozenfeld, R. *et al.* Receptor Heteromerization Expands the Repertoire of Cannabinoid Signaling in Rodent Neurons. *PLOS ONE* **7**, e29239, doi:10.1371/journal.pone.0029239 (2012).

101 He, J. C. *et al.* The Gαo/i-coupled Cannabinoid Receptor-mediated Neurite Outgrowth Involves Rap Regulation of Src and Stat3*. *Journal of Biological Chemistry* **280**, 33426-33434, doi:https://doi.org/10.1074/jbc.M502812200 (2005).

102 Jordan, J. D. *et al.* Cannabinoid Receptor-induced Neurite Outgrowth Is Mediated by Rap1 Activation through Gαo/i-triggered Proteasomal Degradation of Rap1GAPII*. *Journal of Biological Chemistry* **280**, 11413-11421, doi:https://doi.org/10.1074/jbc.M411521200 (2005).

103 Jung, K.-M., Astarita, G., Thongkham, D. & Piomelli, D. Diacylglycerol lipase-alpha and -beta control neurite outgrowth in neuro-2a cells through distinct molecular mechanisms. *Mol Pharmacol* **80**, 60-67, doi:10.1124/mol.110.070458 (2011).

104 Busquets-García, A., Bolaños, J. P. & Marsicano, G. Metabolic messengers: endocannabinoids. *Nature Metabolism* **4**, 848-855 (2022).

105 Farah, S. I., Hilston, S., Tran, N., Zvonok, N. & Makriyannis, A. 1-, 2-and 3-AG as Substrates of the Endocannabinoid Enzymes and Endogenous Ligands of the Cannabinoid Receptor 1. *Biochemical and Biophysical Research Communications* **591**, 31-36 (2022).

106 Steffens, M., Zentner, J., Honegger, J. & Feuerstein, T. J. Binding affinity and agonist activity of putative endogenous cannabinoids at the human neocortical CB1 receptor. *Biochemical Pharmacology* **69**, 169-178, doi:https://doi.org/10.1016/j.bcp.2004.08.033 (2005).

107 Kearn, C. S., Greenberg, M. J., DiCamelli, R., Kurzawa, K. & Hillard, C. J. Relationships between ligand affinities for the cerebellar cannabinoid receptor CB1 and the induction of GDP/GTP exchange. *J Neurochem* **72**, 2379-2387, doi:10.1046/j.1471-4159.1999.0722379.x (1999).

108 Shen, M., Piser, T. M., Seybold, V. S. & Thayer, S. A. Cannabinoid receptor agonists inhibit glutamatergic synaptic transmission in rat hippocampal cultures. *J Neurosci* **16**, 4322-4334, doi:10.1523/JNEUROSCI.16-14-04322.1996 (1996).

109 An, D., Peigneur, S., Hendrickx, L. A. & Tytgat, J. Targeting Cannabinoid Receptors: Current Status and Prospects of Natural Products. *Int J Mol Sci* **21**, 5064, doi:10.3390/ijms21145064 (2020).

110 Eldeeb, K., Leone-Kabler, S. & Howlett, A. C. CB1 cannabinoid receptor-mediated increases in cyclic AMP accumulation are correlated with reduced Gi/o function. *Journal of basic and clinical physiology and pharmacology* **27**, 311-322 (2016).

111 Rinaldi-Carmona, M. *et al.* SR141716A, a potent and selective antagonist of the brain cannabinoid receptor. *FEBS letters* **350**, 240-244 (1994).

112 Bauer, M. *et al.* Identification and quantification of a new family of peptide endocannabinoids (Pepcans) showing negative allosteric modulation at CB1 receptors. *J Biol Chem* **287**, 36944-36967, doi:10.1074/jbc.M112.382481 (2012).

113 Liu, Z. *et al.* Functional Selectivity of a Biased Cannabinoid-1 Receptor (CB1R) Antagonist. *ACS Pharmacology & Translational Science* **4**, 1175-1187, doi:10.1021/acsptsci.1c00048 (2021).

114 Hua, T. *et al.* Crystal structures of agonist-bound human cannabinoid receptor CB(1). *Nature* **547**, 468-471, doi:10.1038/nature23272 (2017).

115 Shim, J.-Y., Bertalovitz, A. C. & Kendall, D. A. Identification of essential cannabinoid-binding domains: structural insights into early dynamic events in receptor activation. *J Biol Chem* **286**, 33422-33435, doi:10.1074/jbc.M111.261651 (2011).

116 Makriyannis, A., Guo, J. & Tian, X. Albumin enhances the diffusion of lipophilic drugs into the membrane bilayer. *Life sciences* **77**, 1605-1611 (2005).

117 Sugiura, T. *et al.* Evidence That the Cannabinoid CB1 Receptor Is a 2-Arachidonoylglycerol Receptor: STRUCTURE-ACTIVITY RELATIONSHIP OF 2-ARACHIDONOYLGLYCEROL, ETHER-LINKED ANALOGUES, AND RELATED COMPOUNDS*. *Journal of Biological Chemistry* **274**, 2794-2801, doi:https://doi.org/10.1074/jbc.274.5.2794 (1999).

118 Farah, S. I., Hilston, S., Tran, N., Zvonok, N. & Makriyannis, A. 1-, 2- and 3-AG as substrates of the endocannabinoid enzymes and endogenous ligands of the cannabinoid receptor 1. *Biochemical and Biophysical Research Communications* **591**, 31-36, doi:https://doi.org/10.1016/j.bbrc.2021.12.105 (2022).

119 Tagen, M. & Klumpers, L. E. Review of delta-8-tetrahydrocannabinol (Δ8-THC): Comparative pharmacology with Δ9-THC. *British journal of pharmacology* **179**, 3915-3933 (2022).

120 Thomas, A. *et al.* Cannabidiol displays unexpectedly high potency as an antagonist of CB1 and CB2 receptor agonists in vitro. *British journal of pharmacology* **150**, 613-623 (2007).

121 Zygmunt, P. M. *et al.* Monoacylglycerols activate TRPV1–a link between phospholipase C and TRPV1. *PloS one* **8**, e81618 (2013).

122 Navia-Paldanius, D., Savinainen, J. R. & Laitinen, J. T. Biochemical and pharmacological characterization of human α/β-hydrolase domain containing 6 (ABHD6) and 12 (ABHD12). *Journal of lipid research*, jlr. M030411 (2012).
123 Hua, T. *et al.* Crystal structures of agonist-bound human cannabinoid receptor CB1. *Nature* **547**, 468-471 (2017).
124 Tham, M. *et al.* Allosteric and orthosteric pharmacology of cannabidiol and cannabidiol-dimethylheptyl at the type 1 and type 2 cannabinoid receptors. *British journal of pharmacology* **176**, 1455-1469 (2019).
125 Ahn, K. H., Mahmoud, M. M., Shim, J.-Y. & Kendall, D. A. Distinct roles of β-arrestin 1 and β-arrestin 2 in ORG27569-induced biased signaling and internalization of the cannabinoid receptor 1 (CB1). *Journal of biological chemistry* **288**, 9790-9800 (2013).
126 Murataeva, N. *et al.* Where's my entourage? The curious case of 2-oleoylglycerol, 2-linolenoylglycerol, and 2-palmitoylglycerol. *Pharmacological research* **110**, 173-180 (2016).
127 Leishman, E., Mackie, K. & Bradshaw, H. B. Elevated levels of arachidonic acid-derived lipids including prostaglandins and endocannabinoids are present throughout ABHD12 knockout brains: novel insights into the neurodegenerative phenotype. *Frontiers in molecular neuroscience* **12**, 142 (2019).
128 Torrens, A. *et al.* Comparative Pharmacokinetics of Δ(9)-Tetrahydrocannabinol in Adolescent and Adult Male Mice. *J Pharmacol Exp Ther* **374**, 151-160, doi:10.1124/jpet.120.265892 (2020).
129 Vozella, V., Zibardi, C., Ahmed, F. & Piomelli, D. Fast and Sensitive Quantification of Δ(9)-Tetrahydrocannabinol and Its Main Oxidative Metabolites by Liquid Chromatography/Tandem Mass Spectrometry. *Cannabis Cannabinoid Res* **4**, 110-123, doi:10.1089/can.2018.0075 (2019).
130 Fezza, F. *et al.* Endocannabinoids, Related Compounds and Their Metabolic Routes. *Molecules* **19**, 17078-17106 (2014).
131 Pertwee, R. G. Cannabinoids and multiple sclerosis. *Pharmacol Ther* **95**, 165-174 (2002).
132 Matsuda, L. A., Lolait, S. J., Brownstein, M. J., Young, A. C. & Bonner, T. I. Structure of a cannabinoid receptor and functional expression of the cloned cDNA. *Nature* **346**, 561-564 (1990).
133 Thomas, B. F., Gilliam, A. F., Burch, D. F., Roche, M. J. & Seltzman, H. H. Comparative receptor binding analyses of cannabinoid agonists and antagonists. *Journal of Pharmacology and Experimental Therapeutics* **285**, 285-292 (1998).
134 Straiker, A., Dvorakova, M., Zimmowitch, A. & Mackie, K. Cannabidiol inhibits endocannabinoid signaling in autaptic hippocampal neurons. *Molecular pharmacology* **94**, 743-748 (2018).
135 Laprairie, R. B., Bagher, A. M., Kelly, M. E., Dupre, D. J. & Denovan-Wright, E. M. Type 1 cannabinoid receptor ligands display functional selectivity in a cell culture model of striatal medium spiny projection neurons. *J Biol Chem* **289**, 24845-24862, doi:10.1074/jbc.M114.557025 (2014).
136 Laprairie, R., Bagher, A., Kelly, M. & Denovan-Wright, E. Cannabidiol is a negative allosteric modulator of the cannabinoid CB1 receptor. *British journal of pharmacology* **172**, 4790-4805 (2015).
137 Jakowiecki, J. *et al.* Allosteric Modulation of the CB1 Cannabinoid Receptor by Cannabidiol—A Molecular Modeling Study of the N-Terminal Domain and the Allosteric-Orthosteric Coupling. *Molecules* **26**, 2456 (2021).
138 Shao, Z. *et al.* Structure of an allosteric modulator bound to the CB1 cannabinoid receptor. *Nature chemical biology* **15**, 1199-1205 (2019).
139 Grygorczyk, R. *et al.* Lytic Release of Cellular ATP: Physiological Relevance and Therapeutic Applications. *Life (Basel)* **11**, doi:10.3390/life11070700 (2021).

140 Rodrigues, R. J., Tomé, A. R. & Cunha, R. A. ATP as a multi-target danger signal in the brain. *Front Neurosci* **9**, 148, doi:10.3389/fnins.2015.00148 (2015).

141 Kennedy, C. The P2Y/P2X divide: How it began. *Biochemical Pharmacology* **187**, 114408, doi:https://doi.org/10.1016/j.bcp.2021.114408 (2021).

142 Chavez-Noriega, L. E. *et al.* Pharmacological characterization of recombinant human neuronal nicotinic acetylcholine receptors hα2β2, hα2β4, hα3β2, hα3β4, hα4β2, hα4β4 and hα7 expressed in Xenopus oocytes. *Journal of Pharmacology and Experimental Therapeutics* **280**, 346-356 (1997).

143 North, R. A. & Surprenant, A. Pharmacology of cloned P2X receptors. *Annu. Rev. Pharmacol. Toxicol.* **40**, 563-580 (2000).

144 Kopp, R., Krautloher, A., Ramírez-Fernández, A. & Nicke, A. P2X7 Interactions and Signaling - Making Head or Tail of It. *Front Mol Neurosci* **12**, 183, doi:10.3389/fnmol.2019.00183 (2019).

145 Andrejew, R. *et al.* The P2X7 Receptor: Central Hub of Brain Diseases. *Front Mol Neurosci* **13**, 124, doi:10.3389/fnmol.2020.00124 (2020).

146 Lu, H.-C. & Mackie, K. Review of the endocannabinoid system. *Biological Psychiatry: Cognitive Neuroscience and Neuroimaging* **6**, 607-615 (2021).

147 Mitrirattanakul, S. *et al.* Site-specific increases in peripheral cannabinoid receptors and their endogenous ligands in a model of neuropathic pain. *Pain* **126**, 102-114, doi:10.1016/j.pain.2006.06.016 (2006).

148 Tanaka, M., Sackett, S. & Zhang, Y. Endocannabinoid Modulation of Microglial Phenotypes in Neuropathology. *Front Neurol* **11**, 87, doi:10.3389/fneur.2020.00087 (2020).

149 Hossain, M. Z., Ando, H., Unno, S. & Kitagawa, J. Targeting Peripherally Restricted Cannabinoid Receptor 1, Cannabinoid Receptor 2, and Endocannabinoid-Degrading Enzymes for the Treatment of Neuropathic Pain Including Neuropathic Orofacial Pain. *Int J Mol Sci* **21**, doi:10.3390/ijms21041423 (2020).

150 Covelo, A., Eraso-Pichot, A., Fernández-Moncada, I., Serrat, R. & Marsicano, G. CB1R-dependent regulation of astrocyte physiology and astrocyte-neuron interactions. *Neuropharmacology* **195**, 108678 (2021).

151 Singh, S. *et al.* Pharmacological characterization of the endocannabinoid sensor GRABeCB2. 0. *bioRxiv*, 2023.2003. 2003.531053 (2023).

152 Walter, L., Dinh, T. & Stella, N. ATP induces a rapid and pronounced increase in 2-arachidonoylglycerol production by astrocytes, a response limited by monoacylglycerol lipase. *J Neurosci* **24**, 8068-8074, doi:10.1523/JNEUROSCI.2419-04.2004 (2004).

153 Witting, A., Walter, L., Wacker, J., Moller, T. & Stella, N. P2X7 receptors control 2-arachidonoylglycerol production by microglial cells. *Proc Natl Acad Sci U S A* **101**, 3214-3219, doi:10.1073/pnas.0306707101 (2004).

154 Baggelaar, M. P. *et al.* Highly Selective, Reversible Inhibitor Identified by Comparative Chemoproteomics Modulates Diacylglycerol Lipase Activity in Neurons. *Journal of the American Chemical Society* **137**, 8851-8857, doi:10.1021/jacs.5b04883 (2015).

155 Hsu, K.-L. *et al.* DAGLβ inhibition perturbs a lipid network involved in macrophage inflammatory responses. *Nat Chem Biol* **8**, 999-1007, doi:10.1038/nchembio.1105 (2012).

156 Eldeeb, K., Leone-Kabler, S. & Howlett, A. C. CB1 cannabinoid receptor-mediated increases in cyclic AMP accumulation are correlated with reduced Gi/o function. *J Basic Clin Physiol Pharmacol* **27**, 311-322, doi:10.1515/jbcpp-2015-0096 (2016).

157 Rinaldi-Carmona, M. *et al.* SR141716A, a potent and selective antagonist of the brain cannabinoid receptor. *FEBS Letters* **350**, 240-244, doi:https://doi.org/10.1016/0014-5793(94)00773-X (1994).

158 Young, M. T., Pelegrin, P. & Surprenant, A. Amino acid residues in the P2X7 receptor that mediate differential sensitivity to ATP and BzATP. *Mol Pharmacol* **71**, 92-100, doi:10.1124/mol.106.030163 (2007).
159 Gómez-Villafuertes, R. *et al.* Ca2+/calmodulin-dependent kinase II signalling cascade mediates P2X7 receptor-dependent inhibition of neuritogenesis in neuroblastoma cells. *The FEBS journal* **276**, 5307-5325 (2009).
160 Donnelly-Roberts, D. L., Namovic, M. T., Han, P. & Jarvis, M. F. Mammalian P2X7 receptor pharmacology: comparison of recombinant mouse, rat and human P2X7 receptors. *Br J Pharmacol* **157**, 1203-1214, doi:10.1111/j.1476-5381.2009.00233.x (2009).
161 Janks, L., Sharma, C. V. R. & Egan, T. M. A central role for P2X7 receptors in human microglia. *Journal of Neuroinflammation* **15**, 325, doi:10.1186/s12974-018-1353-8 (2018).
162 Michel, A. D. & Fonfria, E. Agonist potency at P2X7 receptors is modulated by structurally diverse lipids. *Br J Pharmacol* **152**, 523-537, doi:10.1038/sj.bjp.0707417 (2007).
163 Burnstock, G. Purine and purinergic receptors. *Brain Neurosci Adv* **2**, 2398212818817494, doi:10.1177/2398212818817494 (2018).
164 Honore, P. *et al.* A-740003 [N-(1-{[(cyanoimino)(5-quinolinylamino) methyl] amino}-2, 2-dimethylpropyl)-2-(3, 4-dimethoxyphenyl) acetamide], a novel and selective P2X7 receptor antagonist, dose-dependently reduces neuropathic pain in the rat. *Journal of Pharmacology and Experimental Therapeutics* **319**, 1376-1385 (2006).
165 Reigada, D. *et al.* Diadenosine tetraphosphate (Ap(4)A) inhibits ATP-induced excitotoxicity: a neuroprotective strategy for traumatic spinal cord injury treatment. *Purinergic Signal* **13**, 75-87, doi:10.1007/s11302-016-9541-4 (2017).
166 Eichmann, T. O. & Lass, A. DAG tales: the multiple faces of diacylglycerol—stereochemistry, metabolism, and signaling. *Cellular and Molecular Life Sciences* **72**, 3931-3952, doi:10.1007/s00018-015-1982-3 (2015).
167 Ogasawara, D. *et al.* Rapid and profound rewiring of brain lipid signaling networks by acute diacylglycerol lipase inhibition. *Proc Natl Acad Sci U S A* **113**, 26-33, doi:10.1073/pnas.1522364112 (2016).
168 van Esbroeck, A. C. M. *et al.* Identification of α,β-Hydrolase Domain Containing Protein 6 as a Diacylglycerol Lipase in Neuro-2a Cells. *Front Mol Neurosci* **12**, 286-286, doi:10.3389/fnmol.2019.00286 (2019).
169 Hsu, K.-L. *et al.* Discovery and optimization of piperidyl-1,2,3-triazole ureas as potent, selective, and in vivo-active inhibitors of α/β-hydrolase domain containing 6 (ABHD6). *J Med Chem* **56**, 8270-8279, doi:10.1021/jm400899c (2013).
170 Drysdale, C. *et al.* P2X7-mediated alteration of membrane fluidity is associated with the late stages of age-related macular degeneration. *Purinergic Signal* **18**, 469-479, doi:10.1007/s11302-022-09894-y (2022).
171 Kokona, D. *et al.* The endocannabinoid 2-arachidonoylglycerol and dual ABHD6/MAGL enzyme inhibitors display neuroprotective and anti-inflammatory actions in the in vivo retinal model of AMPA excitotoxicity. *Neuropharmacology* **185**, 108450, doi:https://doi.org/10.1016/j.neuropharm.2021.108450 (2021).
172 Biringer, R. G. The rise and fall of anandamide: processes that control synthesis, degradation, and storage. *Mol Cell Biochem* **476**, 2753-2775, doi:10.1007/s11010-021-04121-5 (2021).
173 Burkey, T. H. *et al.* Relative efficacies of cannabinoid CB1 receptor agonists in the mouse brain. *European Journal of Pharmacology* **336**, 295-298, doi:https://doi.org/10.1016/S0014-2999(97)01255-7 (1997).
174 Graham, E. S. *et al.* Induction of Krox-24 by Endogenous Cannabinoid Type 1 Receptors in Neuro2A Cells Is Mediated by the MEK-ERK MAPK Pathway and Is Suppressed by the

Phosphatidylinositol 3-Kinase Pathway*. *Journal of Biological Chemistry* **281**, 29085-29095, doi:https://doi.org/10.1074/jbc.M602516200 (2006).

175 Erb, L. & Weisman, G. A. Coupling of P2Y receptors to G proteins and other signaling pathways. *Wiley Interdiscip Rev Membr Transp Signal* **1**, 789-803, doi:10.1002/wmts.62 (2012).

176 Surprenant, A. & North, R. A. Signaling at Purinergic P2X Receptors. *Annual Review of Physiology* **71**, 333-359, doi:10.1146/annurev.physiol.70.113006.100630 (2009).

177 Rassendren, F. *et al.* The permeabilizing ATP receptor, P2X7. Cloning and expression of a human cDNA. *J Biol Chem* **272**, 5482-5486, doi:10.1074/jbc.272.9.5482 (1997).

178 Di Virgilio, F., Dal Ben, D., Sarti, A. C., Giuliani, A. L. & Falzoni, S. The P2X7 Receptor in Infection and Inflammation. *Immunity* **47**, 15-31, doi:https://doi.org/10.1016/j.immuni.2017.06.020 (2017).

179 Di Virgilio, F., Sarti, A. C. & Grassi, F. Modulation of innate and adaptive immunity by P2X ion channels. *Current Opinion in Immunology* **52**, 51-59, doi:https://doi.org/10.1016/j.coi.2018.03.026 (2018).

180 Bisogno, T. *et al.* Cloning of the first sn1-DAG lipases points to the spatial and temporal regulation of endocannabinoid signaling in the brain. *J Cell Biol* **163**, 463-468, doi:10.1083/jcb.200305129 (2003).

181 He, Y., Taylor, N., Fourgeaud, L. & Bhattacharya, A. The role of microglial P2X7: modulation of cell death and cytokine release. *J Neuroinflammation* **14**, 135, doi:10.1186/s12974-017-0904-8 (2017).

182 Wang, X. *et al.* P2X7 receptor inhibition improves recovery after spinal cord injury. *Nature Medicine* **10**, 821-827, doi:10.1038/nm1082 (2004).

183 Kanellopoulos, J. M. & Delarasse, C. Pleiotropic Roles of P2X7 in the Central Nervous System. *Front Cell Neurosci* **13**, 401, doi:10.3389/fncel.2019.00401 (2019).

184 Karasawa, A., Michalski, K., Mikhelzon, P. & Kawate, T. The P2X7 receptor forms a dye-permeable pore independent of its intracellular domain but dependent on membrane lipid composition. *Elife* **6**, e31186 (2017).

185 Ren, W. J. & Illes, P. Involvement of P2X7 receptors in chronic pain disorders. *Purinergic Signal* **18**, 83-92, doi:10.1007/s11302-021-09796-5 (2022).

186 Muñoz, M. F., Griffith, T. N. & Contreras, J. E. Mechanisms of ATP release in pain: role of pannexin and connexin channels. *Purinergic Signal* **17**, 549-561, doi:10.1007/s11302-021-09822-6 (2021).

187 Chessell, I. P. *et al.* Disruption of the P2X7 purinoceptor gene abolishes chronic inflammatory and neuropathic pain. *PAIN* **114** (2005).

188 Stella, N. THC and CBD: Similarities and differences between siblings. *Neuron* **111**, 302-327, doi:https://doi.org/10.1016/j.neuron.2022.12.022 (2023).

189 Ford, Z. K. *et al.* Cannabinoid Receptor 1 Expression in Human Dorsal Root Ganglia and CB13-Induced Bidirectional Modulation of Sensory Neuron Activity. *Front Pain Res (Lausanne)* **2**, 721332, doi:10.3389/fpain.2021.721332 (2021).

190 Ghosh, K., Zhang, G.-F., Chen, H., Chen, S.-R. & Pan, H.-L. Cannabinoid CB2 receptors are upregulated via bivalent histone modifications and control primary afferent input to the spinal cord in neuropathic pain. *Journal of Biological Chemistry* **298**, 101999, doi:https://doi.org/10.1016/j.jbc.2022.101999 (2022).

191 Vučković, S., Srebro, D., Vujović, K. S., Vučetić, Č. & Prostran, M. Cannabinoids and Pain: New Insights From Old Molecules. *Frontiers in Pharmacology* **9**, doi:10.3389/fphar.2018.01259 (2018).

192 Thomas, A., Okine, B. N., Finn, D. P. & Masocha, W. Peripheral deficiency and antiallodynic effects of 2-arachidonoyl glycerol in a mouse model of paclitaxel-induced neuropathic pain.

Biomedicine & Pharmacotherapy **129**, 110456, doi:https://doi.org/10.1016/j.biopha.2020.110456 (2020).

193 Thompson, A. L. *et al.* The Endocannabinoid System Alleviates Pain in a Murine Model of Cancer-Induced Bone Pain. *J Pharmacol Exp Ther* **373**, 230-238, doi:10.1124/jpet.119.262337 (2020).

194 Wen, J. *et al.* WWL70 protects against chronic constriction injury-induced neuropathic pain in mice by cannabinoid receptor-independent mechanisms. *Journal of Neuroinflammation* **15**, 9, doi:10.1186/s12974-017-1045-9 (2018).

195 Pellkofer, H. L. *et al.* The major brain endocannabinoid 2-AG controls neuropathic pain and mechanical hyperalgesia in patients with neuromyelitis optica. *PLoS One* **8**, e71500, doi:10.1371/journal.pone.0071500 (2013).

196 Sagar, D. R. *et al.* Dynamic regulation of the endocannabinoid system: implications for analgesia. *Mol Pain* **5**, 59, doi:10.1186/1744-8069-5-59 (2009).

197 Choi, S. I. & Hwang, S. W. Depolarizing Effectors of Bradykinin Signaling in Nociceptor Excitation in Pain Perception. *Biomol Ther (Seoul)* **26**, 255-267, doi:10.4062/biomolther.2017.127 (2018).

198 Turu, G. *et al.* Paracrine transactivation of the CB1 cannabinoid receptor by AT1 angiotensin and other Gq/11 protein-coupled receptors. *J Biol Chem* **284**, 16914-16921, doi:10.1074/jbc.M109.003681 (2009).

199 Zygmunt, P. M. *et al.* Monoacylglycerols activate TRPV1--a link between phospholipase C and TRPV1. *PloS one* **8**, e81618-e81618, doi:10.1371/journal.pone.0081618 (2013).

200 Golias, C., Charalabopoulos, A., Stagikas, D., Charalabopoulos, K. & Batistatou, A. The kinin system--bradykinin: biological effects and clinical implications. Multiple role of the kinin system--bradykinin. *Hippokratia* **11**, 124-128 (2007).

201 Wade, J., McDaid, L., Harkin, J., Crunelli, V. & Kelso, S. Self-repair in a Bidirectionally Coupled Astrocyte-Neuron (AN) System based on Retrograde Signaling. *Frontiers in Computational Neuroscience* **6**, doi:10.3389/fncom.2012.00076 (2012).

202 Duffy, S. S., Hayes, J. P., Fiore, N. T. & Moalem-Taylor, G. The cannabinoid system and microglia in health and disease. *Neuropharmacology* **190**, 108555, doi:https://doi.org/10.1016/j.neuropharm.2021.108555 (2021).

203 Kallendrusch, S. *et al.* Intrinsic up-regulation of 2-AG favors an area specific neuronal survival in different in vitro models of neuronal damage. *PLoS One* **7**, e51208, doi:10.1371/journal.pone.0051208 (2012).

204 Viader, A. *et al.* A chemical proteomic atlas of brain serine hydrolases identifies cell type-specific pathways regulating neuroinflammation. *eLife* **5**, e12345, doi:10.7554/eLife.12345 (2016).

205 Elmes, M. W. *et al.* Fatty acid-binding proteins (FABPs) are intracellular carriers for Δ9-tetrahydrocannabinol (THC) and cannabidiol (CBD). *J Biol Chem* **290**, 8711-8721, doi:10.1074/jbc.M114.618447 (2015).

206 Leboffe, L., di Masi, A., Trezza, V., Polticelli, F. & Ascenzi, P. Human serum albumin: A modulator of cannabinoid drugs. *IUBMB Life* **69**, 834-840, doi:https://doi.org/10.1002/iub.1682 (2017).

207 Latremoliere, A. & Woolf, C. J. Central sensitization: a generator of pain hypersensitivity by central neural plasticity. *J Pain* **10**, 895-926, doi:10.1016/j.jpain.2009.06.012 (2009).

208 Gangadharan, V. & Kuner, R. Pain hypersensitivity mechanisms at a glance. *Dis Model Mech* **6**, 889-895, doi:10.1242/dmm.011502 (2013).

209 Li, W., Blankman, J. L. & Cravatt, B. F. A Functional Proteomic Strategy to Discover Inhibitors for Uncharacterized Hydrolases. *Journal of the American Chemical Society* **129**, 9594-9595, doi:10.1021/ja073650c (2007).

210 Simon, G. M. & Cravatt, B. F. Activity-based proteomics of enzyme superfamilies: serine hydrolases as a case study. *J Biol Chem* **285**, 11051-11055, doi:10.1074/jbc.R109.097600 (2010).

211 van Esbroeck, A. C. M. *et al.* Activity-based protein profiling reveals off-target proteins of the FAAH inhibitor BIA 10-2474. *Science* **356**, 1084-1087, doi:10.1126/science.aaf7497 (2017).

212 Békés, M., Langley, D. R. & Crews, C. M. PROTAC targeted protein degraders: the past is prologue. *Nature Reviews Drug Discovery* **21**, 181-200, doi:10.1038/s41573-021-00371-6 (2022).

213 Miralpeix, C. *et al.* Carnitine palmitoyltransferase 1C negatively regulates the endocannabinoid hydrolase ABHD6 in mice, depending on nutritional status. *Br J Pharmacol* **178**, 1507-1523, doi:10.1111/bph.15377 (2021).

214 Hoover, H. S., Blankman, J. L., Niessen, S. & Cravatt, B. F. Selectivity of inhibitors of endocannabinoid biosynthesis evaluated by activity-based protein profiling. *Bioorg Med Chem Lett* **18**, 5838-5841, doi:10.1016/j.bmcl.2008.06.091 (2008).

215 Aaltonen, N. *et al.* High-Resolution Confocal Fluorescence Imaging of Serine Hydrolase Activity in Cryosections - Application to Glioma Brain Unveils Activity Hotspots Originating from Tumor-Associated Neutrophils. *Biol Proced Online* **22**, 6, doi:10.1186/s12575-020-00118-4 (2020).

216 Rauwerdink, A. & Kazlauskas, R. J. How the Same Core Catalytic Machinery Catalyzes 17 Different Reactions: the Serine-Histidine-Aspartate Catalytic Triad of α/β-Hydrolase Fold Enzymes. *ACS Catal* **5**, 6153-6176, doi:10.1021/acscatal.5b01539 (2015).

217 Bononi, G., Tuccinardi, T., Rizzolio, F. & Granchi, C. α/β-Hydrolase Domain (ABHD) Inhibitors as New Potential Therapeutic Options against Lipid-Related Diseases. *J Med Chem* **64**, 9759-9785, doi:10.1021/acs.jmedchem.1c00624 (2021).

218 Matošević, A. & Bosak, A. Carbamate group as structural motif in drugs: a review of carbamate derivatives used as therapeutic agents. *Arh Hig Rada Toksikol* **71**, 285-299, doi:10.2478/aiht-2020-71-3466 (2020).

219 Tchantchou, F. & Zhang, Y. Selective inhibition of alpha/beta-hydrolase domain 6 attenuates neurodegeneration, alleviates blood brain barrier breakdown, and improves functional recovery in a mouse model of traumatic brain injury. *J Neurotrauma* **30**, 565-579, doi:10.1089/neu.2012.2647 (2013).

220 Tanaka, M. *et al.* WWL70 attenuates PGE2 production derived from 2-arachidonoylglycerol in microglia by ABHD6-independent mechanism. *Journal of Neuroinflammation* **14**, 7, doi:10.1186/s12974-016-0783-4 (2017).

221 Agalave, S. G., Maujan, S. R. & Pore, V. S. Click Chemistry: 1,2,3-Triazoles as Pharmacophores. *Chemistry – An Asian Journal* **6**, 2696-2718, doi:https://doi.org/10.1002/asia.201100432 (2011).

222 Adibekian, A. *et al.* Click-generated triazole ureas as ultrapotent in vivo-active serine hydrolase inhibitors. *Nat Chem Biol* **7**, 469-478, doi:10.1038/nchembio.579 (2011).

223 Marrs, W. R. *et al.* Dual inhibition of alpha/beta-hydrolase domain 6 and fatty acid amide hydrolase increases endocannabinoid levels in neurons. *J Biol Chem* **286**, 28723-28728, doi:10.1074/jbc.M110.202853 (2011).

224 Patel, J. Z. *et al.* Optimization of 1,2,5-thiadiazole carbamates as potent and selective ABHD6 inhibitors. *ChemMedChem* **10**, 253-265, doi:10.1002/cmdc.201402453 (2015).

225 Niphakis, M. J. *et al.* Evaluation of NHS carbamates as a potent and selective class of endocannabinoid hydrolase inhibitors. *ACS Chem Neurosci* **4**, 1322-1332, doi:10.1021/cn400116z (2013).

226 Janssen, F. J. *et al.* Discovery of Glycine Sulfonamides as Dual Inhibitors of sn-1-Diacylglycerol Lipase α and α/β-Hydrolase Domain 6. *J Med Chem* **57**, 6610-6622, doi:10.1021/jm500681z (2014).

227 Deng, H. *et al.* Chiral disubstituted piperidinyl ureas: a class of dual diacylglycerol lipase-α and ABHD6 inhibitors. *MedChemComm* **8**, 982-988, doi:10.1039/C7MD00029D (2017).

228 Malamas, M. S. *et al.* Design and Synthesis of Highly Potent and Specific ABHD6 Inhibitors. *ChemMedChem*, doi:10.1002/cmdc.202100406 (2021).

229 Kawaguchi, A. *et al.* Functional expression of bradykinin B1 and B2 receptors in neonatal rat trigeminal ganglion neurons. *Front Cell Neurosci* **9**, doi:10.3389/fncel.2015.00229 (2015).

230 Wang, H. *et al.* Bradykinin produces pain hypersensitivity by potentiating spinal cord glutamatergic synaptic transmission. *J Neurosci* **25**, 7986-7992, doi:10.1523/jneurosci.2393-05.2005 (2005).

231 Ji, R.-R., Nackley, A., Huh, Y., Terrando, N. & Maixner, W. Neuroinflammation and Central Sensitization in Chronic and Widespread Pain. *Anesthesiology* **129**, 343-366, doi:10.1097/ALN.0000000000002130 (2018).

232 Yam, M. F. *et al.* General Pathways of Pain Sensation and the Major Neurotransmitters Involved in Pain Regulation. *Int J Mol Sci* **19**, doi:10.3390/ijms19082164 (2018).

233 Bononi, G. *et al.* Reversible Monoacylglycerol Lipase Inhibitors: Discovery of a New Class of Benzylpiperidine Derivatives. *J Med Chem* **65**, 7118-7140, doi:10.1021/acs.jmedchem.1c01806 (2022).

VITA

Simar Raj Singh earned a Bachelor of Science degree in Cellular and Molecular Biology followed by a master's degree in pharmacology at the University of Michigan-Ann Arbor. Prior to entering graduate school, he worked in multiple academic labs, including the Gnegy Lab at the University of Michigan and the Kovats Lab at the Oklahoma Medical Research Foundation, where he contributed to several research publications. As a graduate student at the University of Washington Department of Pharmacology, Simar worked in the lab of Dr. Nephi Stella where he studied mechanisms of endocannabinoid signaling.